Distribution Agreement

In presenting this thesis as a partial fulfillment of the requirements for a degree from Emory University, I hereby grant to Emory University and its agents the non-exclusive license to archive, make accessible, and display my thesis in whole or in part in all forms of media, now or hereafter now, including display on the World Wide Web. I understand that I may select some access restrictions as part of the online submission of this thesis. I retain all ownership rights to the copyright of the thesis. I also retain the right to use in future works (such as articles or books) all or part of this thesis.

Alicia Walker April 9, 2020

From epigenetic memory to memory loss: How tau prevents LSD1 from regulating transcription and induces cell death in Alzheimer's disease

by

Alicia Walker

David Katz
Adviser

Neuroscience and Behavioral Biology

David Katz

Adviser

Allan Levey

Committee Member

Roger Deal

Committee Member

2020

From epigenetic memory to memory loss: How tau prevents LSD1 from regulating transcription and induces cell death in Alzheimer's disease

By

Alicia Walker

David Katz

Adviser

An abstract of
a thesis submitted to the Faculty of Emory College of Arts and Sciences
of Emory University in partial fulfillment
of the requirements of the degree of
Bachelor of Science with Honors

Neuroscience and Behavioral Biology

2020

Abstract

From epigenetic memory to memory loss: How tau prevents LSD1 from regulating transcription and induces cell death in Alzheimer's disease

By Alicia Walker

During development, the histone demethylase LSD1 functions as an eraser of epigenetic memory, removing 'bookmarks' of active transcription to induce cellular reprogramming. However, LSD1's role in terminally differentiated cells is unknown. Previously, our lab implicated LSD1 in tau-induced neurodegeneration by showing that LSD1 localizes to pathological tau aggregates in Alzheimer's disease (AD) cases, and that it is continuously required for the survival of hippocampal and cortical neurons in mice. Here, we utilize the P301S tauopathy mouse model to demonstrate that pathological tau can exclude LSD1 from the nucleus in neurons. In addition, we show that reducing LSD1 in these mice is sufficient to highly exacerbate the tauopathy phenotype. We find that overexpressing LSD1 in the hippocampus of tauopathy mice, even after pathology has formed, is sufficient to significantly delay neurodegeneration. These results suggest that inhibiting LSD1 via sequestration contributes to tau-mediated neurodegeneration. In considering the mechanism of the interaction between tau and LSD1, we recognized that both proteins have disordered regions. Tau has been shown to interact with disordered regions of other proteins, therefore we hypothesized that tau might similarly interact with LSD1 in this way. Here, we show preliminary evidence that loss of the N-terminal disordered domain reduces the sequestration of LSD1 by tau aggregates. Additionally, we further conceive that this disordered domain may be partially required for LSD1 functionality *in vivo*. Taken together, this work provides evidence that LSD1, specifically its N-terminal disordered domain, is a promising therapeutic target for tauopathies such as AD.

From epigenetic memory to memory loss: How tau prevents LSD1 from regulating transcription and induces cell death in Alzheimer's disease

By

Alicia Walker

David Katz

Adviser

A thesis submitted to the Faculty of Emory College of Arts and Sciences
of Emory University in partial fulfillment
of the requirements of the degree of
Bachelor of Science with Honors

Neuroscience and Behavioral Biology

2020

Acknowledgements

I would first like to thank Dr. Katz for being an incredible mentor throughout my undergraduate research career. He has provided me with countless opportunities – from funding me to do research over the summer, to helping me find a lab while studying abroad in Australia, to helping get my dream gap-year job as a research assistant in Beth Stevens' lab at Boston Children's Hospital. An additional thank you to my committee members, Dr. Allan Levey and Dr. Roger Deal, for their time and thoughtful questions. I also want to thank my graduate student mentor Amanda Engstrom for teaching me (quite literally) almost everything I know. I am unsure what my life in research will look like without her, as we have learned to anticipate each other's every need in a way that eerily resembles telepathy. I want to extend a special thank you to Dr. Stephanie Kyle for doing the painstaking work to get this project off the ground during her time in the Katz lab. My honors thesis would not be nearly this dope without her hard work. Thank you to the rest of the members of the Katz lab for helping me learn and grow as a scientist and person. Special shoutouts to: Dr. Teresa Lee, for always being an amazing mentor in science and life, Sindy Chavez and Alyssa (A$) Scott for enabling my procrastination by being my coffee break buddies, and to our great rotation students this year (Yu, Kat, Tommy, and Emily) for weighing the mice in the N-terminal colony every week so that I didn't have to!

And finally, thank you to COVID-19 for ruining my senior spring. If it weren't for a literal global pandemic, I'm not sure that I would have had the discipline to stay inside writing this thesis for what felt like an eternity.

Table of Contents

CHAPTER I

Introduction

Our lab is interested in the chromatin modifying enzyme LSD1 (Lysine-specific histone demethylase 1). LSD1 removes mono- and di- methyl groups from lysine 4 of histone H3 (H3K4me1/2) (Shi et al., 2004). H3K4me1/2 are deposited by a methyltransferase that functions in conjunction with RNA Polymerase II elongation, thereby activating chromatin in a transcription-coupled manner (Ng et al., 2003; Mito et al., 2005; Shilatifard, 2012). LSD1 regulates a form of transcriptional memory, a process which allows for the maintenance of specific histone tail modifications, such as H3K4me2, through cell divisions to mark previously active loci (Muramoto et al., 2010). While other active marks on chromatin may induce transcription, transcription-coupled modifications are specifically used to mark RNA Polymerase II's previous targets, 'bookmarking' active loci throughout the process of cell division so that daughter cells can 'hit the ground running' on the same transcriptional program as their parent (Lee and Katz, 2020). Tight regulation of this process is intuitively important when considering transitions of cell fate, such as differentiation or fertilization, in which a cell must abandon its current transcriptional program for an entirely new path. During development, LSD1 functions as an eraser, removing marks of active transcriptional memory to induce cellular reprogramming (Whyte et al., 2012). An example is its function with the REST complex to derepress neuronal genes during stem cell differentiation into neural progenitors, and subsequent maturation to neurons (Ballas et al., 2005). A neuronal specific isoform of LSD1 produced by alternative splicing of exons 2 and/or 8 has been shown to induce neurite morphogenesis upon overexpression (Zibetti et al., 2010). This mechanism has been linked to substrate specificity of LSD1 isoforms, where neuronal specific LSD1 splices specifically demethylate H4K20 or H3K9 (depending on the isoform and its interacting partner) in order to activate neuronal transcriptional programs in response to neuronal activity (Laurent et al., 2015; Wang et al., 2015). Conditional

knockout of a neuronal-specific LSD1 isoform in adult mice results in learning and memory deficits; this deficiency was not explained by anatomical changes, but rather was the result of downregulated transcription factors critical for neuronal activity (Wang et al., 2015). Alternatively, canonical LSD1 acts primarily on H3K4 to erase transcriptional memory as described above. LSD1 is also known to function with REST to prevent neuronal cell fates in non-neuronal cells (Chong et al., 1995) but little else was known about the role of ubiquitously expressed LSD1 outside of development.

With the intent to further understand LSD1 function in the maintenance of differentiated cells, our lab conditionally knocked out *Lsd1* in adult mice using a Cre/Lox tamoxifen inducible system (Christopher et al., 2017). To our surprise, these mice developed massive hippocampal and cortical neurodegeneration, and corresponding learning and memory defects, within weeks of *Lsd1* deletion, demonstrating that LSD1 is required for neuronal survival in adult mice (Christopher et al., 2017). The cell death observed in these animals is correlated with reactivation of pluripotency genes (Christopher et al., 2017). Stem cell networks are particularly vulnerable to the accumulation of inappropriate marks of active transcriptional memory because these genes produce transcription factors which further activate their own production in a positive feedback manner (Lee and Katz, 2020). Taken together, these data suggest that RNA Polymerase II and the H3K4 methyltransferase are continuously landing and elongating on pluripotency genes in these neurons, requiring LSD1 to continuously erase the marks they leave behind to prevent the inappropriate reactivation of a developmental transcriptional program in differentiated cells. When LSD1 is deleted in adult mice and the epigenetic mechanism of maintaining cell fate is lost, neurons in the hippocampus and cortex crucial for learning and memory die. This suggests that the erasure of this epigenetic memory is required for neuronal survival. This result is

separate from the aforementioned behavioral deficits observed in mice with a conditional knockout of the neuronal specific LSD1 splice, which does not occur due to cell death, but rather as a result of inappropriate repression of neuronal activity.

In addition, the patterns of neurodegeneration, behavioral deficits, and expression changes that we observed in *Lsd1* deletion mice closely resemble Alzheimer's Disease (AD) and frontotemporal dementia cases, but not other neurodegenerative diseases (Christopher et al., 2017). These overlaps between our *Lsd1* deletion mice and the human neurodegenerative diseases raise the possibility that LSD1 could be involved in these diseases. Frontotemporal dementia and AD are tauopathies, a class of neurodegenerative disease associated with pathological tau. Interestingly, LSD1 specifically mislocalizes to Tau aggregates in human AD cases, but not Amyloid-beta plaques in AD or alpha-synuclein aggregates in Parkinson's Disease cases (Christopher et al., 2017). These results clearly implicate a relationship between tau and LSD1. The following chapters detail the next two projects we undertook to understand how LSD1 fits into the story of AD pathogenesis.

CHAPTER II

Materials and Methods

The following materials and methods were utilized to collect the results in Chapters III and IV. Methods denoted with an asterisk (*) represent those performed by A.C.W.

A. Solutions and buffers

0.1M Phosphate buffer

0.2M Solution A: NaH_2PO_4 24.0g/L

0.2M Solution B: Na_2HPO_4 28.4g/L

To 1,000mL Solution B, add Solution A slowly to bring pH to 7.3 (about 220mL Solution A).

Dilute 1/2 with diH_2O when needed to make 0.1M

Tail prep buffer

10mL 1M Tris-Cl

20mL 5M NaCl

20mL 0.5M EDTA

50mL 10% SDS

900mL diH_2O

1X TBS

7.88g Tris-Cl

9.0g NaCl

1,000mL diH_2O

10X Citrate Buffer

2.g Citrate Monohydrate

1000mL diH2O

pH to 6.0 with NaOH

dilute 1:10 for working 1X solution

H20 Brij

1,000mL of diH2O

2.5mL of 30% Brij 35 solution (Sigma)

Tris Brij

100mL 1M Tris-Cl pH 7.5

100mL 1M NaCl

5mL 1M MgCl2

2.5mL 30% Brij 35

797.5mL diH2O

Tau secret formula

10mL 1M Tris-Cl pH 7.5

1.5mL 1M NaCl

0.5mL 1M MgCl2

88mL diH2O

B. Mouse work

All mouse work was approved by and conducted in accordance with the Emory University Institutional Animal Care and Use Committee.

i. Mouse lines

Lsd1$^{fl/fl}$ mice (Wang et al., 2007) were crossed to *CAGG-CreERTM* (Hayashi and McMahon, 2002), a tamoxifen inducible Cre, to generate *CAGG-CreER*^{TM}, *Lsd1*$^{fl/+}$ mice, which were then intercrossed to produce *CAGG-CreER*^{TM}, *Lsd1*$^{fl/fl}$ mice. This cross also produced *CAGG-CreER*^{TM} negative animals with *Lsd1*$^{fl/fl}$, which were used as littermate controls in all experiments. The line was maintained by crossing *CAGG-CreER*^{TM} negative, *Lsd1*$^{fl/fl}$ mice with *CAGG-CreER*^{TM}, *Lsd1*$^{fl/fl}$ mice.

Using the same *Lsd1*$^{fl/fl}$ mice we generated *Lsd1*$^{-/+}$ mice that were maintained as heterozygotes. *Lsd1*$^{-/+}$ mice were crossed with PS19 Tau mice (Yoshiyama et al., 2007). PS19 Tau mice are hemizygous for the P301S mutated form of the human tau protein identified from a human patient. PS19 Tau mice were maintained as hemizygotes. These crosses generated four experimental genotypes: wildtype, *Lsd1*$^{-/+}$, PS19 Tau, and PS19;*Lsd1*$^{-/+}$ mice.

We additionally generated a novel mouse line heterozygous for an exon 1 deletion of *Lsd1* (hereafter referred to as *Lsd1*$^{\Delta N/+}$). *Lsd1*$^{\Delta N/+}$ mice were crossed with PS19 Tau mice, generating four experimental genotypes: wildtype, *Lsd1*$^{\Delta N/+}$, PS19 Tau, and PS19;*Lsd1*$^{\Delta N/+}$ (Figure 4.10). PS19;*Lsd1*$^{\Delta N/+}$ mice were crossed with *Lsd1*$^{\Delta N/+}$ mice to generate mice homozygous for the exon 1 deletion of *Lsd1* (hereafter referred to as *Lsd1*$^{\Delta N/\Delta N}$) in the Tau background. These crosses generated six experimental genotypes:

wildtype, PS19 Tau, *Lsd1*$^{\Delta N/+}$, PS19;*Lsd1*$^{\Delta N/+}$, *Lsd1*$^{\Delta N/\Delta N}$ and PS19;*Lsd1*$^{\Delta N/\Delta N}$ (Figure 4.14).

ii. Mouse genotyping by PCR*

At weaning, a 5mm piece of mouse tail was removed with a razor blade and digested overnight in a 50°C water bath with 500µL tail prep buffer and 5µL of 20mg/mL protease K (Ambion). This digest was then phenol/chloroform extracted by adding 500µL phenol/chloroform and vigorously vortexing followed by separation of the aqueous and organic layers by centrifugation (5 minutes). The 250µL of the aqueous (top) layer was extracted, brought back up to 500µL with water, and then re-extracted with 500µL phenol/chloroform. The aqueous layer of the second extraction was recovered (400µL) and DNA was precipitated with ethanol by adding 40µL of 3M sodium acetate and 800µL of ice cold 100% ethanol, followed by inversion. The mixture was then centrifuged at 4°C for 10 minutes to produce a pellet and the supernatant was discarded. The pellet was washed with 150µL of 70% ethanol (room temperature) and centrifuged again for 5 minutes, followed by careful removal of the ethanol. The isolated pellet was allowed to dry at room temperature for 10 minutes and finally reconstituted with water. This DNA served as the template for genotyping PCR reactions.

For genotyping, each PCR reaction contained 3µL of template undiluted DNA (LSD1ΔN deletion) or DNA diluted either 1/100 (Cre, Tau) or 1/1000 (Lsd1) and 22µL of PCR reaction mix. Each PCR reaction mix contained 2.5 µL 10X AmpliTaq Gold 360 buffer, 0.5 µL 10mM dNTPs, 1.0 µL each primer (50 µM stock, Table 2-1), 35.0 µL 25mM MgCl2, 0.2 µL AmpliTaq Gold 360 Polymerase and water. The Lsd1 genotyping

reaction yields two possible products: 483bp for wildtype and 289bp for deleted. The Cre genotyping reaction yields a positive control product (250bp) and 320bp product when the Cre transgene is present. The Tau genotyping reaction yields a positive control product (250bp) and 350bp product when the Tau transgene is present. The LSD1ΔN deletion genotyping reaction yields a 480bp product when the deletion is present, while the LSD1ΔN control genotyping reaction yields a 230bp product.

iii. Euthanasia* and tissue fixation*

Mice were given a lethal dose of isoflurane via inhalation, then transcardially perfused with ice cold 4.0% paraformaldehyde in 0.1M phosphate buffer. Brain and spinal cord were dissected and post fixed in cold paraformaldehyde solution for 2 hours. Brain weights and sizes were taken from mice that were euthanized by cervical dislocation. Brain was dissected, immediately weighed, imaged, and fixed in cold 4.0% paraformaldehyde in 0.1M phosphate buffer overnight. In all cases, tissues were transferred to cold PBS, then serially dehydrated and embedded in paraffin and serially sectioned into 8μm coronal sections.

iv. Quantitative Analysis of Paralysis: Rotarod and grid performance*

We performed experiments on PS19 Tau, *Lsd1*$^{-/+}$, PS19;*Lsd1*$^{-/+}$ mice at 6, 8, and 10 months. For the rotarod experiments, mice were given two practice trials and then placed on the rotating cylinder at 4rpm. Rotational speed then gradually increased over a 5-minute test session up to a maximum rotational speed of 40rpm. Latency to fall off of the accelerating rotarod was used as the dependent variable. We calculated the latency to fall,

maximum speed in rotations per minute, and distance traveled. For grid performance, mice were placed on a horizontal grid that was then inverted so mice are hanging upside down by their paws. Mice were videotaped for 10 seconds, and then scored* for forepaw and back paw distance traveled. Mice that could not hold onto grid for 10 seconds were censored. Investigators were blinded to the genotypes for both experiments.

v. Mouse magnetic resonance imagining (MRI)

MRI studies were conducted on PS19 Tau, *Lsd1*$^{-/+}$, PS19;*Lsd1*$^{-/+}$ mice at 6 months and 10 months (*n*=3/genotype). Mice were anesthetized with isoflurane, and monitored for heart rate and temperature changes while anesthetized. MRI measurements were performed using a 9.4 T/20 cm horizontal bore Bruker magnet, interfaced to an AVANCE console (Bruker, Billerica, MA, USA). A two-coil actively decoupled imaging set-up was used (a 2 cm diameter surface coil for reception and a 7.2 cm diameter volume coil for transmission). Axial T2-weighted images were acquired with a RARE (Rapid Acquisition with Refocused Echos) sequence. Its imaging parameters were as follows: TR = 3000 ms, Eff.TE = 64 ms, RARE factor = 4, field of view (FOV) = 23.04 × 23.04 mm2, matrix = 192 × 192, Avg = 4, slice thickness (thk) = 0.6 mm, number of slice(NSL)=20. Specific emphasis was placed on the neocortex and hippocampus in the coronal images (1.0 – 4.0 mm posterior to the bregma).

vi. Stereotaxic surgery and viral infusion

All surgical procedures were approved by and conducted in accordance with the Emory University Institutional Animal Care and Use Committee. Mice were anesthetized with isoflurane (3% induction, 1-2% maintenance) and administered the analgesic

meloxicam (5 mg/kg). Using a Stoeling Quintessential Stereotaxic Injector pump and Hamilton syringe, mice were injected with either the control AAV-DJ- HA virus, the AAV-DJ-LSD1- HA virus, or the AAV-DJ-LSD1ΔN-HA virus into both hippocampi. Each virus was injected into the rostral (AP: -2.5, ML:± 2.2, DV: -1.6, relative to bregma) and caudal (AP: -3.1, ML:± 3.0, DV: -3.5) hippocampus of both hemispheres (four injection sites total). Infusion volumes were 0.5 µL per injection site, administered at a rate of 0.15 µL/min. Following surgery, mice were monitored daily for the duration of the experiment. Brains were extracted 3 months post-surgery which allows sufficient time for viral expression. Injection accuracy was confirmed by HA positive staining, and those mice where staining was outside the hippocampus or that did not fully reach hippocampus were censored.

C. Staining

i. Histology* and histological quantification*

Hematoxylin and eosin staining was performed according to standard procedures. Briefly, sections were dewaxed with xylenes and serial ethanol dilutions then stained with Eosin using the Richard-Allan Scientific Signature Series Eosin-Y package (ThermoScientific). To derive unbiased estimates of neuronal loss in the hippocampus, the number of primordial neurons in CA1 and CA3 (corresponding approximately to bregma coordinates -2.0 mm and -3.0 mm) were counted from 2 randomly selected regions in the field of a Zeiss Axiophot ocular graticule grid and measured manually using digital micrographs of H&E-stained preparations. Investigators were blinded to the genotype or treatment.

ii. Immunohistochemistry* and Immunofluorescence*

Sections were dewaxed with xylenes and serial ethanol dilutions, then treated with 3% hydrogen peroxide at 40°C for 5 minutes to quench endogenous peroxidase activity, blocked in 2% serum at 40°C for 15 minutes, and incubated with primary Ab (Table S1) overnight at 4°C. Slides were washed, then incubated with biotinylated secondary Ab (Biotinylated Goat α Rabbit, 1:200, Vector Labs BA-1000 or Biotinylated Horse α Mouse, 1:200, Vector Labs BA-9200) at 37°C for 30 minutes. Signal amplification was then carried out by incubating at 37°C for 1 hour with Vector Labs Elite ABC reagent (PK-6200). Slides were developed with DAB for 1-5 minutes, counterstained with hematoxylin for 1 minutes, and coverslipped.

For immunofluorescence, dewaxed sections were first rinsed with TBS. Antigen retrieval was performed by microwaving at 10% power 2X for 5 minutes in 0.01M sodium citrate. Slides were then cooled, washed with TBS, permeabilized in 0.5% Triton X-100 for 20 minutes, followed by blocking in 10% goat serum 20 minutes. Primary Abs (Table 2-2) were incubated overnight at 4°C. Slides were then washed and incubated in secondary Abs (Invitrogen A1 1001 and Invitrogen A11012) for 1 hour at room temperature, followed by TBS washes, counterstained with DAPI, and then coverslipped.

iii. Quantification of tau accumulation

For the assessment of tau accumulation, six random sections (sampling from CA1, CA3, and cerebral cortex) per sample were manually counted using digital micrographs of AT8 stained preparations in the field of a Zeiss Axiophot ocular graticule grid. Investigators were blinded to the genotype or treatment. Imaging for immunofluorescence of LSD1 staining was performed on a spinning-disk confocal

Nikon-Tie controlled with the software NIS Elements (Nikon). Imaging for all other immunofluorescence staining was performed on an Eclipse Ti2 inverted microscope (Nikon, Toyko, Japan) controlled with the software NIS Elements (Nikon). Image J software ((NIH, http://imagej.nih.gov/ij/) was used for viewing all images.

iv. Protein quantification

Protein levels were determined by homogenizing brains in 1 ml/g of tissue in ice-cold lysis buffer (150mM NaCl, 1% Triton X-100, 0.5% Na-deoxycholate, 1% SDS, 50mM Tris, pH8.0) in a dounce homogenizer, followed by end-over-end spin at 4°C for 2 hours, and centrifugation at 20,000 x g for 20 minutes at 4°C. Protein concentrations were determined following standard BCA protocol (Pierce BCA Protein Assay Kit). Equal amounts of protein for each sample were loaded and run on a 12% SDS-PAGE gel, transferred (Semi-dry transfer using BIO RAD Trans-Blot Turbo Transfer System), blocked in 5% BSA, and probed with primary Ab (Table S1) over night at 4°C. Blots were rinsed and stained with HRP-conjugated secondary Ab, and detected by chemiluminescence using ChemiDoc MP Imaging System (BIO RAD). Protein levels were normalized using total protein calculated using BIO RAD ImageLab software.

D. RNA sequencing

i. RNA isolation

Mice were euthanized by cervical dislocation, hippocampi were dissected and snap frozen with liquid nitrogen in 1mL Trizol, and stored at -80°C. For RNA isolation, samples were thawed at 37°C then kept on ice prior to homogenization with Polytron homogenizer with a 5 second pulse. After a 5 minute incubation at room temperature, one

tenth the sample volume of 1-bromo-3chloropropane was added, mixed by inversion and incubated for 3 minutes at room temperature. Samples were then centrifuged at 13,000 X g for 15 minutes at 4°C to separate the aqueous and organic layers. As much of the aqueous layer was recovered as possible, then RNA was precipitated with isoproponal. Pellets were then washed with 75% ethanol and resuspended in 50μL of dionized water.

RNA library preparation and sequencing were performed by HudsonAlpha Genomic Services Lab. RNA was Poly(A) selected and 300bp size selected. Libraries were sequenced for 25 million 50bp paired end reads. All RNA-seq FASTQ files will be uploaded to Gene Expression Omnibus (GEO).

ii. RNA sequencing analysis

Short read FASTQ files were quality trimmed using FASTX toolkit (v. 0.0.14) to trim three bases from the 5' end of the reads. Paired-end reads were then mapped to the mm9 genome using TopHat2 (Kim et al., 2013) and the UCSC knownGene gtf file. The following parameters were used in the TopHat2 call "-N 1 –g 1 –read-gap-length 1 –mate-inner-dis 170". Reads that had the same starting location and strand with mate-pairs that also had the same location and strand were considered to be PCR duplicates and removed from subsequent analyses using Picard tools (v.1.103). Differentially expressed transcripts were determined using Cufflinks and Cuffdiff (v2.1.1) (Trapnell et al., 2010). Downstream analyses were performed in R/Bioconductor (Gentleman et al., 2004) and used gene summarized expression levels normalized using Fragments Per Kilobase per Million (FPKM) from Cufflinks. Hierarchical clustering was performed using the pvclust R package were significance was determined using bootstrapping (Suzuki and

Shimodaira, 2006). Principle Components Analysis (PCA) was conducted using the "prcomp" function of the stats package in R/ Bioconductor. Enriched gene ontologies were determined using the package "GOstats" (v. 3.1.1) (Falcon and Gentleman, 2007). Gene Set Enrichment Analysis (GSEA) was performed using a pre-ranked gene list determined by cuffdiff test statistic and GSEA (v. 2.1.0) (Mootha et al., 2003; Subramanian et al., 2005). Hierarchical clustering of gene expression data was performed using average clustering in the heatmap.2 package. UCSC-style display of gene expression data were plotted using the "rtracklayer" package (Lawrence et al., 2009) and custom R scripts as previously described (Scharer et al., 2013).

The sequencing data were uploaded to the Galaxy web platform, and *we used the public server at* usegalaxy.org *to analyze the data ((Afgan et al., 2016; Afgan et al., 2018)).* FASTQ files were quality assessed using FASTQC (v.0.11.7), trimmed using Trimmomatic (v.0.36.5) and minimum QC score of 20 and minimum read length of 36bp. Paired-end reads were subsequently mapped to the GRCm38 genome using HISAT2 (v.2.1.0). Unmapped, unpaired and multiply mapped reads were removed using Filter SAM or BAM (v.1.1.2). Assignment of transcripts to GRCm38 genomic features was performed using Featurecounts (v.1.6.0.6) and the Ensembl GRCm38.93 gtf file. Differentially expressed transcripts were determined using DESEQ2 (v.2.11.40.2) (Afgan et al., 2018). For all datasets, a cutoff of adjusted p-value < 0.3 and abs (log_2 fold change) > 0.58 was applied. TPM values were calculated from raw data obtained from Featurecounts output. Subsequent downstream analysis was performed using R and normalized counts and adjusted P-values from DESEQ2 (v.2.11.40.2). Heatmaps were produced and hierarchical clustering was done using the gplots package (v. 3.0.1) and

normalized counts (B. B. Gregory R. Warens, 2019). Volcano plots were produced using the enhanced volcano package (v.0.99.16) and adjusted p-values ((Blighe, 2019)). Additionally, Gene Set Enrichment Analysis (Pre-ranked list) was performed using the online platform WebGestalt ((Zhang et al., 2005; Wang et al., 2013; Wang et al., 2017; Liao et al., 2019)). Custom R-scripts available upon request.

iii. Comparison to human gene expression data

Normalized gene expression data from late onset Alzheimer's disease (LOAD) (Zhang et al., 2013), frontal temporal dementia (FTD) (Chen-Plotkin et al., 2008) and Parkinson's disease (PD) (Zhang et al., 2005) patients were downloaded from Gene Expression Omnibus gene sets GSE44772, GSE13162 and GSE20295, respectively. Comparison to *Lsd1*^{CAGG} gene expression data was performed by mapping mouse and human genes using the NCBI homologene database (Wheeler et al., 2001). Correlation of *Lsd1*^{CAGG} gene expression changes and those found in LOAD, FTD and PD patients were assessed using Spearman's rank correlation (ρ). P-values were determined by analysis of variance (ANOVA).

Table 2-1 Genotyping Primers

Mouse genotyping for the *Lsd1* control and deleted alleles, the *Tau* transgene, and the *Lsd1ΔN* deletion allele were performed with the listed primers. Lyophilized stocks were reconstituted to 50μM. The Lsd1 Forward and Reverse were mixed in equal parts and the Tau Forward, Tau Reverse, Cre/Tau Control Forward and Cre/Tau Control Reverse were mixed in equal parts prior to use in the PCR reaction. The Lsd1ΔN deletion Forward and Reverse were not pre-mixed and were used in equal parts in the PCR reaction.

Lsd1	Forward	5'-GCACCAACACTAAAGAGTATCC-3'
	Reverse	5'-CCACAGAACTTCAAATTACTAAT-3'
Cre transgene	Forward	5'-GAACCTGATGGACATGTTCAGG-3'
	Reverse	5'-AGTGCGTTCGAACGCTAGAGCCTGT-3'
Tau transgene	Forward	5'-GGGGACACGTCTCCACGGCATCTCAGCAATGTCTCC-3'
	Reverse	5'-TCCCCCAGCCTAGACCACGAGAAT-3'
Cre and Tau control	Forward	5'-TTACGTCCATCGTGGACAGC-3'
	Reverse	TGGGCTGGGTGTTAGCCTTA-3'
Lsd1ΔN deletion	Forward	5'-GATATGCTGGGTCGCACTCC-3'
	Reverse	5'-GTAGACAAACGCGTCGGGAA-3'
Lsd1ΔN control	Forward	5'-GCCCATGGAGACCGGAATA-3'
	Reverse	5'-cacacaggtagacaaacgcg-3'

Table 2-2 Primary Antibodies

Primary antibodies for immunohistochemistry and immunofluorescence staining experiments are given. Also listed are the manufacturer and catalog number, experiment, and dilution used.

Target	**Manufacturer**	**Clone**	**Lot number**	**Experiment**	**Dilution**
NeuN	Millipore MAB377	A60	2392283	Mouse IF	1:500
LSD1	Abcam 17721		GR3193508-2	Mouse IF	1:100
				Mouse IHC	1:500
PHF-Tau	ThermoFisher MN 1020	AT8	TI2611431	Mouse IHC	1:1,000
		AT8	TI2611431	Mouse IF	1:200
HA	Abcam ab130275	16B12	GR3190856-12	Mouse IHC	1:500
		16B12	GR3190856-12	Mouse IF	1:100
HA	Abcam ab9110		GF3224022-1	Mouse IF	1:500
GFAP	Dako	Z0334	20047046	Mouse IHC	1:100
IBA1	Synaptic System 234004		2-16	Mouse IF	1:100
Neurofilament (phospho)	Millipore NE1022	SMI-31R		Mouse IHC	1:500
PHF-1	Peter Davies (Albert Einstein College of Medicine, NY)			Mouse IHC	1:1,000
LSD1	Cell Signaling 2139		5	Immunoblot	1:1,000
TLR2	Abcam ab9100	TL2.1	GR3189369-7	Mouse IF	1:100

CHAPTER III

The inhibition of LSD1 via sequestration contributes to tau-mediated neurodegeneration

Engstrom AK, Walker AC*, Moudgal RA, Myrick DA, Kyle SM, Katz DJ (2020) The inhibition of LSD1 via sequestration contributes to tau-mediated neurodegeneration. bioRxiv:745133.

This manuscript is currently under review by Review Commons and is openly accessible on bioRxiv.

INTRODUCTION

Tauopathies such as corticobasal degeneration, progressive supranuclear palsy, and frontotemporal lobar degeneration with tau inclusions are neurodegenerative diseases pathologically defined by different forms of tau positive intraneuronal deposits (Goedert et al., 1988; Wischik et al., 1988; Holtzman et al., 2016; Wang and Mandelkow, 2016; Orr et al., 2017). In addition to these primary tauopathies, neuropathological observations of postmortem Alzheimer's disease (AD) brains show the presence of neurofibrillary tangles (NFTs) of hyperphosphorylated tau protein, as well as plaques containing β-amyloid (Aβ) peptide (Barage and Sonawane; Hardy and Selkoe, 2002; Duyckaerts et al., 2009; Bloom, 2014). AD is the leading cause of age-related dementia, resulting from neuronal cell death in the frontal and temporal cortices, as well as the hippocampus (Barage and Sonawane). As dementia progresses, the spatial pattern of tau pathology highly correlates with the level of cognitive impairment (Arriagada et al., 1992; Gomez-Isla et al., 1997; Karran et al., 2011; Bejanin et al., 2017). In addition, Aβ oligomers and/or plaques can enhance tau pathology in various mouse models (Hurtado et al., 2010; He et al., 2018), and there is increasing evidence that accumulation of Aβ plaques can contribute to tau pathology (Braak and Braak, 1997; Choi et al., 2014; Holtzman et al., 2016). The most well-defined physiological role of tau is in stabilizing microtubules, particularly in neuronal axons (Wang and Mandelkow, 2016). However, in the pathological state, tau becomes aberrantly phosphorylated (Morishima-Kawashima et al., 1995; Hanger et al., 1998; Wang and Mandelkow, 2016), truncated (Wischik et al., 1988; Orr et al., 2017), and aggregates into oligomers and larger insoluble filaments (Arendt et al., 2016; Castellani and Perry, 2019). This pathology is thought to trigger synaptic loss, dramatic genome-wide expression changes, increased inflammatory response, and neuronal cell death (Masliah et al., 2001; Ingelsson et al.,

2004; Rubio-Perez and Morillas-Ruiz, 2012; Kinney et al., 2018). These data suggest that pathological tau may be a downstream mediator of the neurotoxic effects leading to neuronal degeneration in AD.

Previously, our lab demonstrated that deleting the histone demethylase *Lsd1* in adult mice leads to significant neuronal cell death in the hippocampus and cortex with associated learning and memory defects (Christopher et al., 2017). In this mouse model, loss of *Lsd1* induces genome-wide expression changes that significantly overlap with those observed in the brains of postmortem human AD cases, but not other neurodegenerative diseases, such as Parkinson's disease or amyotrophic lateral sclerosis (ALS) cases. Consistent with this overlap, we observed LSD1 protein mislocalized to cytoplasmic NFTs, but it was not associated with Aβ plaques in AD cases or with Lewy bodies of α-synuclein in Parkinson's disease cases (Christopher et al., 2017). These data highlight the requirement for LSD1 in neuronal survival and suggest that the nuclear function of the histone demethylase LSD1 could be disrupted by mislocalization to pathological tau.

To investigate how LSD1 may contribute to tau-mediated neurodegeneration, we utilized the PS19 P301S tauopathy mouse model (hereafter referred to as PS19 Tau). PS19 Tau mice express a P301S mutated form of the human tau protein, originally identified in a frontotemporal dementia with parkinsonism (FTDP-17) patient, driven by the prion promoter throughout the nervous system (Yoshiyama et al., 2007). When expressed in mice, the P301S tau protein is prone to hyperphosphorylation and somatodendritic aggregation, without the presence of Aβ plaques. PS19 Tau mice develop a heavy pathological tau burden and have been well characterized for the temporal progression of tau pathology and disease-related phenotypes

(Bellucci et al., 2004; Iba et al., 2015). However, the mechanism of neuronal cell death caused by pathological tau is still unknown.

Here, we provide functional data that the inhibition of LSD1 function contributes to tau induced neurodegeneration. We demonstrate in PS19 Tau mice that pathological tau sequesters LSD1 in the cytoplasm of neurons throughout the brain. This results in depletion of LSD1 from the nucleus. Additionally, we provide genetic and molecular evidence that pathological tau contributes to neurodegeneration by disrupting LSD1. Finally, we show that overexpressing LSD1 in hippocampal neurons is sufficient to suppress neuronal cell death even after pathological tau has formed. We propose that pathological tau contributes to neuronal cell death by sequestering LSD1 in the cytoplasm, depleting the nuclear pool of LSD1 that is required for neuronal survival.

RESULTS

Tau pathology depletes LSD1 from the nucleus in the PS19 Tau mouse model

Previously, we showed in human AD cases that LSD1 protein inappropriately colocalizes with NFTs in the cell body of hippocampal and cortical neurons, while in unaffected controls LSD1 was properly localized exclusively to the nucleus (Christopher et al., 2017). However, because neurons in AD cases with intracellular NFTs presumably die and are cleared, it was difficult to determine whether tau prevents LSD1 from localizing to the nucleus in a dying neuron. To address this possibility, we performed LSD1 immunofluorescence on 12 month old PS19 Tau mice, which have significant tau pathology (Yoshiyama et al., 2007). Because PS19 Tau mice undergo neurodegeneration over a shortened period, there are more neurons undergoing neurodegeneration at any given time point. Thus, we reasoned that it may be possible to observe

LSD1 depletion from the nucleus. Similar to what we observe in humans, LSD1 protein in 12 month old Wild Type mice was localized to the nucleus of neurons in the cerebral cortex (Fig. 3.1A-C) and the hippocampus (Fig. S1 A-C). However, in 12 month old PS19 Tau mice, LSD1 protein was sequestered in the cytoplasm and depleted from the nucleus both in the cerebral cortex (Fig. 3.1D-F) and the hippocampus (Fig. S1 D-F). These are both regions where we observe substantial cytoplasmic tau pathology (Fig. 3.1G-I; Fig. S1 G-I). Similarly, in other brain regions that accumulate tau pathology, such as the thalamus and amygdala, LSD1 was localized to the nucleus in 12 month old Wild Type control mice (Fig. S1 J-O), but abnormally localized to the cytoplasm in PS19 Tau mouse littermates (Fig. S1 P-U). Overall, we observed sequestration of LSD1 in 6 out of 7 mice analyzed. In each of the 6 mice, there were varying levels of sequestration ranging from LSD1 found in both the nucleus and cytoplasm (Fig. S1 V-X), to depletion from the nucleus (Fig. S1 Y-DD).

Reduction of LSD1 increases the mouse tauopathy phenotype

If the presence of pathological tau in the cytoplasm is leading to neuronal cell death through the sequestration and nuclear depletion of LSD1, we would expect that lowering the overall levels of LSD1 would accelerate depletion and exacerbate the progression of disease. To test this, we made PS19 Tau mice heterozygous for *Lsd1* (hereafter referred to as PS19;*Lsd1*$^{-/+}$, Fig. S2 A). *Lsd1* heterozygotes (hereafter referred to as *Lsd1*$^{-/+}$) have a functioning copy of *Lsd1* and don't have phenotypes associated with LSD1 loss of function (Foster et al., 2010; Jin et al., 2013; Lyons et al., 2013). Thus, *Lsd1* heterozygosity does not completely compromise LSD1 function. Instead mice that are heterozygous for *Lsd1* are sensitized to mechanisms affecting LSD1 localization and function. Consistent with this, we observed a 30% reduction in transcript levels (Fig. S2 B) and a 35% reduction in protein levels (Fig. S2 C,D) in *Lsd1*$^{-/+}$ mice compared to their

Lsd1$^{+/+}$ littermates. Surprisingly, PS19 Tau mice have a 20% increase in LSD1 protein levels compared to *Lsd1*$^{+/+}$ littermates. Nevertheless, consistent with the reduction in LSD1 that we observe in *Lsd1*$^{-/+}$ mice, PS19;*Lsd1*$^{-/+}$ mice have a similar 26% reduction in transcript levels (Fig. S2 B) and a 31% reduction in protein levels (Fig. S2 C,D) compared to PS19 Tau littermates. In addition, all genotypes were born at normal Mendelian ratios with equal male/female ratios.

As expected, *Lsd1*$^{-/+}$ mice had normal survival (Fig. 3.2A). In contrast, PS19 Tau mice had a reduced overall survival (Fig. 3.2A) (Yoshiyama et al., 2007). When one copy of *Lsd1* was removed from PS19 Tau mice, their reduced survival was significantly exacerbated (P-value = 0.0017, Fig. 3.2A). As expected, there was little effect on the onset of reduced viability. The initial decline in the survival of PS19;*Lsd1*$^{-/+}$ mice started only slightly earlier than PS19 Tau mice, but after the appearance of pathological tau in neurons (Fig. S6 K-M) (Yoshiyama et al., 2007). This suggests that pathological tau may have to be present before *Lsd1* heterozygosity has deleterious effects. Subsequently, PS19;*Lsd1*$^{-/+}$ mice had a 14% reduction in median lifespan compared to PS19 Tau mice and reached median survival 44 days earlier then PS19 Tau mice. In addition, there was a further exacerbation of reduced lifespan as pathology became more severe. PS19;*Lsd1*$^{-/+}$ mice reached the point when there was only 10% of the population remaining 83 days earlier than PS19 Tau mice, and all but one of the last 25% of PS19;*Lsd1*$^{-/+}$ mice died between 11.5-13.5 months, compared to 13.5-19 months in PS19 Tau mice. As a result, 28% of PS19 Tau mice were still alive after all but one of the PS19;*Lsd1*$^{-/+}$ mice had died (Fig. 3.2A).

PS19 Tau mice develop paralysis starting with hind limb clasping which progresses until they are unable to feed (Yoshiyama et al., 2007). In our hands, PS19 Tau mice displayed intermittent hind limb clasping starting at approximately 6 months of age. At 12 months, these mice had a severe clasp, but were still mobile. This is delayed compared to what was originally

reported by Yoshiyama and colleagues (Yoshiyama et al., 2007). PS19;*Lsd1*$^{-/+}$ mice also displayed intermittent hind limb clasping beginning at approximately 6 months of age. However PS19;*Lsd1*$^{-/+}$ mice became terminally paralyzed at a faster rate compared to PS19 Tau mouse littermates. At 12 months, when PS19 Tau mice were still mobile, PS19;*Lsd1*$^{-/+}$ mice were severely paralyzed and typically terminal (Movie S1). To quantitatively assess paralysis we performed rotarod and grid performance tests. In the rotarod, we assessed the ability of the mice to stay on the rotating rod (latency to fall) (Fig. 3.2B), the speed of the rod at which they fall off the rotarod (rotations per minute) (Fig. 3.2C), and the total distance traveled (Fig. 3.2D). All genotypes performed the same at 6 months and 8 months (Fig. 3.2B-D). However, at 10 months, when PS19 Tau mice still performed normally, PS19;*Lsd1*$^{-/+}$ mice had a significant deficit in mobility (P-value < 0.01, Fig. 3.2B,C). A deficit in PS19;*Lsd1*$^{-/+}$ mice was also observed at 10 months in the total distance traveled (Fig. 3.2D) and in grid performance testing (Fig. S3 A), though neither were statistically significant.

To further investigate the exacerbation of paralysis we examined the spinal cord motor neurons. Healthy motor neurons from *Lsd1*$^{+/+}$ control mice express LSD1 (Fig. S3 B-D) and are classically identified by circular nuclei at the center of a large cell body. In contrast to the healthy motor neurons we observed in 12 month old PS19 Tau mice (Fig. S3 E), many of the motor neurons in PS19;*Lsd1*$^{-/+}$ mice at 12 months had abnormal morphology, with the nucleus skewed to the edge of the cell body (Fig. S3 E vs. S3 F) and a ballooned cell body (Fig. S3 F). Within the cell body we found aberrant hyperphosphorylated NFH (heavy chain neurofilament), which is a sign of activated neuronal stress pathways (Fig S3 G vs. S3 H) (Giasson and Mushynski, 1996; Liu et al., 2008). This abnormal morphology is highly reminiscent of a well-established process known as chromatolysis, which is characterized by swelling of the neuronal

cell body, disruption of Nissl granules, and pyknotic or shrunken nuclei abnormally skewed to the edge of the cell body (Cragg, 1970; Moon, 2018). Chromatolysis, which is linked to neuronal stress and often leads to apoptosis (Cragg, 1970), has been observed in AD and other neurodegenerative diseases (Cataldo et al., 1994; Riancho et al., 2014; Sil et al., 2014; Moon, 2018).

Reduction of LSD1 exacerbates PS19 Tau neurodegeneration

In addition to accelerating the paralysis phenotype, reducing the level of *Lsd1* in PS19 Tau mice exacerbated neuronal cell death in the brain. At 6 months and 8 months, we observed no difference between genotypes in the overall morphology in the hippocampus (Fig. S4 A-H) based on histological analysis. There was also no difference between $Lsd1^{+/+}$ and $Lsd1^{-/+}$ mice at 10 months or 12 months (Fig. 3.3A,B; Fig. S4 I,J,M,N; Fig. S5 A,B,E,F,I,J,M,N). At 10 months, PS19 Tau mice had very little cell loss in the hippocampus compared to $Lsd1^{+/+}$ and $Lsd1^{-/+}$ control mice (Fig. S4 I-K, M-O). In contrast, at 10 months, PS19;$Lsd1^{-/+}$ mice had dramatic cell loss both in the CA1 region of the hippocampus and throughout the posterior hippocampus (Fig. S4 L,P). At 12 months, the PS19 Tau mice had a slight decrease in CA1 and CA3 neurons spanning the hippocampal pyramidal cell layer compared to $Lsd1^{+/+}$ control mice (17% and 19.4% respectively, Fig. 3.3A,B; Fig. S5 A-C, E-G). In comparison, PS19;$Lsd1^{-/+}$ mice had a 52% and 54% decrease in the CA1 and CA3 respectively (Fig. 3.3A,B; Fig. S5 D,H) compared to $Lsd1^{+/+}$ control mice. This resulted in decreased overall brain size (Fig. 3.3C) and brain weight (Fig. 3.3D) in PS19;$Lsd1^{-/+}$ mice compared to PS19 Tau and $Lsd1^{-/+}$ mouse littermates. Additionally, at 12 months there were increased levels of cell loss in the Dentate Gyrus (Fig. S5 I-L), and throughout the posterior hippocampus (Fig. S5 M-P).

Along with the histology, we monitored the progression of neuronal cell death in the same individual over time by performing magnetic resonance imaging (MRI) at 6 months and again at 10 months (Movie S2). At 6 months, there was no sign of cell loss or ventricular dilatation in *Lsd1*$^{-/+}$, PS19 Tau, or PS19;*Lsd1*$^{-/+}$ mice (Fig. 3.3E-G). However, at 10 months the MRI showed that there was dramatic ventricular dilatation in PS19;*Lsd1*$^{-/+}$ mice, as evidenced by high-intensity areas in T2- weighted imaging, with substantial hippocampal and neocortical atrophy (Fig. 3.3J vs. 3H, Movie S2). At this timepoint, PS19 Tau mice had some ventricular dilatation and hippocampal atrophy throughout the hippocampus (Fig. 3.3I), but much less than PS19;*Lsd1*$^{-/+}$ mice (Fig. 3.3J, Movie S2. 0:51sec vs. 1:00sec).

Tau pathology is not affected by change in LSD1 levels

Since LSD1 is a chromatin regulator, it is possible that reducing LSD1 protein levels affects the PS19 Tau transgene. However, we confirmed that there was no difference between PS19 Tau mice and PS19;*Lsd1*$^{-/+}$ mice in the endogenous mouse *Mapt* RNA expression, nor in the human P301S MAPT transgene expression (Fig. S6 A). It is also possible that LSD1 affects tau pathology. To test this, we performed immunohistochemistry staining for a hyperphosphorylated form of tau (AT8). As expected, we did not observe any AT8 positive staining in *Lsd1*$^{-/+}$ at 6, 8, or 10 months (Fig. S6 B,E,H). Additionally, we observed very little AT8 positive immunoreactivity at 6 months in both PS19 Tau or PS19;*Lsd1*$^{-/+}$ mice (Fig. S6 C,D). At 8 months both PS19 Tau and PS19;*Lsd1*$^{-/+}$ mice had low but consistent levels of AT8 positive immunoreactivity (Fig. S6 F,G), and by 10 months both PS19 Tau and PS19;*Lsd1*$^{-/+}$ mice developed the same high level of AT8 positive tau immunoreactivity (Fig. S6 I,J). This was consistent throughout both the CA1 and CA3 regions of the hippocampus and the cerebral cortex (Fig. S6 K-M). We also did not observe any difference between PS19 Tau mice and PS19;*Lsd1*$^{-/+}$

mice when assaying PHF1 (an alternative phospho-tau antibody) immunoreactivity in the CA1 region of the hippocampus at 8 months (Fig. S7 A-C, G) and 10 months (Fig. S7 D-F, G), nor in the CA3 region of the hippocampus or the cerebral cortex at 8 and 10 months (Fig. S7 H,I).

The functional interaction between tau pathology and LSD1 inhibition is specific

To test the specificity of the functional interaction between tau pathology and LSD1, we investigated the overlap in the effected molecular pathways associated with both pathological tau and *Lsd1* heterozygosity. To address this, we performed RNA sequencing on the hippocampus of 9 month *Lsd1*$^{+/+}$, *Lsd1*$^{-/+}$, PS19 Tau, and PS19;*Lsd1*$^{-/+}$ littermates. As opposed to analyzing transcriptional changes at the terminal stage of disease, this time point allows us to assess molecular changes prior to the onset of neuronal cell death. This is also the time point that we observed the earliest signs of exacerbation of paralysis in PS19;*Lsd1*$^{-/+}$ mice. Because of this early stage in the progression of the disease, we would not expect dramatic changes in transcription overall. Nevertheless, if tau pathology is inhibiting LSD1 function, we would expect that the genome-wide expression changes induced by tau might be exacerbated by a reduction in LSD1. The RNA-seq analysis detected 54 significant gene expression changes in PS19 Tau mice compared to *Lsd1*$^{+/+}$ (Fig S8 A,B), and 271 significant gene expression changes in PS19;*Lsd1*$^{-/+}$ mice compared to *Lsd1*$^{+/+}$ (Fig S8 C,D). Importantly, *Lsd1*$^{-/+}$ mice had only 4 gene expression changes observed genome-wide (Fig. S8 E,F), indicating that the partially reduced level of LSD1 expression had very little effect on transcription on its own. This is consistent with the lack of phenotype in these animals.

We first examined the relationship between tau-induced expression changes and the effects of *Lsd1* heterozygosity by comparing the transcriptional changes observed in PS19 Tau mice with PS19;*Lsd1*$^{-/+}$ mice. In PS19 Tau mice that do not yet have significant

neurodegeneration, we identified 54 genes (36 up and 18 down) that were differentially expressed. Of these 54 genes, 50 were changed in the same direction in PS19;*Lsd1*$^{-/+}$ mice (93%). In addition, amongst the 50 genes changed in the same direction, 36 (72%) had exacerbated expression in PS19;*Lsd1*$^{-/+}$ mice compared to PS19 Tau mice (Fig. 3.4A). Based on this overlap, we further compared the expression changes between PS19 Tau mice and PS19;*Lsd1*$^{-/+}$ mice genome-wide. Amongst the transcripts that were changed in both PS19 Tau mice and PS19;*Lsd1*$^{-/+}$ mice compared to *Lsd1*$^{+/+}$ mice, 71% changed in the same direction (either up or down). Consistent with this overlap in gene expression, Gene Set Enrichment Analysis demonstrated that the pathways that are affected in both PS19 Tau mice and PS19;*Lsd1*$^{-/+}$ mice are very similar (Fig. S8 G-J). However, the genes affected in both sets of mice tended to be further exacerbated in PS19;*Lsd1*$^{-/+}$ mice compared to PS19 Tau mice. Amongst the 71% of genes that changed in the same direction in both PS19 Tau mice and PS19;*Lsd1*$^{-/+}$ mice, 76% of these transcripts had a higher fold-change in PS19;*Lsd1*$^{-/+}$ mice compared to PS19 Tau mice (Fig. 3.4B).

Overexpression of LSD1 rescues neurodegeneration in the hippocampus of PS19 Tau mice

Our data demonstrate that reduction of LSD1 protein exacerbates the tauopathy phenotype in PS19 Tau mice. Based on this, we considered the possibility that overexpression of LSD1 might counter the loss of LSD1 from the nucleus and protect against neurodegeneration in PS19 Tau mice. To address this possibility, we injected PS19 Tau mice with a neuronal specific virus (AAV-DJ driven by the synapsin promoter) expressing either the full length LSD1 protein with an N-terminal HA tag (hereafter referred to as PS19- LSD1 inj) or a control virus expressing only the HA tag (hereafter referred to as PS19- HA inj). Additionally, to control for the effects of viral injection, we injected Wild Type littermates with the HA only expressing virus (hereafter

referred to as WT- HA inj). All injections were performed directly into the hippocampus at 8-8.5 months, when tau pathology is already present throughout the nervous system. Immunolabeling for the HA tag demonstrated that the virus is specific to NeuN+ neurons (Fig. S9 A-D), with no HA expression observed in IBA+ microglia (Fig. S9 E-H), or GFAP+ astrocytes (Fig. S9 I-L). It also confirmed that virally expressed LSD1 is nuclear (Fig. S9 M) and confined to the hippocampus (Fig. S9 N). After 3 months of overexpression, 11-11.5 month old mice were euthanized, and the brains were analyzed. Injections resulted in a ~6-fold increase in expression of LSD1 in the hippocampus compared to endogenous LSD1 in the PS19- HA inj mice, but no increase in the cerebellum (Fig. S9 O,P). As expected, because the viral injections were restricted to the hippocampus, the mice injected with LSD1 still developed paralysis (Movie S3). This confirms that the tau transgene is expressed and functioning. Additionally, we did not observe a difference in total levels of AT8 positive tau immunoreactivity (Fig. S9 Q-T). Therefore, any modulation to the phenotype was not due to changes in tau pathology.

Injected mice were evaluated for cell death by neuronal cell counts in the hippocampus. Injection of LSD1 virus into the hippocampus of PS19 Tau mice rescued the neurodegeneration phenotype. At 11 months, compared to WT-HA inj control mice, 70% of the PS19-HA inj mice had hippocampal cell counts that were below the lowest WT-HA inj control, while none of the Tau mice injected with the LSD1 virus were below this level. Overall, we observed significantly more neurons (P-value <0.05) spanning the pyramidal cell layer (84% of WT- HA inj CA1 counts) compared to their PS19- HA inj littermates (59% of WT- HA inj CA1 counts), such that overall the neuronal cell count in PS19- LSD1 inj mice was not statistically different from the WT- HA inj (Fig. 3.5A-D). Additionally, in the histological analysis we observed a large number of cells infiltrating the hippocampus in PS19- HA inj mice compared to WT- HA inj littermates

(Fig. 3.5B vs. 3.5C). Marker analysis demonstrated that this was due to a strong inflammatory response, with a large increase in the number of GFAP+ astrocytes (Fig. S10 A-C vs. D-F) and TRL2+ activated microglia (Fig. S10 J-L vs. M-O, S-V vs. W,Z, EE). Injection of PS19 Tau mice with LSD1 virus rescued this inflammatory response. For example, all but one (9 out of 10 analyzed) of the PS19- LSD1 inj mice had a reduction in the number of GFAP+ astrocytes (Fig. S10 G-I vs. D-F) and TRL2+ activated microglia (Fig. S10 P-R vs. M-O, AA-DD vs. W-Z, EE). Of note, the one PS19- LSD1 inj mouse where we did observe increased glial cells, similar to PS19- HA inj mice, had the lowest neuronal cell count (74% of WT- HA inj CA1 neurons). It is possible that this mouse was already undergoing neurodegeneration prior to the injection of the LSD1 overexpression virus.

Although the number of hippocampal neurons in PS19- LSD1 inj mice did not differ from WT- HA inj controls, in 6 of the 10 PS19- LSD1 inj mice we observed cells with abnormal blebbed nuclei at varying numbers throughout the hippocampus (Fig. 3.5E). These abnormal cells are rare in PS19- HA inj mice, which have a reduced overall number of cells in the pyramidal cell layer compared to WT- HA inj control mice. One possibility is that these abnormal cells with blebbing nuclei represent an intermediate state between a healthy neuron and a dying neuron that is prolonged by rescue via LSD1 overexpression. Interestingly, these abnormal cells also differed in the localization of HA-tagged LSD1. The four mice with normal nuclei had HA-tagged LSD1 protein localized uniformly throughout the nucleus (Fig. 3.5F). In contrast, the six mice with abnormal nuclear blebbing had some HA-tagged LSD1 that was mislocalized to the cytoplasm (Fig. 3.5G). This includes the one PS19- LSD1 inj mouse that had an elevated number of astrocytes and TRL2 positive microglia. Thus, the blebbing state

correlates with when the viral produced LSD1 begins to be sequestered in the cytoplasm, similar to the endogenously produced LSD1.

DISCUSSION

In this study we investigate a potential downstream mediator of tau pathology in neurodegenerative disease. We find that modulation of the chromatin modifying enzyme LSD1 can alter neurodegeneration in a tauopathy mouse model. Previously, we showed that LSD1 colocalizes with tau pathology in the cell body of neurons in AD cases (Christopher et al., 2017). This suggested that LSD1 might be disrupted in tauopathies such as AD, by being excluded from the nucleus. To address this directly, we utilize the PS19 tauopathy mouse model. In these mice, we find that LSD1 is sequestered in the cytoplasm, in some cases being completely depleted from the nucleus. This provides the first cytological evidence that pathological tau can prevent LSD1 from properly localizing to the nucleus in hippocampal and cortical neurons, where we have previously shown it is continuously required.

Based on the ability of pathological tau to sequester LSD1, we hypothesized that neuronal cell death may be due, at least partly, to LSD1 being sequestered in the cytoplasm and depleted from the nucleus. In this case, reducing LSD1 levels should make it easier for tau to deplete LSD1 from the nucleus, resulting in a faster progression of neurodegeneration and/or a more severe neurodegenerative phenotype. Importantly, LSD1 heterozygosity alone induces only 4 significant gene expression changes and does not lead to any neurodegeneration. This suggests that any effects observed in PS19;*Lsd1*$^{-/+}$ mice are not simply due to LSD1 haploinsufficiency. Normally, PS19 Tau mice develop paralysis and neurodegeneration, along with reduced survival. In contrast, when we reduce LSD1 in the PS19 Tau mice, PS19;*Lsd1*$^{-/+}$ mice die significantly

earlier, most likely due to the increased rate of paralysis. Additionally, PS19;*Lsd1*$^{-/+}$ mice have increased neuronal cell death and clearance in the hippocampus. This suggests that pathological tau functions through LSD1 to cause neurodegeneration *in vivo* in mice.

PS19;*Lsd1*$^{-/+}$ mice have a 31% reduction in LSD1 protein levels compared to PS19 Tau mice from birth. This reduction should theoretically make mice sensitive to LSD1 depletion at any time. However, tau pathology starts at 6-8 months in PS19 Tau mice. As a result, if *Lsd1* heterozygosity is functioning by making it easier for pathological tau to deplete LSD1 from the nucleus, we would not expect to see any exacerbation until after pathological tau is present. The exacerbation of the PS19 Tau mouse neurodegenerative phenotype does not occur until after pathological human tau was present. This suggests that the effect of *Lsd1* heterozygosity requires the presence of pathological tau, placing LSD1 downstream of tau. Consistent with LSD1 being downstream of pathological tau, we found no evidence that *Lsd1* heterozygosity affects the expression of the tau transgene, or the buildup of pathological tau in PS19 Tau mice.

To test whether the functional interaction between pathological tau and reduced LSD1 is specific, we used RNA-seq to determine whether the downstream molecular pathways altered in PS19 Tau mice are exacerbated in PS19;*Lsd1*$^{-/+}$ mice. This analysis was performed at the time of earliest signs of neuronal distress, allowing us to assess molecular changes prior to cell death and clearance. LSD1 heterozygosity induces only 4 significant expression changes. In addition, the pathways are affected in both PS19 Tau mice and PS19;*Lsd1*$^{-/+}$ mice are very similar. This suggests that reducing LSD1 did not induce any additional neurodegeneration pathways. In contrast, when LSD1 is reduced in PS19 Tau mice, the genome-wide expression changes induced by pathological tau are specifically exacerbated. This suggests that the functional

interaction that we observe between pathological tau and reduced LSD1 is occurring through the tau pathway.

Our previous data implicated LSD1 in the tau-mediated neurodegeneration pathway. Utilizing the PS19 Tau mouse model, we now show a functional interaction between pathological tau and LSD1. Importantly, because PS19 Tau mice do not have Aβ plaque accumulation, this functional interaction is specific to tau. Based on these data we propose the following model (Movie S4): in healthy hippocampal and cortical neurons, LSD1 is translated in the cytoplasm and transported into the nucleus where it is continuously required to repress inappropriate transcription. In tauopathy, pathological tau accumulates in the cytoplasm blocking LSD1 from nuclear import. This interferes with the continuous requirement for LSD1, resulting in neuronal cell death. Recently, it has been observed that the nuclear pore breaks down in AD (Sheffield et al., 2006; Frost et al., 2016; Eftekharzadeh et al., 2018). It should be noted that this mechanism would potentially exacerbate the model that we propose.

This model makes a direct prediction: if tau is predominantly functioning through LSD1, then increasing the levels of LSD1 should rescue the tau-induced neurodegenerative phenotype. To address this, we overexpressed LSD1 in the hippocampal neurons of PS19 Tau mice. Overexpression of LSD1 specifically in hippocampal neurons rescues the neuronal cell death and limits the inflammatory response. This rescue is neuronal specific, suggesting that the functional interaction between LSD1 and tau is occurring in neurons. In addition, this rescue occurs despite there being no effect on tau aggregation. This negates the possibility that the tau transgene is simply not functioning when LSD1 is overexpressed. The ability of LSD1 overexpression to overcome tau-mediated neurodegeneration in the presence of pathological tau aggregates, provides further evidence that pathological tau is functioning through the inhibition of LSD1.

Importantly, overexpressing LSD1 should not prevent it from being sequestered. Rather overexpressing LSD1 should make it more difficult for pathological tau to sequester all of the LSD1 protein, allowing some LSD1 to be transported to the nucleus. Thus, overexpressing LSD1 would be expected to temporarily rescue the ability of pathological tau to kill neurons. Consistent with this, LSD1 overexpression delays the effect of pathological tau rather than permanently rescuing. In 60% of the mice, the surviving neurons have abnormal morphology, and the overexpressed version of LSD1 is also sequestered. observation that neurons fail to maintain their morphology when the overexpressed LSD1 begins to be sequestered in the cytoplasm provides further support for the model that tau mediates neurodegeneration through the sequestration of LSD1. Nevertheless, our data suggest that overexpression of LSD1 cannot permanently overcome pathological tau. To permanently overcome pathological tau, it would likely be necessary to permanently disrupt the interaction between pathological tau and LSD1. This work is currently ongoing in the lab. Overall, our data establish LSD1 as a major downstream effector of tau-mediated neurodegeneration. Based on these data, we propose that the LSD1 pathway is a potential late stage target for intervention in tauopathies, such as AD.

FIGURES

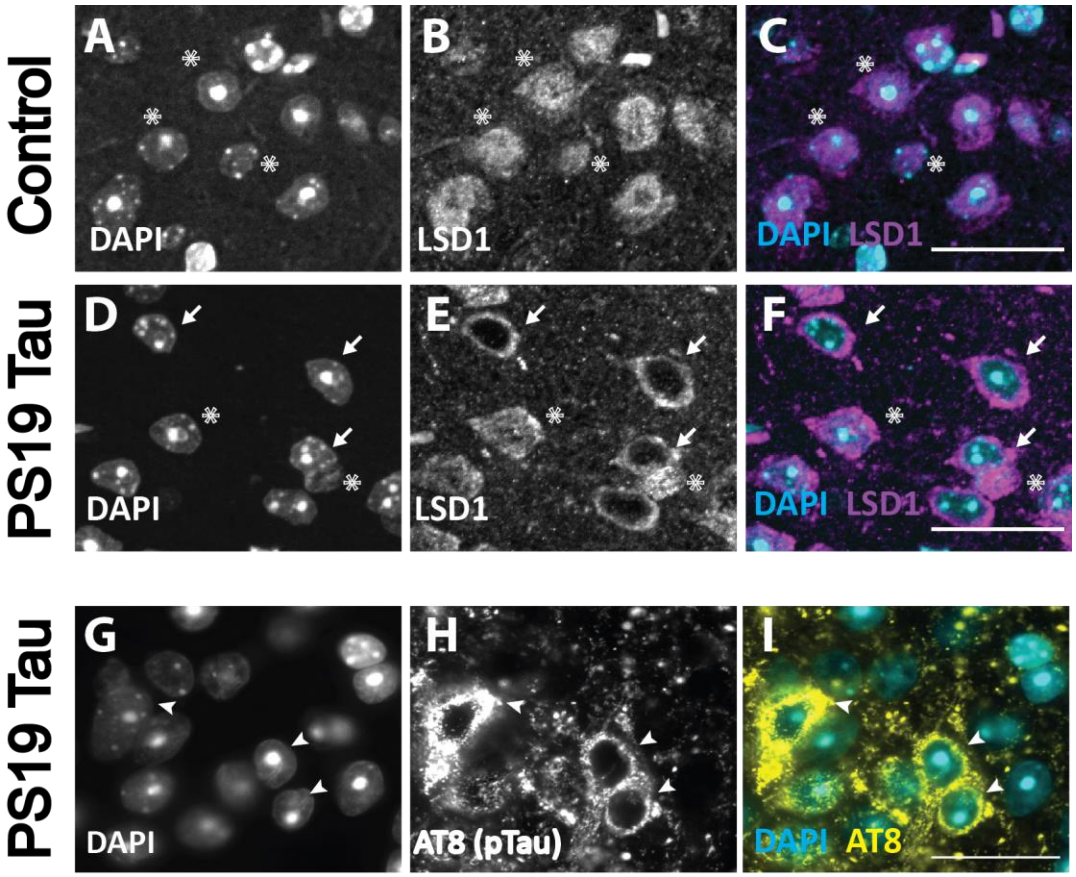

Fig. 3.1 | LSD1 sequestration and tau accumulation in PS19 Tau mice. A-C, Representative immunofluorescence of 12 month old control Wild Type mice showing DAPI (**A**), LSD1 (**B**), and merged (**C**) in the cerebral cortex where LSD1 is localized specifically to DAPI positive nuclei. **D-F**, Representative image of the cerebral cortex in 12 month old PS19 Tau mice. Staining for DAPI (**D**), LSD1 (**E**), and merged (**F**) shows that LSD1 is localized outside the nucleus, and depleted from the DAPI positive nucleus. Arrows denote cells where LSD1 is localized outside of the nucleus, and asterisks denote LSD1 localized specifically to the nucleus. **G-I,** Representative immunofluorescence of 12 month old PS19 Tau mouse with staining for DAPI (**G**), AT8 positive hyper-phosphorylated tau (**H**) and merge (**I**) where hyper-phosphorylated tau accumulates in the cytoplasm of the cell body. Arrowheads denote hyper-phosphorylated tau. Scale bars=25μm.

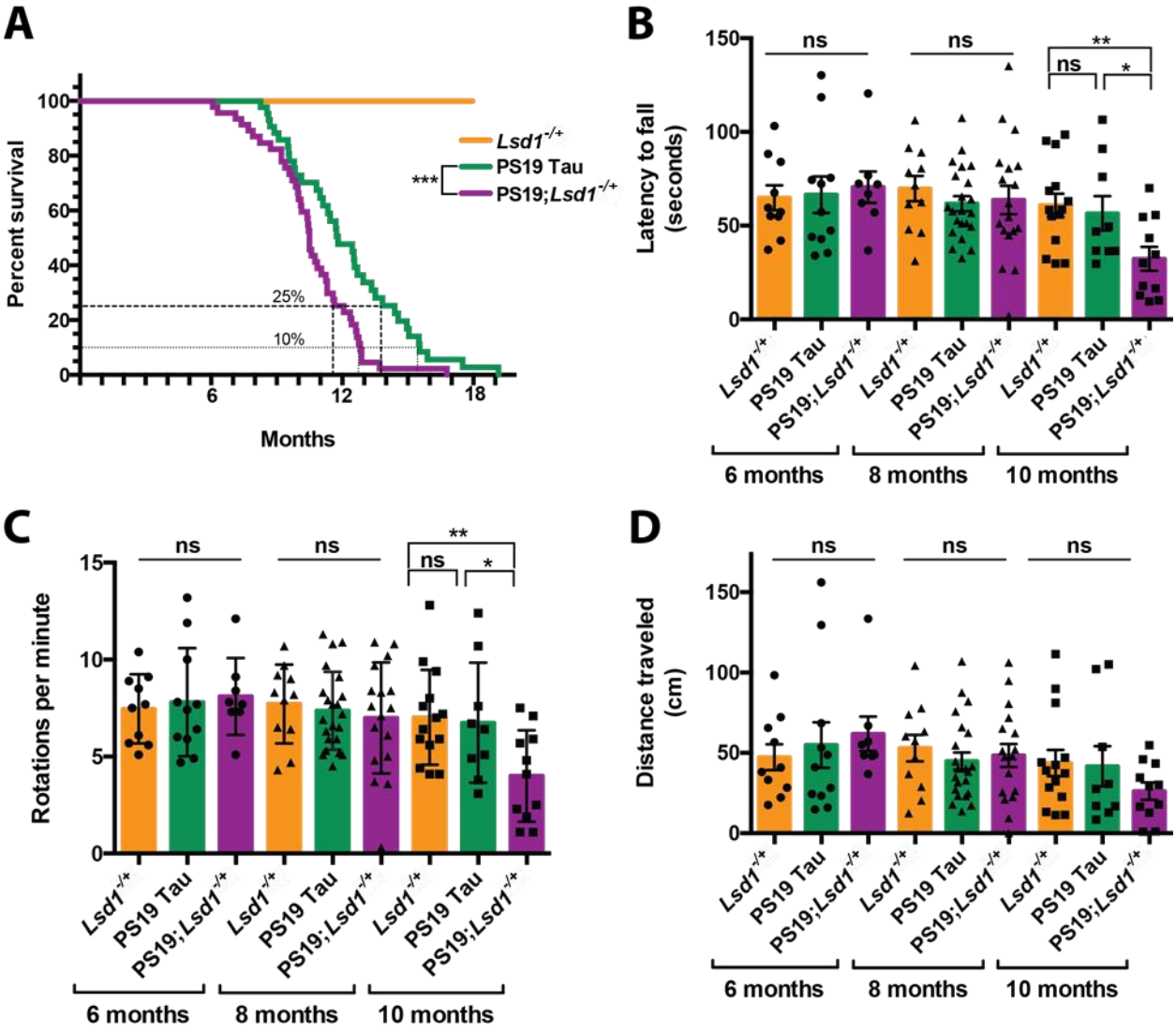

Fig. 3.2 | Reduction of *Lsd1* exacerbates the PS19 Tau mouse paralysis phenotype. A, Lifespan curve showing that no *Lsd1*$^{-/+}$ mice died before 18 months (orange, *n*=20). PS19;*Lsd1*$^{-/+}$ mice (purple, *n*=44) have a significant reduction in survival compared to PS19 Tau mice with wild-type levels of *Lsd1* (green, *n*=37)(Log-rank Mantle-Cox test ***P<0.005). **B-D**, Rotarod testing of latency to fall (in seconds) (**B**), rotations per minute (when the mouse fell) (**C**), and distance traveled (in centimeters) (**D**) for mice at age 6, 8 and 10 months. *Lsd1*$^{-/+}$ (orange, *n*=10,11,14), PS19 Tau (green, *n*=11,22,9), and PS19;*Lsd1*$^{-/+}$ (purple, *n*=8,17,11). Values are

mean ± SEM (two-way analysis of variance (ANOVA) with Tukey's post hoc test *P<0.05 **P<0.01, ns=not significant).

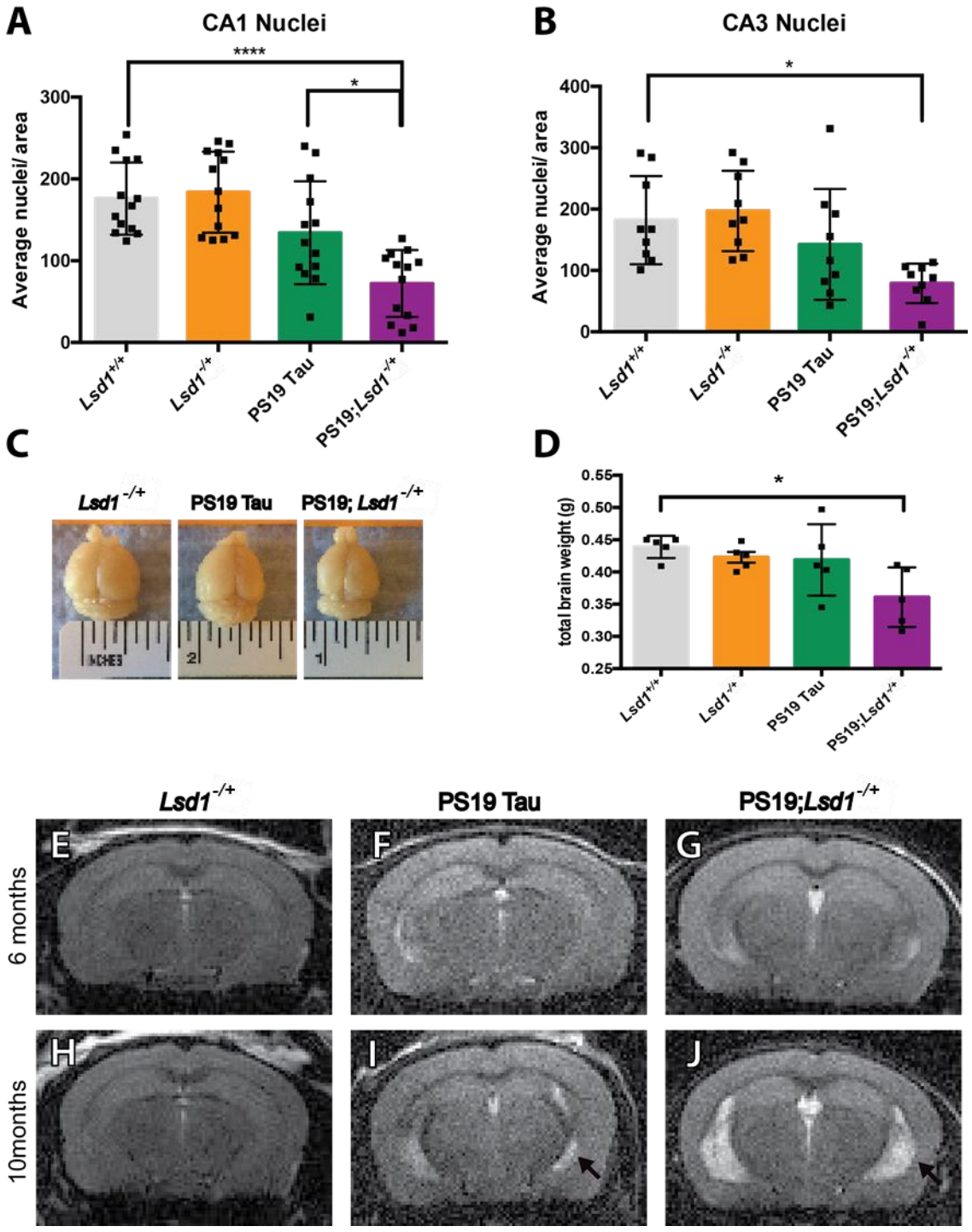

Fig. 3.3 | Reduction of *Lsd1* exacerbates neurodegeneration in PS19 Tau mice. A,B, Average nuclei per area in the CA1 (**A**) and CA3 (**B**) regions of the hippocampus in 12 month old *Lsd1*$^{+/+}$, *Lsd1*$^{-/+}$, PS19 Tau, and PS19;*Lsd1*$^{-/+}$ mice. Quantification from histology represented in **Fig. S5 A-H**. Values are mean ± SD (**A**, *n*=13 & **B,** *n*=9). **C,** Representative image of the brains of 12 month old *Lsd1*$^{-/+}$, PS19 Tau, and PS19;*Lsd1*$^{-/+}$ littermates. **D,** Total brain weight of 12 month old littermates represented in **Fig. 3.3C.** Values are mean ± SD (*n*=5). For all graphs: one-way analysis of variance (ANOVA) with Tukey's post hoc test (two-sided) *P<0.05,****P<0.001. **E-J,** Representative image of T2- weighted RARE coronal MRI taken from 6 months (**E-G**) and 10 months (**H-jJ**) of age in *Lsd1*$^{-/+}$ (**E,H**), PS19 (**F,J**), and PS19;*Lsd1*$^{-/+}$ (**G,J**) mice (*n*=3). Arrow denotes region of hippocampal atrophy.

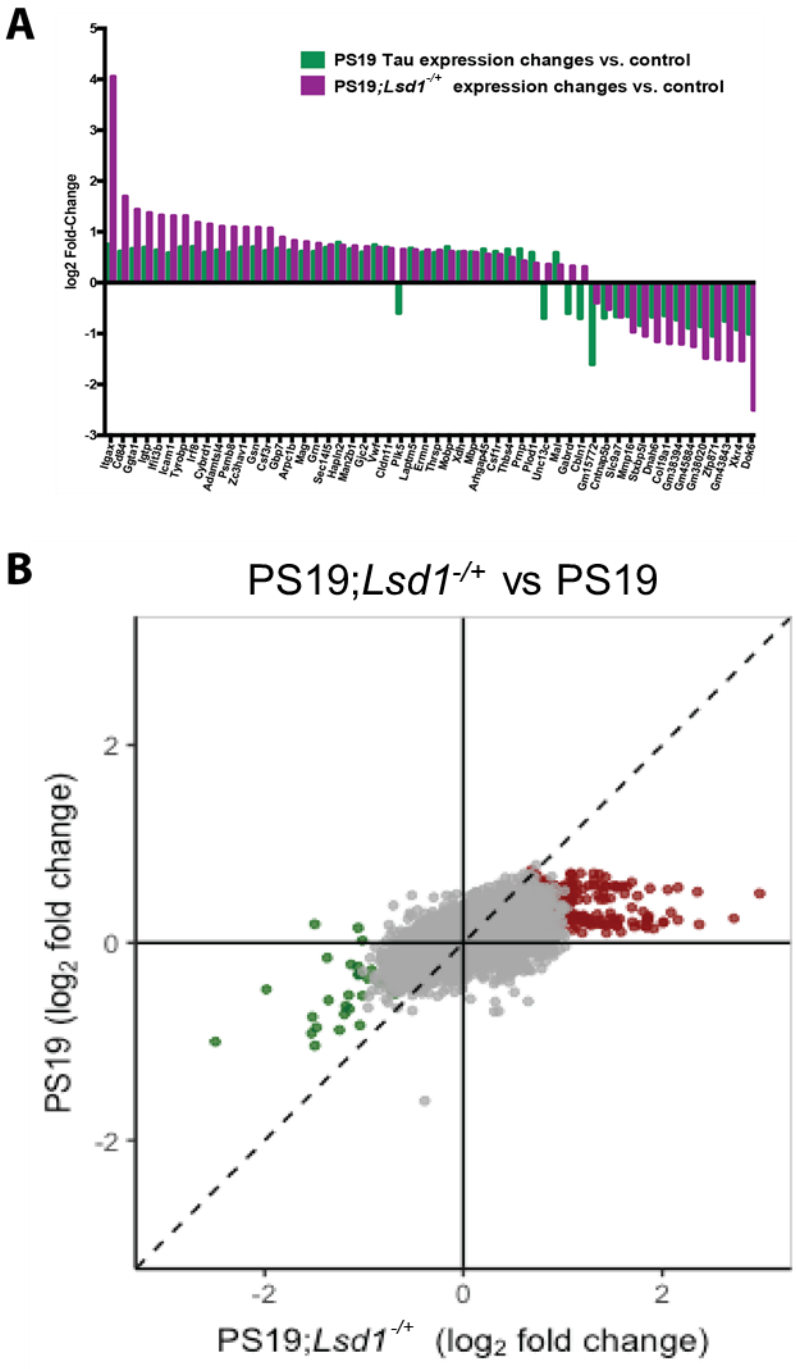

Fig. 3.4 | Molecular overlap between loss of LSD1 function and tauopathy. A, Histogram (log_2 fold change) of the 54 genes that have significant changes in expression in the PS19 Tau mouse (green) and their corresponding expression changes in the PS19;*Lsd1*$^{-/+}$ mouse (purple). **B,** Scatter plot showing the correlation between the genome-wide log_2 fold change in gene

expression between PS19 Tau and PS19;*Lsd1*$^{-/+}$. The most significantly changed genes in PS19;*Lsd1*$^{-/+}$ mouse are shown in red (upregulated) and green (downregulated). All other genes are shown in grey. Dotted line represents 1:1 relationship between gene expression changes in PS19 Tau vs. PS19;*Lsd1*$^{-/+}$. Exacerbated genes fall to the right of the dotted line in the positively correlated quadrant and to the left of the dotted line in the negatively correlated quadrant. Genes with correlated expression changes are found in the top right and bottom left quadrants, while genes that do not correlate are found in the opposite quadrants.

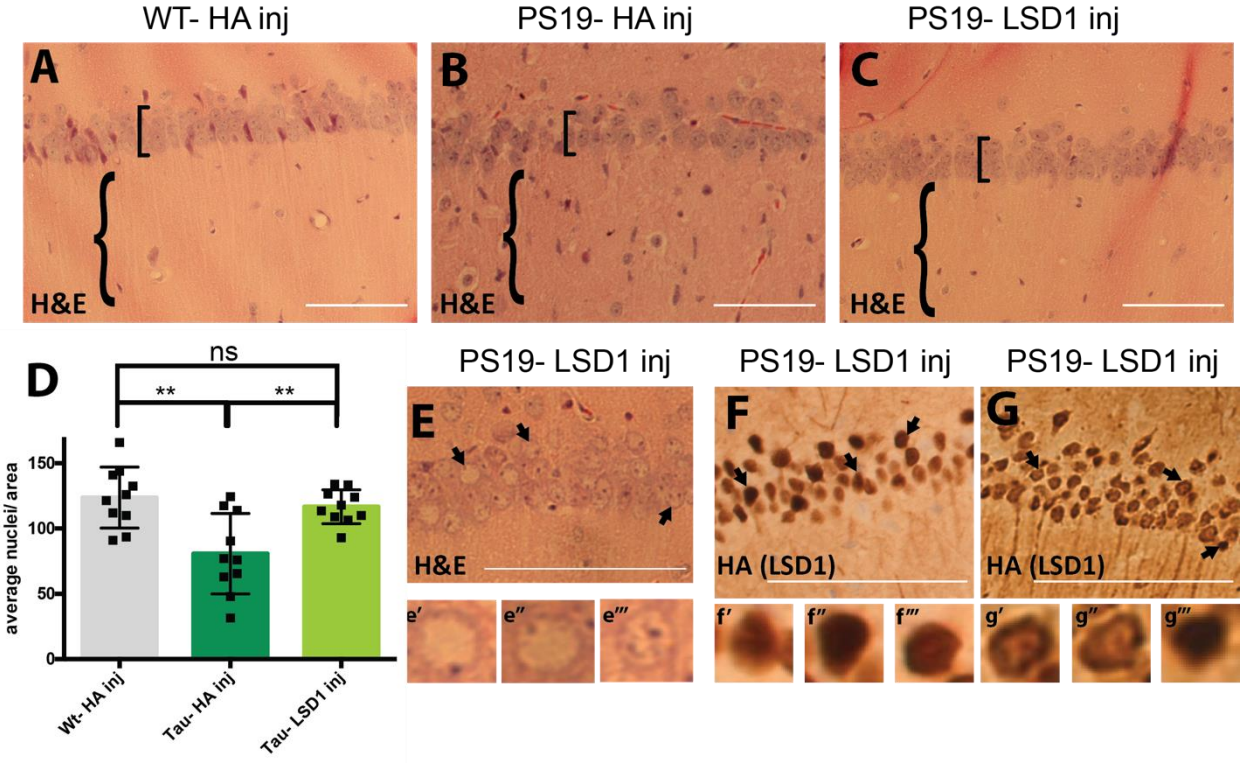

Fig. 3.5 | LSD1 overexpression rescues the neurodegenerative phenotype in the hippocampus of 11 month old PS19 Tau mice. A-C, Representative image of H&E stained CA1 region of the hippocampus of 11 month old Wild Type mice injected with HA control virus (WT- HA inj) (**A**), PS19 Tau mice injected with HA control virus (PS19- HA inj) (**B**), and PS19

Tau mice injected with *Lsd1* overexpressing virus (PS19- LSD1 inj) (**C**). Square brackets denote thickness of pyramidal layer of the CA1 of the hippocampus and curvy brackets denote hippocampal region with or without infiltrating cells. **D,** Quantification of the average number of nuclei in the pyramidal layer of the hippocampus per area per mouse from histology represented in **Fig. 3.5A-C**. Values are mean ± SD (*n*=10, one-way analysis of variance (ANOVA) with Tukey's post hoc test, **p<0.01, ns=not significant). **E,** Representative H&E of PS19- LSD1 inj mouse with abnormal nuclei blebbing in the CA1 region of the hippocampus. **E'-E''',** High magnified image of cells denoted by arrows in **Fig. 3.5E** of individual nuclei that are either abnormally blebbed (**E', E"**) or normal (**E'''**). **F,G,** Immunohistochemistry staining of HA(LSD1) in 11 month PS19- LSD1 inj mice. HA is either localized specifically to the nucleus in all nuclei (**F**) or in only a few nuclei while it is partially sequestered in the cytoplasm in others (**G**). **F'-F''',** High magnified image of cells denoted by arrows in **Fig. 3.5F** of nuclear HA localization in individual nuclei. **G'-G''',** High magnified image of cells denoted by arrows in **Fig. 3.5G** of individual nuclei with HA(LSD1) either sequestered to the cytoplasm (**G', G"**) or confined to the nucleus (**G'''**). Scale bars=50μm.

SUPPLEMENTAL DATA

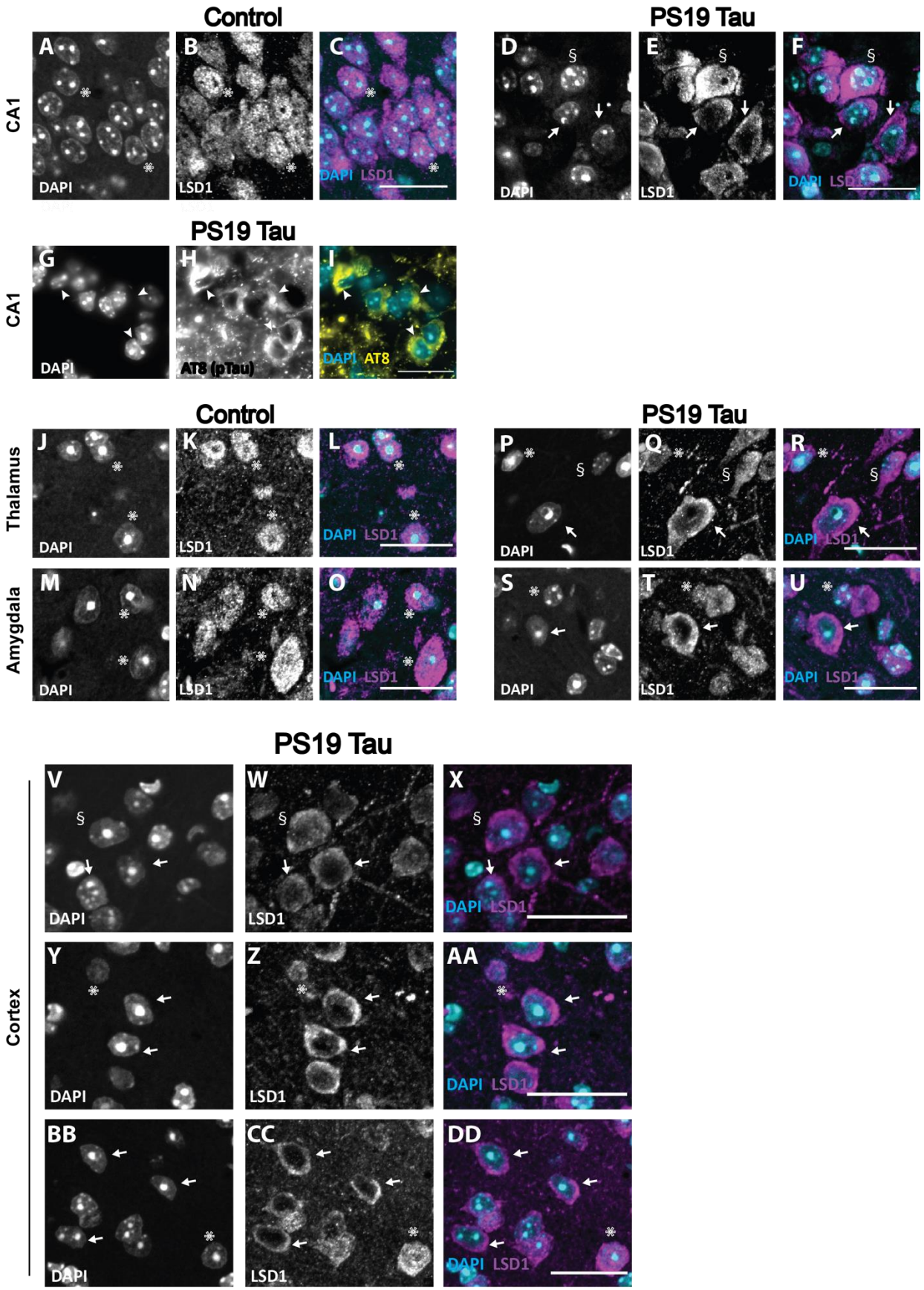
Control
PS19 Tau
CA1
A
B
C
D
E
F
DAPI
LSD1
DAPI LSD1
§
PS19 Tau
CA1
G
H
I
DAPI
AT8 (pTau)
DAPI AT8
Control
PS19 Tau
Thalamus
Amygdala
J
K
L
P
Q
R
M
N
O
S
T
U
PS19 Tau
Cortex
V
W
X
Y
Z
AA
BB
CC
DD

Fig. S1: Sequestration of LSD1 in PS19 Tau mice. A-F, Representative immunofluorescence showing DAPI (**A,D**), LSD1 (**B,E**), and merged (**C,F**) images in the CA1 region of the hippocampus in 12 month old Wild Type (**A-C**) and PS19 mice (**D-F**). **G-I**, Representative immunofluorescence showing DAPI (**G**), AT8 positive hyper-phosphorylated tau (**H**), and merged (**I**) in the CA1 region of the hippocampus of 12 month old PS19 Tau mice showing hyper-phosphorylated tau accumulation in the cytoplasm of the cell bodies. Arrowheads denote hyper-phosphorylated tau. **J-U,** Representative immunofluorescence showing DAPI (**J,M,P,S**), LSD1 (**K,N,Q,T**), and merged (**L,O,R,U**) images in the thalamus (**J-L,P-R**) and amygdala (**M-O,S-U**). In 12 month old control Wild Type mice (**J-O**), LSD1 is localized specifically to the DAPI positive nuclei, but in 12 month old PS19 Tau mice (**P-U**) LSD1 is localized outside of the nucleus. **V-DD,** Additional examples of immunofluorescence showing DAPI (**V,Y,BB**), LSD1 (**W,Z,CC**), and merged (**X,AA,DD**) of the cerebral cortex of 12 month old PS19 Tau mice. Arrows denote cells where LSD1 is localized outside of the nucleus, asterisks denote LSD1 localized specifically to the nucleus, and § denotes cells where LSD1 is both nuclear and cytoplasmic. *n*=7 mice analyzed (images representative of 6 of the 7 mice analyzed). Scale bars=25μm.

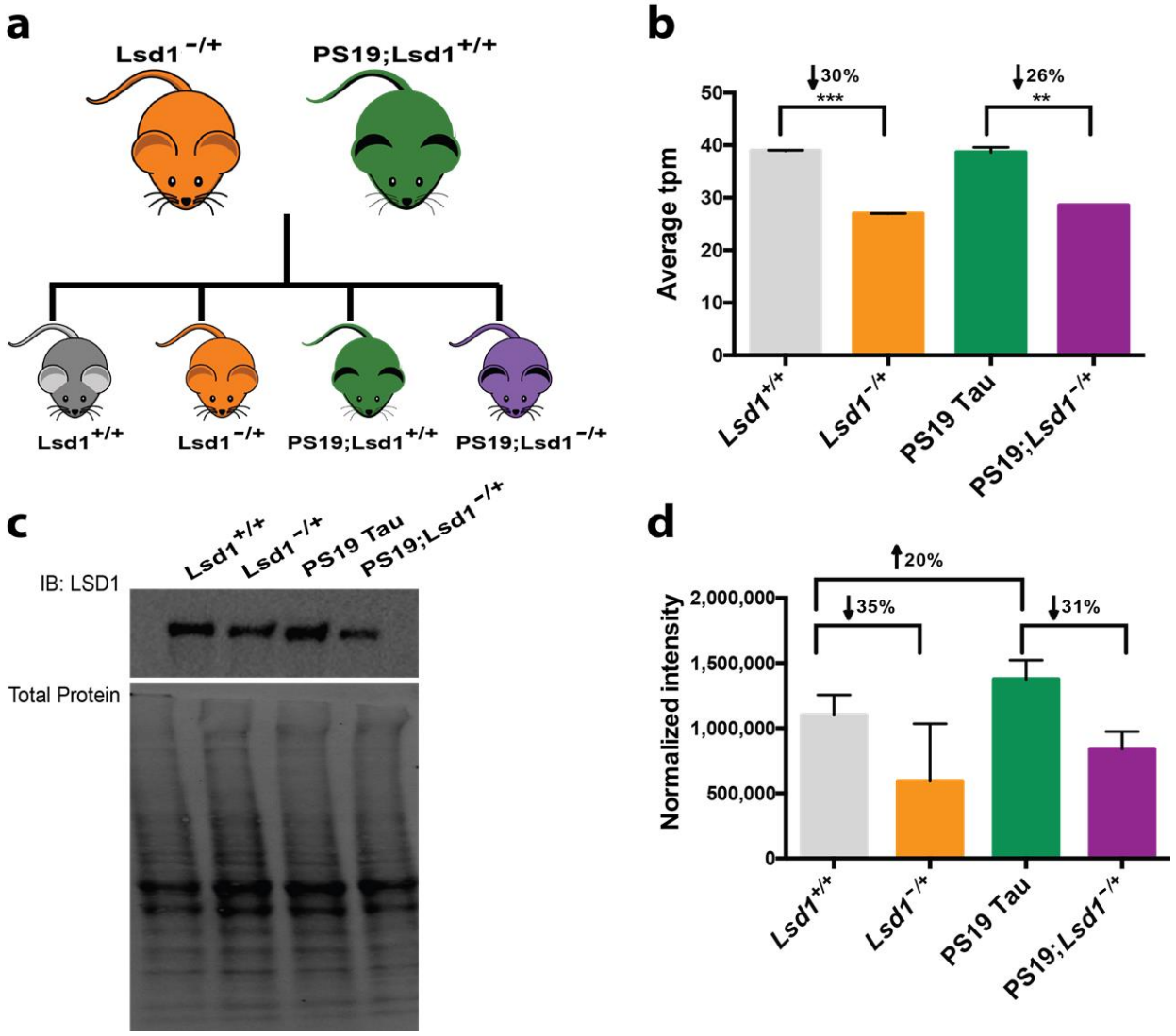

Fig. S2: Generation of PS19 Tau mice with reduced levels of LSD1. a, PS19 Tau mice carrying the P301S human tau transgene that are wild-type for *Lsd1* were crossed with *Lsd1* heterozygous mice. These crosses generated four genotypes: Wild Type mice ($Lsd1^{+/+}$, grey), *Lsd1* heterozygous mice ($Lsd1^{-/+}$, orange), PS19 Tau mice that are wild-type for *Lsd1* (PS19;$Lsd1^{+/+}$ referred to as PS19 Tau, green), and PS19 Tau mice that are heterozygous for *Lsd1* (PS19;$Lsd1^{-/+}$, purple). Colors designated here are maintained throughout all figures. **b,** Average transcripts per million (tpm) from RNA-sequencing of *Lsd1* expression in the hippocampus of $Lsd1^{+/+}$, $Lsd1^{-/+}$, PS19 Tau, and PS19;$Lsd1^{-/+}$ mice. $Lsd1^{-/+}$ mice had a 30%

reduction in expression compared to *Lsd1*$^{+/+}$ mice, and PS19;*Lsd1*$^{-/+}$ had a 26% reduction in expression compared to PS19 Tau mice. Values are mean ± SD (*n*=2, one-way analysis of variance (ANOVA) **P<0.01, ***P<0.005). **c,** Representative image of protein levels in the brain of *Lsd1*$^{+/+}$, *Lsd1*$^{-/+}$, PS19 Tau, and PS19;*Lsd1*$^{-/+}$ mice from LSD1 immunoblot and corresponding total protein blot. **d,** Quantification of immunoblot for LSD1 normalized to total protein loaded per sample as represented in **Extended Data Fig. 2c**. Compared to *Lsd1*$^{+/+}$ mice, *Lsd1*$^{-/+}$ mice had a 35% reduction and PS19 Tau mice had 20% increase in LSD1 protein levels. PS19; *Lsd1*$^{-/+}$ mice had a 31% reduction in LSD1 protein level compared to PS19 Tau mice. Values are mean ± SD (*n*=3, one-way analysis of variance (ANOVA)).

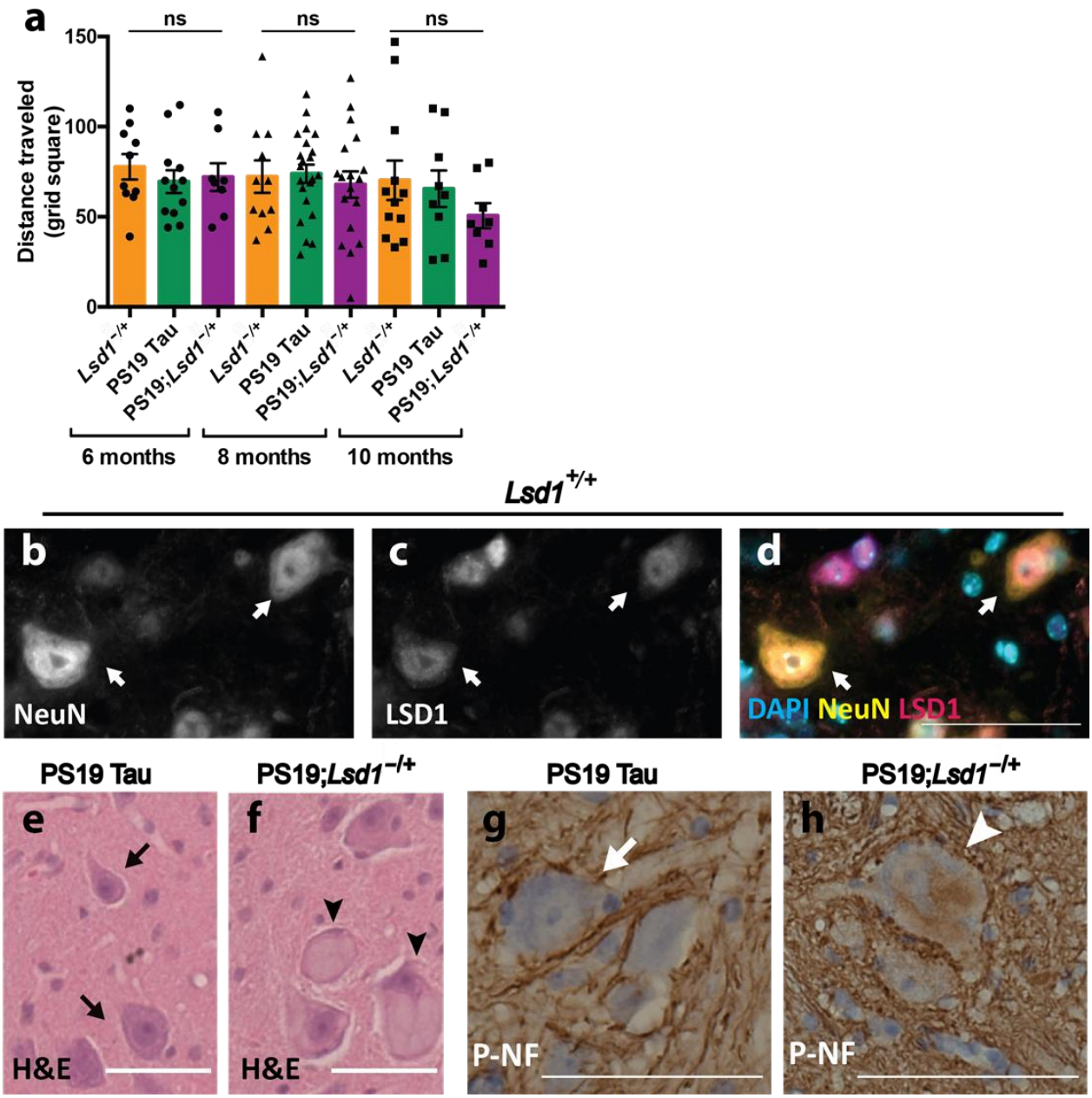

Fig. S3: Reduction of *Lsd1* affects spinal cord in PS19 Tau mice. a, Grid performance test measuring the distance traveled (grid squares traversed) with both forelimbs and hindlimbs in 6, 8, and 10 month old mice. *Lsd1*$^{-/+}$ (orange, *n*=10,11,12), PS19 Tau (green, *n*=12,22,9), and PS19;*Lsd1*$^{-/+}$ (purple, *n*=8,18,8). Values are mean ± SEM (two-way analysis of variance (ANOVA) with Tukey's post hoc test. ns=not significant). **b-d,** Immunofluorescence staining of

NeuN (**b**), LSD1 (**c**), and merged with DAPI (**d**) in spinal cord motor neurons of 12 month old *Lsd1*$^{+/+}$ control mice. **e,f,** Representative image of hematoxylin and eosin (H&E) staining of motor neurons in 12 month old PS19 Tau mice (**e**) and PS19;*Lsd1*$^{-/+}$ (**f**) littermates. **g,h,** Representative image of immunohistochemistry staining for phospho-nuerofilament (brown) counterstained with DAPI (blue) in the motor neurons of 12 month old PS19 Tau mice (**g**) and PS19;*Lsd1*$^{-/+}$ (**h**) littermates. Arrows denote healthy motor neurons. Arrowheads denote abnormal motor neurons. Scale bars=50μm.

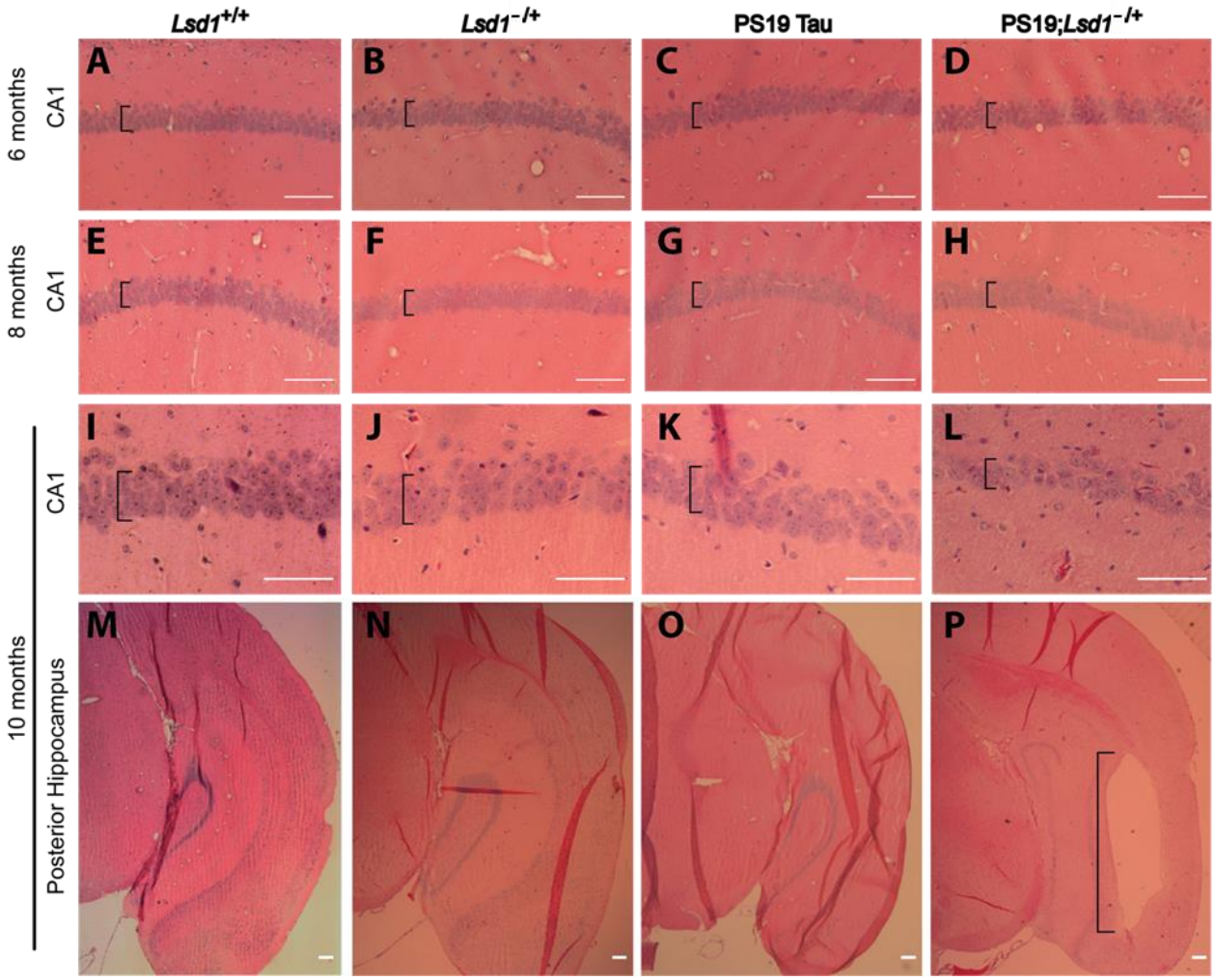

Fig. S4: There is no exacerbation of neurodegeneration in PS19 Tau mice with reduced *Lsd1* until 10 months of age. a-p, Representative image of H&E staining of *Lsd1*$^{+/+}$ (**a,e,i,m**), *Lsd1*$^{-/+}$ (**b,f,j,n**), PS19 Tau (**c,g,k,o**), and PS19;*Lsd1*$^{-/+}$ (**d,h,l,p**) littermates at 6 months (**a-d**), 8 months (**e-h**) and 10 months (**i-p**) in the CA1 (**a-l**) and posterior hippocampus (**m-p**). Brackets denote thickness of pyramidal layer of the CA1 (**a-l**), and region of cell clearance in posterior hippocampus (**p**). Scale bars=50μm.

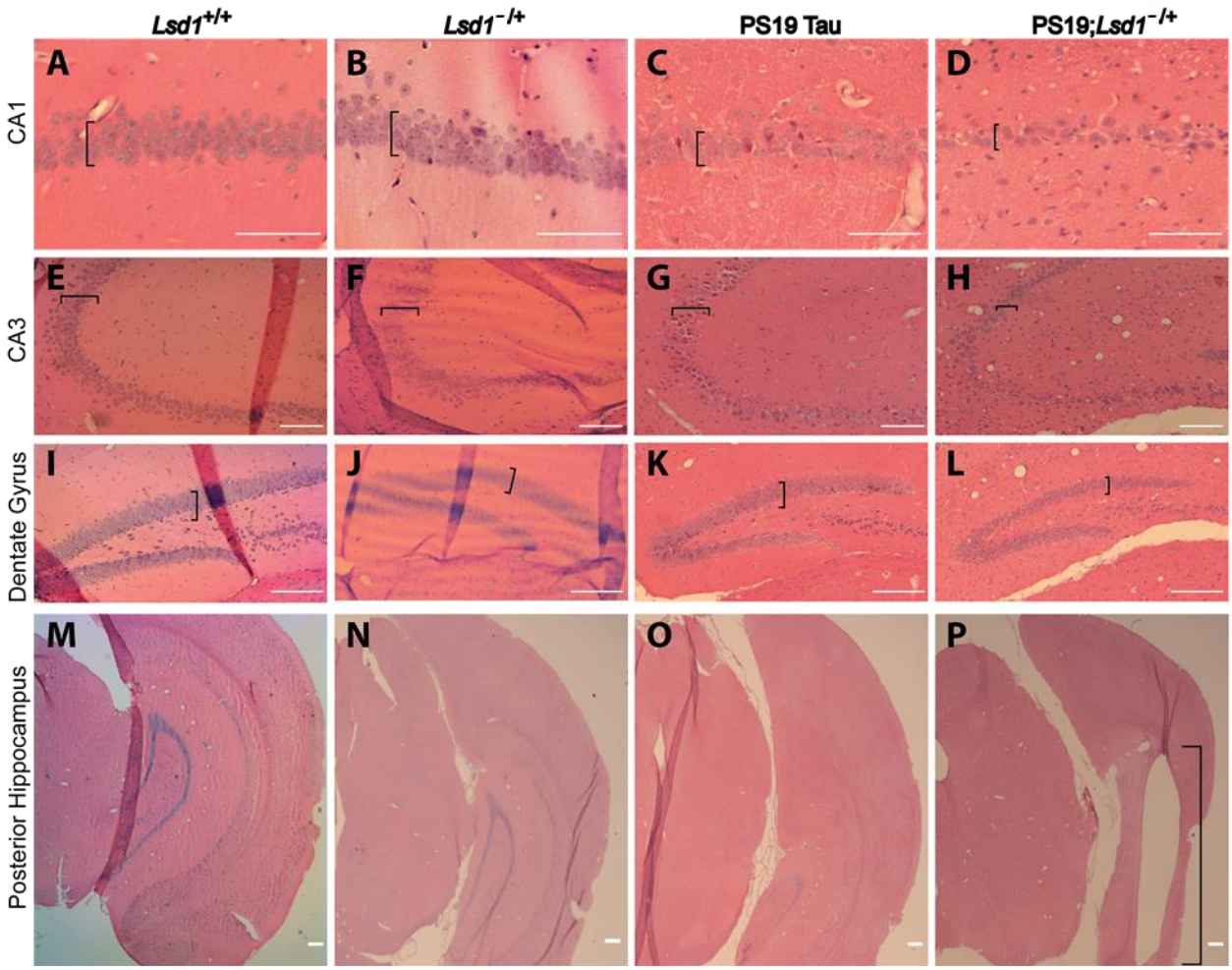

Fig. S5: Increased neurodegeneration throughout the hippocampus and cortex of 12 month old mice. a-p, H&E staining of 12 month old *Lsd1*$^{+/+}$ (**a,e,i,m**), *Lsd1*$^{-/+}$ (**b,f,j**,**n**), PS19 Tau (**c,g,k,o**), and PS19;*Lsd1*$^{-/+}$ (**d,h,l,p**) littermates in the CA1 (**a-d**) and CA3 (**e-h**) regions of the hippocampus, the dentate gyrus (**i-l**), and the posterior hippocampus (**m-p**). Brackets denote thickness of pyramidal layer of the CA1 (**a-d**), CA3 (**e-h**), the granule cell layer of the Dente Gyrus (**i-l**), and region of cell clearance in posterior hippocampus (**p**). Scale bars=50μm.

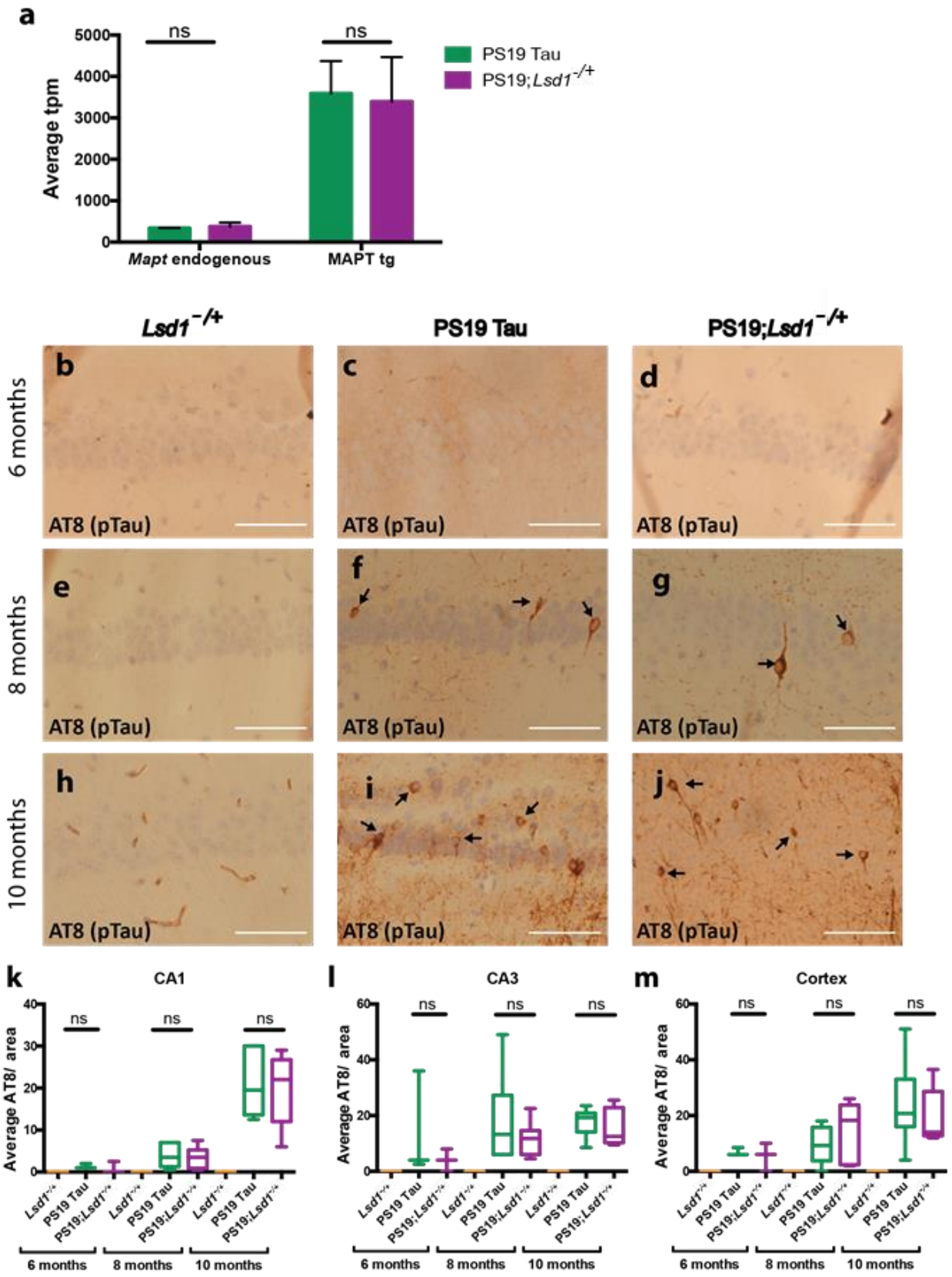
a
Average tpm
5000
4000
3000
2000
1000
0
ns
ns
PS19 Tau
PS19;Lsd1-/+
Mapt endogenous
MAPT tg
Lsd1-/+
PS19 Tau
PS19;Lsd1-/+
6 months
8 months
10 months
b
c
d
e
f
g
h
i
j
AT8 (pTau)
k
CA1
l
CA3
m
Cortex
Average AT8/ area
ns
Lsd1+/+
PS19 Tau
PS19;Lsd1+/+
6 months
8 months
10 months

Fig. S6: Reduction of *Lsd1* does not affect AT8 positive tau pathology. a, Average transcripts per million (tpm) from RNA sequencing of endogenous MAPT and the expression of the human P301S MAPT transgene in the hippocampus of PS19 Tau, and PS19; *Lsd1*$^{-/+}$ mice. Values are mean ± SD (*n*=2). **b-j,** Representative image of immunohistochemistry staining of phosphorylated tau (AT8 antibody) of the CA1 region of the hippocampus in *Lsd1*$^{-/+}$ (**b,e,h**) , PS19 Tau (**c,f,i**), and PS19;*Lsd1*$^{-/+}$ (**d,g,j**) littermates at 6 months (**b-d**), 8 months (**e-g**), and 10 months (**h-j**). Arrows denote AT8 positive immunoreactivity. Scale bars=50μm. **k-m,** Quantification of the average AT8 positive tau immunoreactivity per area from histology represented in **Extended Data Fig. 6b-j** in the CA1 (**k**) and CA3 (**l**) regions of the hippocampus, and the cerebral cortex (**m**) (6 months *n*=3, 8 months *n*=6, and 10 months *n*=6, box plot edges are 25th and 75th percentile, central line is the median, and whiskers are max and min). For all graphs: one-way analysis of variance (ANOVA) with Tukey's post hoc test (two-sided), ns=not significant.

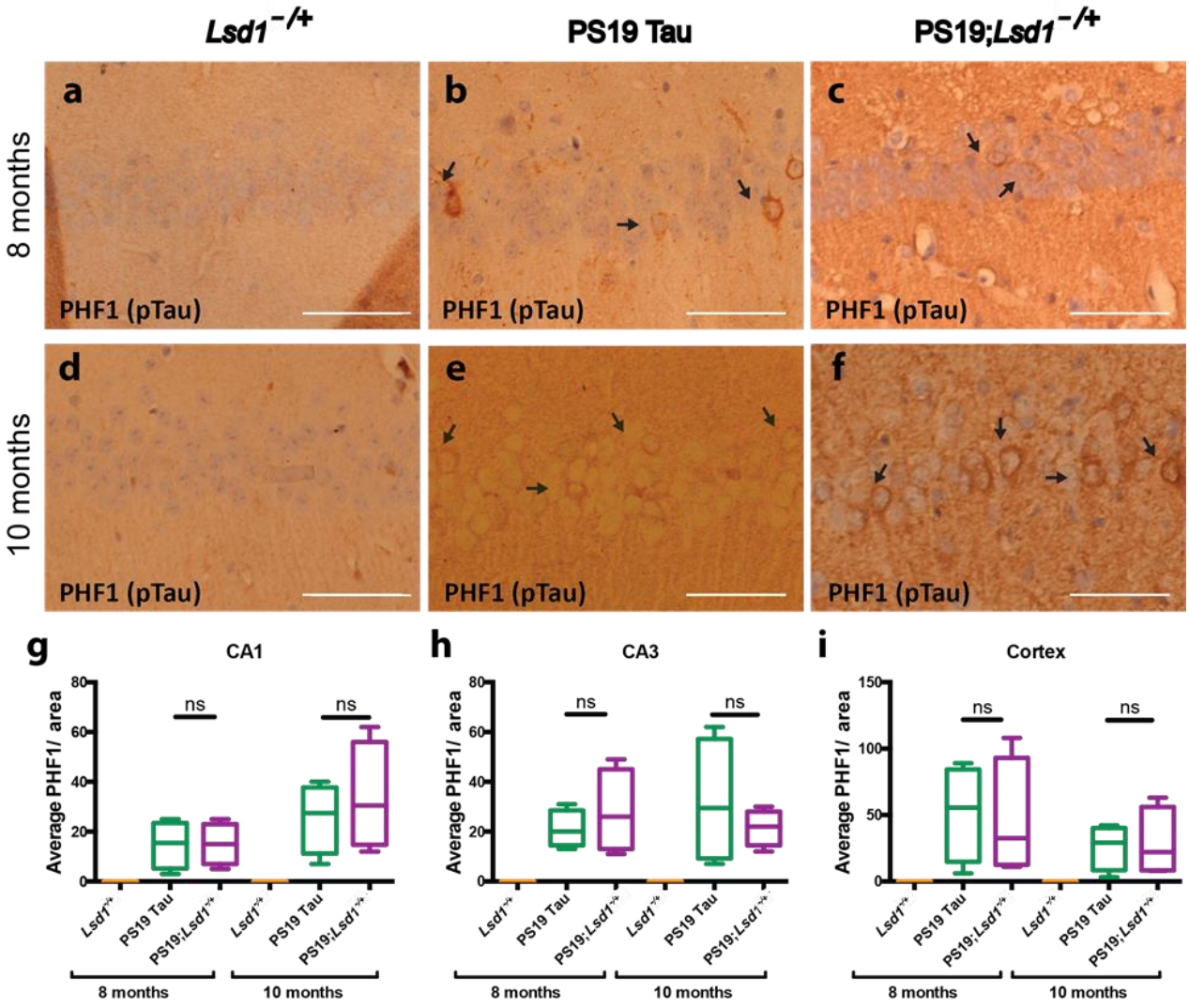

Fig. S7: Reduction of *Lsd1* does not affect PHF1 positive tau pathology. a-f, Representative image of immunohistochemistry staining of PHF1 in the CA1 region of the hippocampus in *Lsd1*$^{-/+}$ (**a,d**), PS19 Tau (**b,e**), and PS19;*Lsd1*$^{-/+}$ (**c,f**) littermates at 8 months (**a-c**) and 10 months (**d-f**). Arrows denote PHF1 positive immunoreactivity. Scale bars=50μm. **g-i,** Quantification of average PHF1 positive tau immunoreactivity per area from histology represented in **Extended Data Fig. a-f** in the CA1 (**g**) and CA3 (**h**) regions of the hippocampus, and the cerebral cortex (**i**) (*n*=4 box plot edges are 25th and 75th percentile, central line is the median, and whiskers are max

and min). For all graphs: one-way analysis of variance (ANOVA) with Tukey's post hoc test (two-sided), ns=not significant.

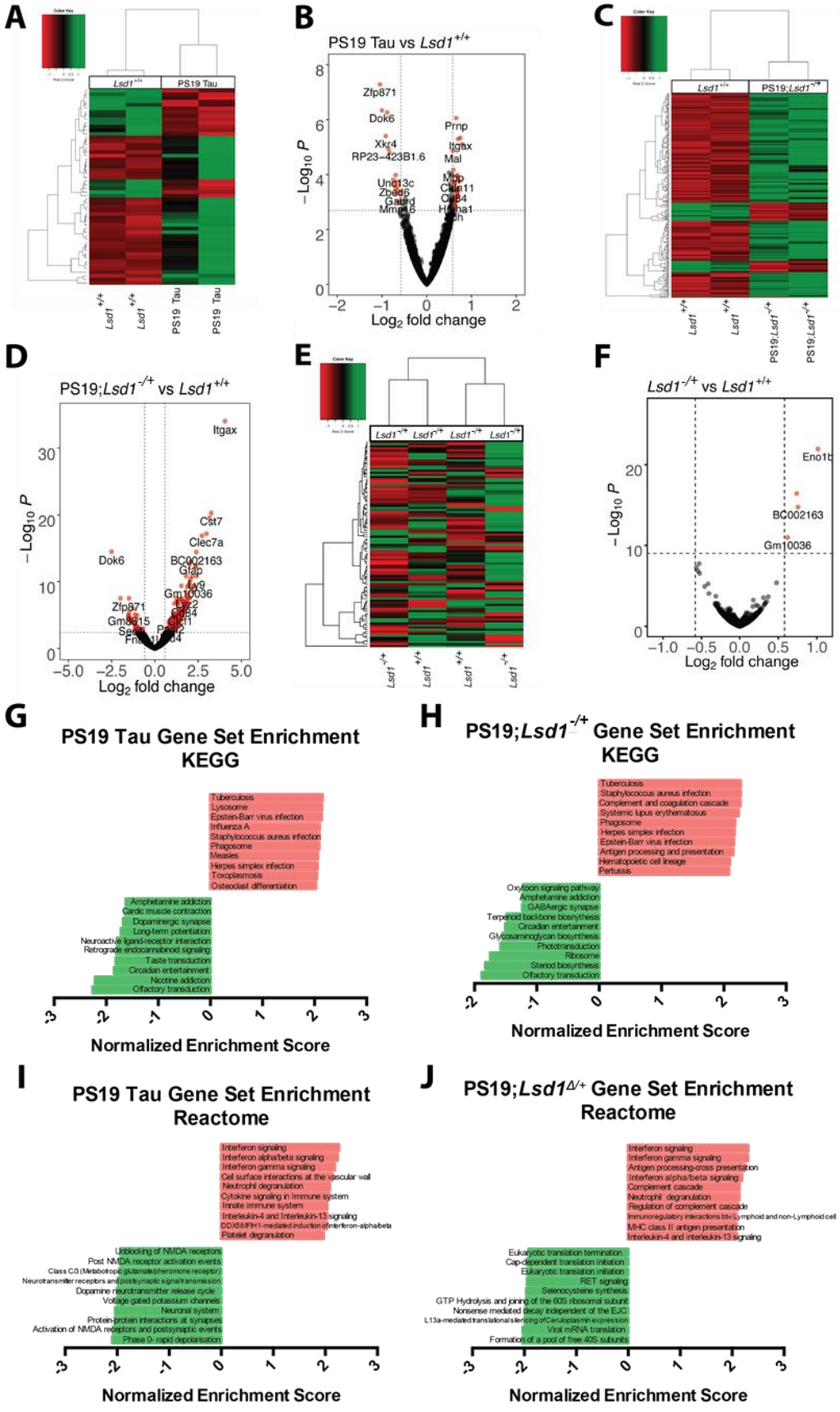
A
B
PS19 Tau vs Lsd1+/+
Zfp871
Dok6
Xkr4
RP23−423B1.6
Prnp
Itgax
Mal
Mbp
Cldn11
Cst7
Hbb−a1
Log2 fold change
C
PS19;Lsd1−/+
D
PS19;Lsd1−/+ vs Lsd1+/+
Itgax
Cst7
Clec7a
Dok6
BC002163
Glap
Gm10036
Zfp871
Gm8915
E
F
Lsd1−/+ vs Lsd1+/+
Eno1b
BC002163
Gm10036
G
PS19 Tau Gene Set Enrichment
KEGG
Tuberculosis
Lysosome
Epstein-Barr virus infection
Influenza A
Staphylococcus aureus infection
Phagosome
Measles
Herpes simplex infection
Toxoplasmosis
Osteoclast differentiation
Amphetamine addiction
Cardiac muscle contraction
Dopaminergic synapse
Long-term potentiation
Neuroactive ligand-receptor interaction
Retrograde endocannabinoid signaling
Taste transduction
Circadian entertainment
Nicotine addiction
Olfactory transduction
Normalized Enrichment Score
H
PS19;Lsd1−/+ Gene Set Enrichment
KEGG
Tuberculosis
Staphylococcus aureus infection
Complement and coagulation cascade
Systemic lupus erythematosus
Phagosome
Herpes simplex infection
Epstein-Barr virus infection
Antigen processing and presentation
Hematopoietic cell lineage
Pertussis
Oxytocin signaling pathway
Amphetamine addiction
GABAergic synapse
Terpenoid backbone biosynthesis
Circadian entertainment
Glycosaminoglycan biosynthesis
Phototransduction
Ribosome
Steroid biosynthesis
Olfactory transduction
Normalized Enrichment Score
I
PS19 Tau Gene Set Enrichment
Reactome
Interferon signaling
Interferon alpha/beta signaling
Interferon gamma signaling
Cell surface interactions at the vascular wall
Neutrophil degranulation
Cytokine signaling in Immune system
Innate immune system
Interleukin-4 and Interleukin-13 signaling
DDX58/IFIH1-mediated induction of interferon-alpha/beta
Platelet degranulation
Unblocking of NMDA receptors
Post NMDA receptor activation events
Class C3 (Metabotropic glutamate/pheromone receptor)
Neurotransmitter receptors and postsynaptic signal transmission
Dopamine neurotransmitter release cycle
Voltage gated potassium channels
Neuronal system
Protein-protein interactions at synapses
Activation of NMDA receptors and postsynaptic events
Phase 0- rapid depolarisation
Normalized Enrichment Score
J
PS19;Lsd1Δ/+ Gene Set Enrichment
Reactome
Interferon signaling
Interferon gamma signaling
Antigen processing-cross presentation
Interferon alpha/beta signaling
Complement cascade
Neutrophil degranulation
Regulation of complement cascade
Immunoregulatory interactions btw Lymphoid and non-Lymphoid cell
MHC class II antigen presentation
Interleukin-4 and Interleukin-13 signaling
Eukaryotic translation termination
Cap-dependent translation initiation
Eukaryotic translation initiation
RET signaling
Selenocysteine synthesis
GTP Hydrolysis and joining of the 60S ribosomal subunit
Nonsense mediated decay independent of the EJC
L13a-mediated translational silencing of Ceruloplasmin expression
Viral mRNA translation
Formation of a pool of free 40S subunits
Normalized Enrichment Score

Fig. S8. Differential expression in 9 month old *Lsd1*$^{-/+}$, PS19 Tau, and PS19;*Lsd1*$^{-/+}$ hippocampus. A,C,E, Heatmap of differentially expressed RNA-seq transcripts between *Lsd1*$^{+/+}$ and PS19 Tau (**A**), PS19; *Lsd1*$^{-/+}$ (**C**), and *Lsd1*$^{-/+}$ (**E**) mouse hippocampus. Samples are hierarchically clustered by relative expression of differentially expressed transcripts. Relative higher (red) and lower (green) expression is indicated. **B,D,F,** Volcano plot of $\log_2$ fold-changes in gene expression (x-axis) by statistical significance ($-\text{Log}_{10}$ P-value; y-axis) in PS19 Tau (**B**), PS19; *Lsd1*$^{-/+}$ (**D**), and *Lsd1*$^{-/+}$ (**F**) compared to *Lsd1*$^{+/+}$ mouse hippocampus. Each dot represents a transcript, and the dotted line represents a significance $\log_2$ fold change cut off of 0.5. **G-J,** Histogram of Gene Set Enrichment Analysis compared to KEGG pathways (**G,H**) and the Reactome (**I,J).** The top ten most enriched (red) and depleted (green) gene sets in the PS19 Tau (**G,I**) and PS19; *Lsd1*$^{-/+}$ (**H,J**) are shown with normalized enrichment scores.

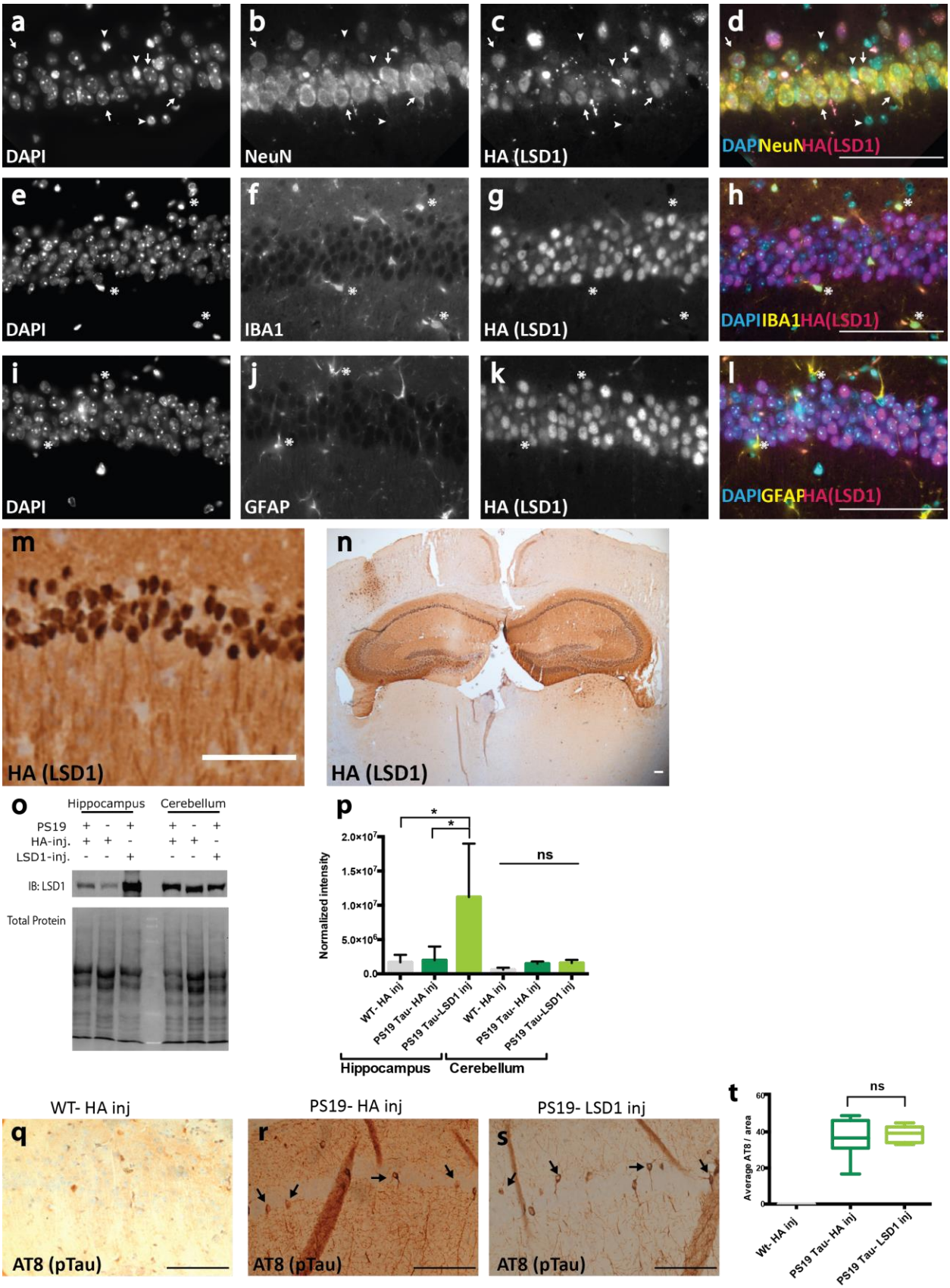
a
DAPI
b
NeuN
c
HA (LSD1)
d
DAPNeuNHA(LSD1)
e
DAPI
f
IBA1
g
HA (LSD1)
h
DAPIBA1HA(LSD1)
i
DAPI
j
GFAP
k
HA (LSD1)
l
DAPIGFAPHA(LSD1)
m
HA (LSD1)
n
HA (LSD1)
o
Hippocampus
Cerebellum
PS19 + - + + - +
HA-inj. + + - + + -
LSD1-inj. - - + - - +
IB: LSD1
Total Protein
p
Normalized intensity
2.0×10^7
1.5×10^7
1.0×10^7
5.0×10^6
0.0
*
*
ns
WT- HA inj
PS19 Tau- HA inj
PS19 Tau-LSD1 inj
WT- HA inj
PS19 Tau- HA inj
PS19 Tau-LSD1 inj
Hippocampus
Cerebellum
WT- HA inj
PS19- HA inj
PS19- LSD1 inj
q
AT8 (pTau)
r
AT8 (pTau)
s
AT8 (pTau)
t
ns
Average AT8 / area
60
40
20
0
Wt- HA inj
PS19 Tau- HA inj
PS19 Tau- LSD1 inj

Fig. S9: LSD1 overexpression in hippocampal neurons of PS19 Tau mice. a-d, Representative immunofluorescence labeling in a WT- HA inj mouse showing DAPI (**a**), NeuN (**b**), HA (which represents the LSD1 virus, hereafter denoted as HA(LSD1)) (**c**), and merged (**d**). Viral produced LSD1 is present in NeuN+ neurons. Arrows denote NeuN+ cells that have HA expression. Arrowheads denote cells that lack NeuN staining and also lack HA expression. **e-h,** Representative immunofluorescence labeling showing DAPI (**e**), IBA1 (**f**), HA(LSD1) (**g**), and merged (**h**). Asterisks denote cells stained positive for IBA1 (**e-h**), which lack HA expression. **i-l,** Representative immunofluorescence labeling showing DAPI (**i**), GFAP (**j**), HA(LSD1) (**k**), and merged (**l**) images. Asterisks denote cells stained positive for GFAP (**i-l**), which lack HA expression. **m-n,** Immunohistochemistry staining for HA(LSD1) showing expression localized to the nucleus of neurons (**m**) specifically within the hippocampus (**n**). **o,** Representative image of immunoblot for LSD1 protein and corresponding total protein blot in the hippocampus versus the cortex of mice injected with either LSD1 or HA only expressing virus. **p,** Quantification of immunoblot for LSD1 normalized to total protein loaded per sample as represented in **Extended Data Fig. 9o** shows overexpression in the hippocampus, but not the cortex. Values are mean ± SD (*n*=3, one-way analysis of variance (ANOVA) with Tukey's post hoc test (two-sided), *P<0.05, ns=not significant. **q-r,** Representative image of immunohistochemistry staining of phosphorylated tau (AT8 antibody) in the CA1 region of the hippocampus in 11 month old WT-HA inj (**q**), PS19- HA inj (**r**), and PS19- LSD1inj (**s**) mice. Arrows denote AT8 positive immunoreactivity. Scale bars=50μm. (**t**) Quantification of average AT8 positive tau immunoreactivity per area from histology represented in **Extended Data Fig. 9q-s**. Box plot edges are 25^{th} and 75^{th} percentile, central line is the median, and whiskers are max and min (*n*=8,

one-way analysis of variance (ANOVA) with Tukey's post hoc test (two-sided), ns=not significant).

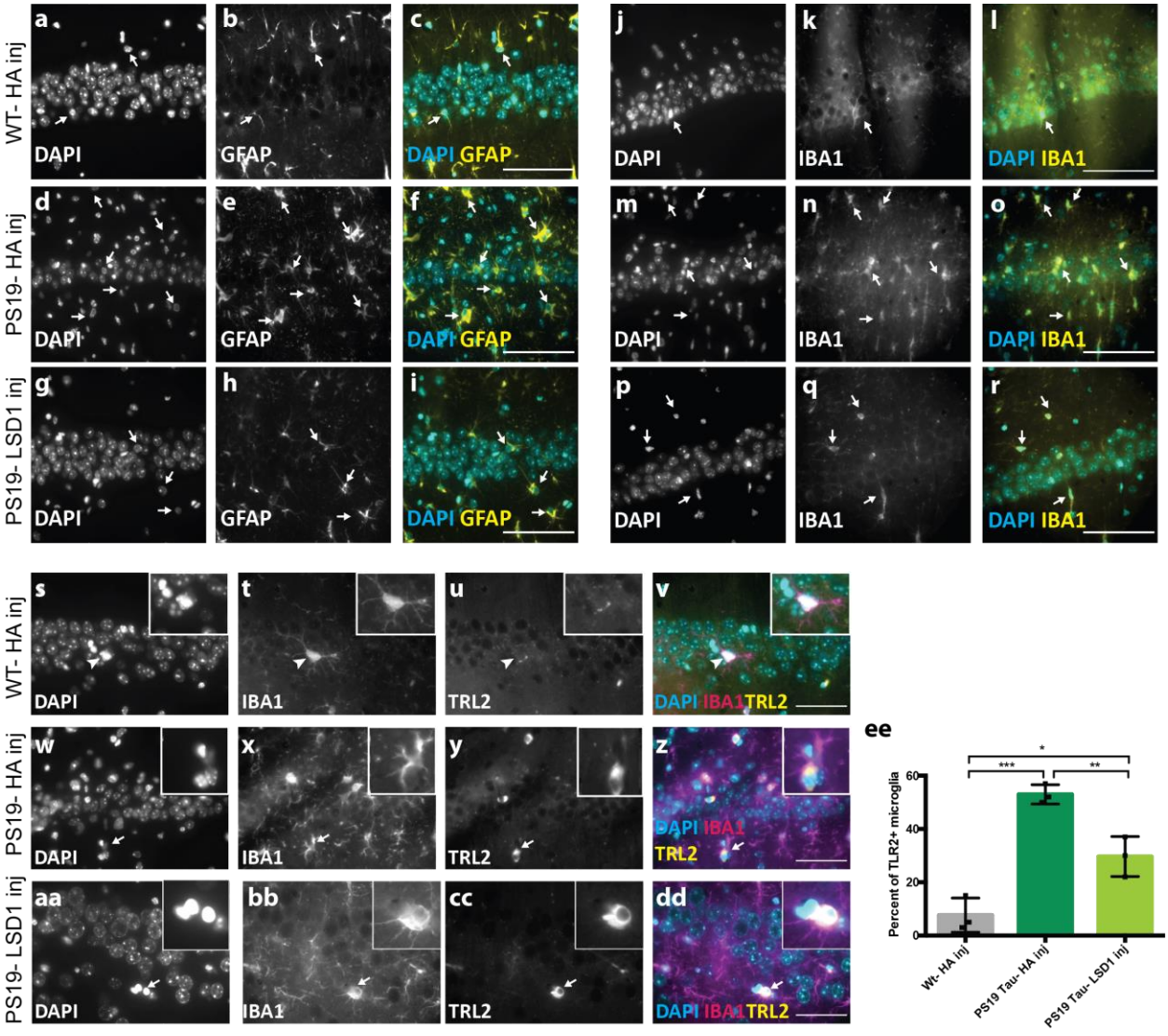

Fig. S10: LSD1 overexpression reduces the gliosis in PS19 Tau mice. a-i, Representative immunofluorescence showing DAPI (**a,d,g**), astrocyte marker GFAP (**b,e,h**), and merged (**c,f,i**) images in WT- HA inj (**a-c**), PS19- HA inj (**d-f**), and PS19- LSD1 inj (**g-i**). Arrows denote GFAP+ astrocytes. **j-r,** Representative immunofluorescence showing DAPI (**j,m,p**), microglia

marker IBA1 (**k,n,q**), and merged (**l,o,r**) images in WT- HA inj (**j-l**), PS19-HA inj (**m-o**), and PS19- LSD1 inj (**p-r**). Arrows denote IBA1+ microglia. **s-dd,** Representative immunofluorescence labeling showing DAPI (**s,w,aa**), microglia marker IBA1 (**t,x,bb**), activated microglia marker TRL2 (**u,y,cc**), and merged (**v,z,dd**) images in WT-Ha inj (**s-v**), PS19-HA inj (**w-z**), and PS19-LSD1 inj (**aa-dd)**. Inset of microglia that is IBA1 positive but TRL2 negative (**s-v,** denoted by arrowhead) or both IBA1 and TRL2 positive (**w-dd**, denoted by arrow). All images are from the CA1 region of the hippocampus Scale bars=50μm. **ee,** Quantification of the percentage of microglia that are TRL2+ in WT- HA inj, PS19- HA inj, and PS19- LSD1 inj mice represented in **Extended Data Fig. 10s-dd**. Values are mean ± SD are (*n*=3, one- way analysis of variance (ANOVA) with Tukey's post hoc test, *p<0.05, **p<0.01, ***p<0.005).

Movie S1. Reduction of LSD1 in PS19 Tau mice exacerbates paralysis. (0-0:06 sec), Tail suspension of 12 month old *Lsd1*$^{-/+}$ mouse that has full mobility in hindlimbs and no paralysis. **(0:07-0:13 sec)**, Tail suspension of 12 month old PS19 Tau mouse that has a hindlimb clasp, seen by holding legs contracted inward and not moving them, but is still mobile upon release. **(0:14-0:19 sec)**, Tail suspension of 12 month old PS19;*Lsd1*$^{-/+}$ mouse that is terminally paralyzed.

Movie S2. Magnetic Resonance Imaging of hippocampal atrophy throughout the brain when LSD1 is reduced in PS19 Tau mice. (0-0:33), Serial coronal slices from T2-weighted RARE MRI, starting posterior ending anteriorly, through the brain of a 6 month old *Lsd1*$^{-/+}$ mouse (**0:03-0:13**), PS19 Tau mouse (**0:13-0:22**), and PS19;*Lsd1*$^{-/+}$ mouse (**0:23-0:32**). (**0:33-1:05**), Serial coronal slices from T2-weighted RARE MRI, starting posterior ending anteriorly,

through the brain of the same mouse *Lsd1*$^{-/+}$ mouse (**0:35-0:45**), PS19 Tau mouse (**0:45-0:55**), and PS19;*Lsd1*$^{-/+}$ mouse (**0:55-1:05**) at 10 months old. High intensity areas (white/light grey) signify ventricular dilatation.

Movie S3. Hippocampal injection of viral LSD1 did not affect development of paralysis in PS19 mice. (0-0:13 sec), Tail suspension of 11 month old WT- HA inj mouse that has full mobility in hindlimbs and no paralysis. **(0:14-0:28 sec)**, Tail suspension of 11 month old PS19-HA mouse that has a hindlimb clasp, seen by holding legs contracted inward and not moving them, but is still mobile upon release. **(0:29-37sec)**, Tail suspension of 11 month old HA- LSD1 inj mouse that similarly has a hindlimb clasp holding legs contracted inward and not moving them, but is still mobile upon release.

Movie S4. Pathological Tau Induces Neurodegeneration by sequestering and inhibiting LSD1. In healthy hippocampal and cortical neurons, LSD1 is translated in the cytoplasm and transported through the nuclear pore into the nucleus where it is continuously required to repress inappropriate transcription. In tauopathy, LSD1 is translated in the cytoplasm, but as pathological tau accumulates in the cytoplasm it blocks LSD1 from being imported into the nucleus. This interferes with the continuous requirement for LSD1, resulting in neuronal cell death.

Data S1. (separate file)

Expression changes in 9 month old *Lsd1*$^{-/+}$, PS19 Tau, PS19;*Lsd1*$^{-/+}$ mice. Spreadsheets for all, significantly upregulated, and significantly downregulated transcripts. Provided for each genotype with two biological replicates are the log2 fold change, P-value, and p adjusted-value as determined by DESEQ2.

CHAPTER IV

Investigating the interaction between pathological tau and the N-terminal disordered domain of LSD1

INTRODUCTION

Currently, our model posits that in healthy hippocampal and cortical neurons, LSD1 is translated in the cytoplasm and transported into the nucleus, where it is continuously required to repress inappropriate transcription. In tauopathy, pathological tau accumulates in the cytoplasm and blocks LSD1 from being imported into the nucleus. This failed import interferes with the cell's continuous nuclear requirement of LSD1 to erase transcriptional memory, resulting in inappropriate transcription and neuronal cell death. Despite convincing evidence for this model, the mechanism of LSD1's interaction with pathological tau remains unknown. The following project aims to elucidate this mechanism by investigating the *in vivo* interaction between LSD1 and hyperphosphorylated tau (pTau).

As previously stated, tau is a phosphoprotein known to promote and stabilize the formation of tubulin into microtubules in mature neurons (Weingarten et al., 1975), a function that is critical for axonal maintenance and neuronal function (Alonso et al., 2018). Post-translational modifications influence protein structure and function; in the case of tau, phosphorylation promotes tubulin depolymerization (Lindwall and Cole, 1984; Castellani and Perry, 2019). Therefore, regulation of this modification allows for modulation of tau function. In healthy brains, the degree of tau phosphorylation is strictly regulated throughout development (Alonso et al., 2018). In tauopathy cases, tau protein becomes aberrantly hyperphosphorylated, disrupting microtubule stability and promoting tau oligomerization and somatodendritic aggregation (Arendt et al., 2016; Castellani and Perry, 2019). Aggregated human tau has been shown to exhibit prion disease properties, in which misfolding and subsequent aggregation can induce further misfolding of both tau and other proteins (Sanders et al., 2014). Furthermore, it has been shown that introduction of aggregated human tau into the brains of young P301S mice

not yet exhibiting tau pathology induces immediate onset of tau aggregation that can be transferred and maintained across several generations (Sanders et al., 2014).

The tau protein is itself highly disordered (Fig. 4.1A) meaning it has little secondary or tertiary structure (Iqbal et al., 2010). Highly disordered proteins have the structural flexibility necessary to interact with multiple targets in a wide array of cellular processes (Wright and Dyson, 1999; Skrabana et al., 2006). In the case of tau, flexibility may be advantageous for improved interaction with an array of tubulins. Alternatively, LSD1 is highly structured, and is thought to have completely ordered functional domains (Forneris et al., 2005; Jin et al., 2014). However, human LSD1 also has an intrinsically disordered N-terminal domain of 172 amino acids (Fig. 4.1B, indicated by arrows) whose functionality, besides the embedded nuclear localization sequence, remains enigmatic (Forneris et al., 2005; Zibetti et al., 2010; Jin et al., 2014). Interestingly, Tau has been shown to interact with the disordered domains of other proteins such as the small nuclear ribonucleoprotein U1-70K (Diner et al., 2014; Bishof et al., 2018). We therefore propose that tau associates with LSD1 via LSD1's intrinsically disordered N-terminal domain, blocking the embedded nuclear localization sequence and preventing LSD1 from entering the nucleus, resulting in neurodegeneration.

To investigate whether pTau interacts with LSD1 via its N-terminal disordered domain, we aimed to remove this domain *in vivo* in tau transgenic mice. In doing so, we first had to consider whether loss of this domain would disrupt or alter LSD1's function. LSD1 is evolutionarily conserved among mammals, *Drosophila*, *C. elegans*, and *Arabidopsis* (Fig. 2) (Shi et al., 2004). However, the N-terminal disordered domain is only partially conserved across these species (Fig. 2, indicated by arrows) (Forneris et al., 2005; Jin et al., 2014). Absence of this domain in *C. elegans* and *Arabidopsis* suggests that LSD1 can still function without it in those

organisms *in vivo*. Indeed, LSD1 exhibits conserved functionality in *C. elegans* (Katz et al., 2009), and *Arabidopsis* (Jiang et al., 2007) despite absence of the N-terminal disordered domain. Additionally, *in vitro* studies investigating LSD1 functionality utilize an N-terminally truncated clone, which was found to exhibit demethylase activity comparable to *in vivo* studies (Forneris et al., 2005; Zibetti et al., 2010). Considering these findings, we predict that N-terminally deleted LSD1 can act as a functional demethylase in mammals.

We have taken two approaches to understand the interaction between LSD1 and pTau. The first utilizes neuronal-specific viral vectors to overexpress either an N-terminally truncated LSD1 protein or the full length LSD1 protein in the hippocampi of PS19 mice. This approach will allow us to interrogate the role of the N-terminal disordered domain of LSD1 in the interaction with pTau. LSD1 is translated in the cytoplasm and imported into the nucleus via direct interaction between importin α proteins and the nuclear localization sequence found in the N-terminal domain of LSD1 (Jin et al., 2014). Removal of the N-terminus including this nuclear localization signal would abolish nuclear import of LSD1 (Jin et al., 2014). To resolve this issue, we added the nuclear localization sequence back into the N-terminally truncated *Lsd1* virus (LSD1ΔN) (Fig 4.3). We aim to answer two questions with this AAV approach: 1) is LSD1ΔN present in the nucleus despite tau aggregates, implying that the N-terminal disordered domain is required for interaction with pTau? And 2) does overexpression of LSD1ΔN in the hippocampus rescue tau-mediated neurodegeneration at least as well as full length LSD1, indicating that the N-terminal disordered domain is not required for functionality *in vivo*?

Because the viral injection approach can only influence neurodegeneration in the hippocampus and does not discount crosstalk-induced degeneration throughout the rest of the CNS, injected PS19 mice still develop paralysis and die at the same rate as un-injected tauopathy

mice (Engstrom et al., 2020), limiting our ability to observe the viral product's localization and effects on cell death beyond the onset of paralysis. Our second approach aims to create PS19 mice that produce a functional LSD1 product impervious to sequestration by tau aggregates. As indicated in Figure 4.3, the unstructured domain of LSD1 spans the amino acids encoded by exon 1 and a small part of exon 2. The intronic sequence between exons 1 and 2 of *Lsd1* contains important regulatory elements, so we generated a tau mouse with a complete exon 1 deletion in one copy of the *Lsd1* gene (PS19;$Lsd1^{\Delta N/+}$). We predict that the truncated protein will no longer be sequestered by pTau, due to the elimination of most of its disordered domain, allowing LSD1ΔN to enter the nucleus unencumbered. Because $Lsd1^{-/+}$ mice appear phenotypically wildtype (Engstrom et al., 2020), we predict that one copy of *Lsd1ΔN* would be enough to maintain the nuclear pool of LSD1, despite tau-mediated sequestration of the full-length protein. The best-case scenario is that the heterozygous (PS19;$Lsd1^{\Delta N/+}$) mice will not develop any neurodegenerative or paralysis phenotype; however, there are multiple potential outcomes that will inform us about the functionality of the N-terminus *in vivo*. By comparing the survival and paralysis outcomes of these mice to tau (PS19) and tau mice with reduced LSD1 (PS19;$Lsd1^{-/+}$), we can start to deduce the degree of functionality, if any, of the N-terminal disordered domain, and whether removal of the N-terminus of LSD1 can reduce sequestration by pTau.

RESULTS

Overexpression of LSD1ΔN rescues as well as full length LSD1 until one year of age

Our data from Chapter 3 demonstrate that overexpression of full length LSD1 in PS19 mice (PS19- LSD1 inj) after the onset of tau pathology temporarily rescues neurodegeneration,

as measured by hippocampal cell counts in 11 month old mice (Engstrom et al., 2020). Here, we assessed whether overexpression of N-terminally truncated LSD1 in PS19 mice (hereafter referred to as PS19- LSD1ΔN inj) would recapitulate this rescue. First, we counted the cells in the injected hippocampus of terminally paralyzed mice (ranging from 8.9-13.1 months) from images of hematoxylin and eosin (H&E) stained tissue. As expected, we observed significant neuronal cell death in PS19 mice injected with the HA-control virus compared to wildtype (Fig. 4.4A,B,E p=0.0002). Continued from our data in Chapter 3, we show a statistically significant rescue of the neuronal cell death seen in the PS19- HA group upon overexpression of full length LSD1 (Fig. 4.4B,C,E p=0.0079). The PS19- LSD1ΔN inj is not significantly different from the wildtype, indicating that overexpression of the LSD1ΔN may have rescued (Fig 4.4A,D,E). However, the PS19- LSD1ΔN inj group is also not statistically significant from the PS19- HA group (Fig. 4.4E – p = 0.7803, comparing means of the PS19- LSD1ΔN inj group to the PS19- HA inj group). This suggests that the rescue may be incomplete. Nevertheless, despite the lack of significant difference between the PS19- LSD1ΔN inj group and the PS19- HA group, there is a clear absence of the degenerating population in the PS19- LSD1ΔN inj group that is clearly present in the Tau- HA inj group (Fig. 4.4B,D,E). This suggests that there is a rescue of at least the most significantly affected population. Finally, comparing the PS19-LSD1 full length rescued mice to the potential rescue seen in the PS19- LSD1ΔN inj group indicates that the LSD1ΔN protein may not be as functional as the full protein. Although more numbers would be needed to determine definitively whether this is the case, this interpretation is further supported by survival data from the PS19;*Lsd1*$^{\Delta N/+}$ mice (Fig. 4.8).

Injection with truncated LSD1 does not result in neuronal blebbing

Previously we showed that the rescue produced by full-length LSD1 overexpression is incomplete – the majority of 'rescued' animals with high cell counts show blebbing morphology that we propose to be a marker of slowed, ongoing cell death (Engstrom et al., 2020). Here we show that 60% of all PS19- LSD1 inj mice exhibit CA1 blebbing (Fig. 4.7E, representative histology Fig. 4.7A,C), while no PS19- LSD1ΔN inj mice exhibit CA1 blebbing (Fig. 4.7E, representative histology Fig. 4.7B,D). Furthermore, 100% of PS19- LSD1 inj animals show blebbing in some region of the hippocampus (Fig. 4.7E), while this number is substantially reduced in animals overexpressing truncated LSD1 (38%). In comparison, we observed both CA1 and other hippocampal blebbing in a single PS19- HA inj mouse (11%). The comparative lack of blebbing in the PS19- LSD1ΔN inj mice raises the possibility that neurons that don't die in these mice are potentially more rescued than what we observe in PS19 mice rescued by the full-length protein. This finding is potentially consistent with a small group of PS19;*Lsd1*$^{\Delta N/+}$ mice that may be more rescued (see below; Fig. 4.9).

Overexpressed LSD1ΔN localizes to the nucleus more consistently than full length LSD1

We observed that the blebbing morphology detected in H&E correlates to cytoplasmic diffuse HA staining, which we suggest represents sequestration of the viral product preceding cell death and clearance (Engstrom et al., 2020). We have recapitulated that result in this sample of PS19- LSD1 inj mice, where all three animals with CA1 blebbing show cytoplasmic diffuse HA staining in that region (two of the three shown in Fig. 4.6A,C), suggesting sequestration. Contrastingly, PS19- LSD1ΔN inj mice show persistent nuclear HA staining (Fig. 4.6B,D), even as late as 12.3 months of age (Fig. 4.6D), well past the onset of tau pathology. This suggests that LSD1ΔN evades tau aggregates to be successfully imported into the nucleus. This finding could potentially account for the lack of blebbing that we observe in PS19- LSD1ΔN inj mice (see

above; Fig. 4.7), as well as a small group of PS19;*Lsd1*$^{\Delta N/+}$ mice that may be more rescued (see below; Fig. 4.9).

PS19;*Lsd1*$^{\Delta N/+}$ mice show an intermediate survival phenotype to PS19 and PS19;*Lsd1*$^{-/+}$ mice

To further explore the function of the N-terminal disordered domain of LSD1, we generated a novel mouse line heterozygous for an exon 1 deletion of *Lsd1* (hereafter referred to as *Lsd1*$^{\Delta N/+}$). With the goal of creating PS19 mice that produce a functional LSD1 product impervious to sequestration by tau aggregates, *Lsd1*$^{\Delta N/+}$ mice were crossed with PS19 mice, generating four experimental genotypes at equal ratios: wildtype, *Lsd1*$^{\Delta N/+}$, PS19, and PS19;*Lsd1*$^{\Delta N/+}$ (Figure 4.7). We would expect different phenotypes in these mice based on the degree to which LSD1's N-terminal disordered domain contributes to enzyme function and association with pTau. If the N-terminal disordered domain is entirely required for LSD1 function, we would anticipate PS19;*Lsd1*$^{\Delta N/+}$ mice to have a similar phenotype to PS19 mice with reduced LSD1 (PS19;*Lsd1*$^{-/+}$, see Chapter 3), because the truncated product from the *Lsd1ΔN* allele would be entirely compromised and no better than a null allele. If the N-terminal disordered domain is partially required for LSD1 function and therefore the *Lsd1ΔN* allele is hypomorphic, then we might expect PS19;*Lsd1*$^{\Delta N/+}$ mice to have a phenotype slightly better or worse than PS19 mice, depending on the degree to which truncation affects LSD1's functionality, as well as the disordered domain's requirement for association with pTau. Finally, if the N-terminal disordered domain is dispensable to LSD1 functionality and is required for sequestration by pTau, we would anticipate a complete rescue of the PS19 phenotype. The PS19;*Lsd1*$^{\Delta N/+}$ mice would be effectively equivalent to our Lsd1$^{-/+}$ mice, who do not present any phenotypes. As seen in Figure 4.8A, PS19;*Lsd1*$^{\Delta N/+}$ mice (orange) appear to have a survival

phenotype intermediate between normal tau mice (green) and tau mice that are heterozygous for an *Lsd1* loss of function allele (30% reduction in LSD1) (purple; data taken from Fig. 3.2A). This suggests that the $Lsd1^{\Delta N/+}$ allele may be hypomorphic for LSD1 function. However, because this experiment is ongoing, and a survival curve is most informative once the entire population is deceased, the remaining living mice >11 months were plotted by age in days in Figure 4.8B. This figure more legibly represents the remainder of the colony.

PS19;$Lsd1^{\Delta N/+}$ mice show a bimodal paralysis phenotype

Although we have not yet performed an objective measure of paralysis (i.e. rotarod, grid performance) in the PS19;$Lsd1^{\Delta N/+}$ animals, we did record the age at clasp onset for all mice during weekly monitoring. Figure 4.9 shows age at clasp onset (black dots), or current age for mice that have no paralysis phenotype (blue dots, y = current age), for all living PS19 and PS19;$Lsd1^{\Delta N/+}$ mice >11 months. All of the longest-lived PS19;$Lsd1^{\Delta N/+}$ mice show no sign of paralysis, despite being older than one year of age. While the majority of the PS19;$Lsd1^{\Delta N/+}$ population developed terminal paralysis as indicated by Figure 4.8A, this evidence shows that certain animals remain unaffected into old age, suggesting a potential bimodal distribution of the paralysis phenotype. However, this interpretation is potentially mitigated by the presence of control PS19 mice that also do not have a clasp at this advanced age.

Generation of $Lsd1^{\Delta N/\Delta N}$ animals will rule out the N-terminal disordered domain as required for LSD1 function

$Lsd1^{-/-}$ mice are embryonic lethal, arresting at E5.5 and are resorbed by E7.5 (Wang et al., 2007; Wang et al., 2009). Therefore, if LSD1's N-terminal disordered domain is functionally required then we will not be able to breed mice homozygous for the exon 1 deletion of *Lsd1*. We have set

up these crosses in both wildtype and tau backgrounds, with the latter expected to generate six experimental genotypes: wildtype, PS19 Tau, *Lsd1*$^{\Delta N/+}$, PS19;*Lsd1*$^{\Delta N/+}$, *Lsd1*$^{\Delta N/\Delta N}$, and PS19;*Lsd1*$^{\Delta N/\Delta N}$ (Figure 4.10). However, we are having some difficulties genotyping the wildtype band for the exon 1 deletion. As a result, we currently cannot distinguish between heterozygotes and homozygotes. We are in the process of optimizing a new PCR genotyping reaction to detect the wildtype band. Once that reaction is functioning, we will be able to determine if *Lsd1*$^{\Delta N/\Delta N}$ mice are viable, and whether they have any phenotype. So far, these crosses have repeatedly generated large litters (9+ pups), which decreases the likelihood that any genotype is embryonic lethal. Furthermore, we have not observed perinatal lethality in these progeny.

DISCUSSION

We have previously shown that modulation of the histone demethylase LSD1 can alter neurodegeneration in a tauopathy mouse model. We produced the first cytological evidence that pathological tau can prevent LSD1 from properly localizing to the nucleus in hippocampal and cortical neurons, where we previously showed it is continuously required. Based on studies that have implicated tau's intrinsic disorder in its association with the disordered domains of other proteins (Diner et al., 2014; Bishof et al., 2018), we predicted that tau associates with LSD1's N-terminal disordered domain, blocking LSD1's nuclear localization sequence from interacting with importin proteins, and thereby sequestering it in the cytoplasm. From this proposed mechanism we hypothesized that removal of LSD1's disordered domain would prevent sequestration by tau, resulting in persistent nuclear localization despite the presence of tau pathology. We observed improved persistence in the nuclear localization of exogenous LSD1ΔN

compared to full length LSD1, as late as one year of age, well past the onset of tau pathology. This preliminary data suggests that LSD1's N-terminal disordered domain is required for association with tau.

We further hypothesized that removal of the N-terminal disordered domain would not alter LSD1's function. We demonstrated that overexpression of LSD1ΔN eliminates the degenerating population consistently seen in age-matched samples of PS19- HA animals, suggesting an effective rescue at this time point. Additionally, the presence of significant blebbing in PS19- LSD1 inj mice and relative lack thereof in PS19- LSD1ΔN inj animals potentially suggests an improved rescue by overexpression of truncated LSD1. However, we do not currently have evidence that overexpressed LSD1ΔN rescues cell death longer than full length (past 12 months), because these experiments are currently ongoing.

The majority of our PS19;*Lsd1*$^{\Delta N/+}$ mice have paralysis. Presence of this phenotype could be interpreted in one of two ways: 1) perhaps the exclusive deletion of exon 1 left enough of the disordered domain remaining to allow for interaction with and sequestration by tau; and/or 2) the N-terminal disordered domain, specifically the sequence encoded by exon 1, is partially required for LSD1 functionality *in vivo*. We have three old PS19;*Lsd1*$^{\Delta N/+}$ mice living with no sign of paralysis. While there are PS19 mice of a similar age that have yet to show a clasp, we feel confident that those animals will eventually develop paralysis (Yoshiyama et al., 2007). It is possible that the PS19;*Lsd1*$^{\Delta N/+}$ mice will show the same stochasticity as the PS19 mice; however, it is also possible that these mice will never develop paralysis. This preliminary result indicates that PS19;*Lsd1*$^{\Delta N/+}$ mice may be bimodally distributed, in that most are phenotypically similar to PS19 mice, while some appear phenotypically wildtype and have a normal lifespan.

Overall, PS19;*Lsd1*$^{\Delta N/+}$ mice show a survival phenotype intermediate to PS19 and PS19;*Lsd1*$^{-/+}$ mice. The fact that the PS19;*Lsd1*$^{\Delta N/+}$ mice show a worse survival phenotype than PS19 mice with two normal copies of *Lsd1* suggests that LSD1ΔN is functionally compromised compared to the full-length protein. However, because PS19;*Lsd1*$^{\Delta N/+}$ mice appear to have a better survival phenotype than PS19;*Lsd1*$^{-/+}$ animals, we argue that LSD1ΔN retains partial functionality *in vivo*. This finding is consistent with the observation that full length LSD1 potentially rescues slightly better than the truncated version. In this case the possibility that a hypomorphic allele can rescue at all may only be due to the viral expression, which results in 6-fold overexpression compared to endogenous levels (Engstrom et al., 2020). This abundance of partially functioning LSD1 could be compensatory, facilitating the elimination of the degenerating population we observed in the viral injection experiment.

Alternatively, when the hypomorphic allele is expressed at normal levels in the mouse colony, we can observe the consequences of its functional shortcomings in the form of paralysis and shortened survival. Combined with our evidence that truncated LSD1 is impervious to sequestration by tau, the argument that *Lsd1ΔN* is a hypomorphic allele potentially further explains the bimodal pattern of paralysis observed in the PS19;*Lsd1*$^{\Delta N/+}$ mice. This is because the neuronal cell death and paralysis would be explained by a combination of 1) the amount of LSD1ΔN versus full length LSD1 any cell is producing, 2) the tau burden in that animal, and 3) how the loss of the N-terminal disordered domain ultimately affects LSD1 function.

As an epigenetic enzyme with a wide array of target loci, it is possible that LSD1's disordered domain is necessary for binding to certain targets or interacting partners (Sandhu, 2009), particularly in the case of transcriptional condensates at highly specific genomic loci as proposed by Richard Young's group at MIT (Shrinivas et al., 2019). If removal of the N-terminal

disordered domain *in vivo* precludes LSD1 from demethylating a few specific targets, it is possible that moving forward we will continue to observe a bimodal distribution of mice that die early of paralysis, and mice that appear phenotypically normal and are long-lived. If this is the case, we might anticipate that homozygosity of the N-terminal deletion would exacerbate this bimodal distribution, where some homozygotes become terminal even younger than their heterozygous counterparts and some remain unaffected. In the affected animals, neurons would accumulate transcription-coupled H3K4me2 on the loci where truncated LSD1 cannot demethylate. This would lead to inappropriate transcription of those loci, as well as further accumulation of active epigenetic 'bookmarks'. This would result in disruption of the cell's transcriptional program, leading to its dysfunction or death (Lee and Katz, 2020).

Alternatively, it is possible that homozygotes would show an improved phenotype compared to heterozygotes because all their LSD1 would be truncated and therefore impervious to sequestration. Despite the partial loss of function in LSD1ΔN, persistent nuclear localization despite aggregation of tau could allow for LSD1 to demethylate targets most crucial to cell survival, creating improved paralysis and survival phenotypes. Our preliminary data from the PS19;*Lsd1*$^{\Delta N/+}$ colony only allow for speculation at this time, but as we continue to breed and age these mice, we will soon have a much clearer idea of what is happening.

FIGURES

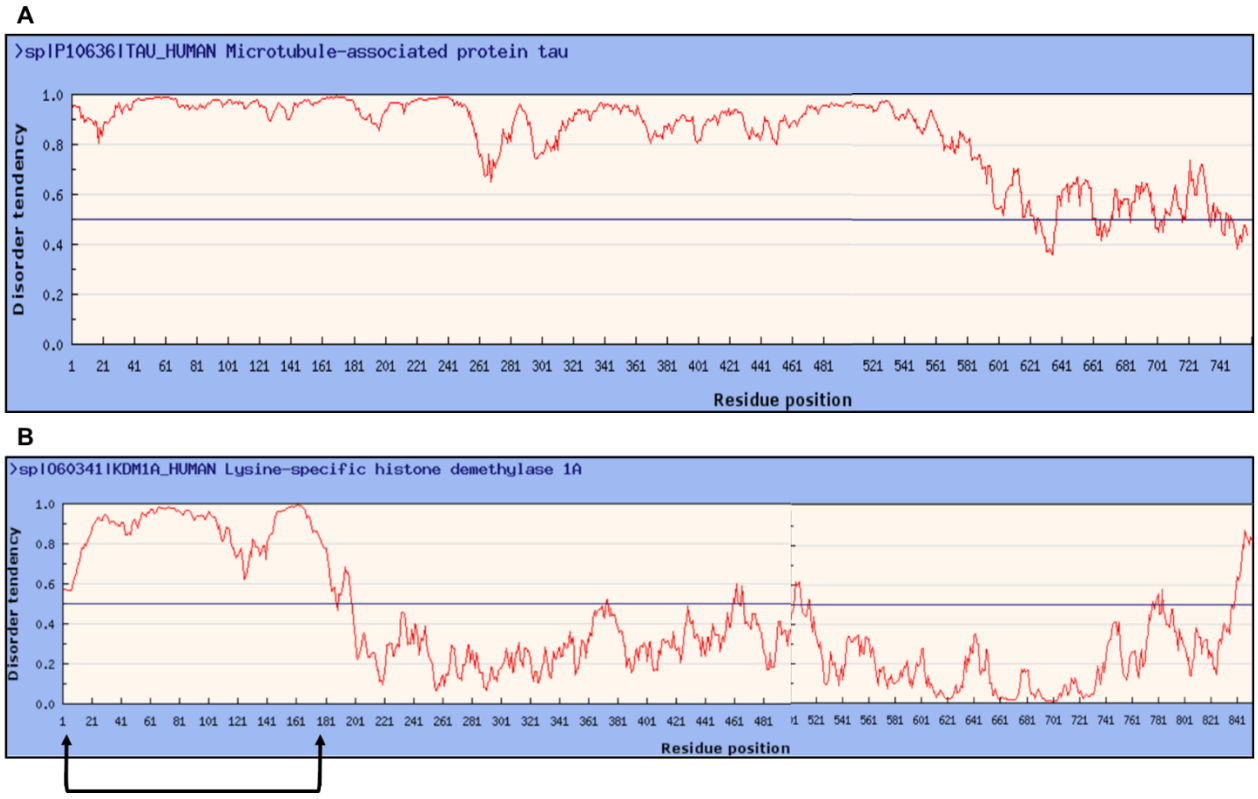

Fig. 4.1 | Tau and LSD1 both have disordered regions. (A, B) Disorder frequency by amino acid residue of human proteins tau and LSD1. **(A)** Tau is a highly disordered protein with very little secondary structure **(B)** LSD1 is highly ordered, apart from the 172 amino acid intrinsically disordered N-terminal domain indicated by bracket arrows. This figure generated at http://iupred.elte.hu/ courtesy of Dr. David J. Katz and Dr. Stephanie M. Kyle.

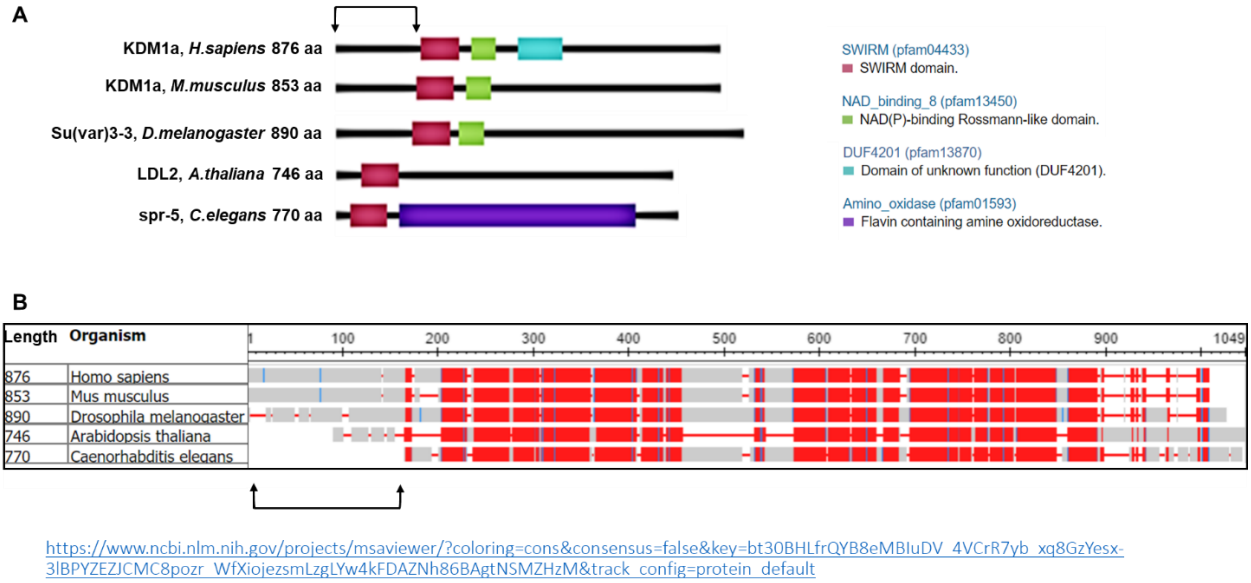

https://www.ncbi.nlm.nih.gov/projects/msaviewer/?coloring=cons&consensus=false&key=bt30BHLfrQYB8eMBIuDV_4VCrR7yb_xq8GzYesx-3lBPYZEZJCMC8pozr_WfXiojezsmLzgLYw4kFDAZNh86BAgtNSMZHzM&track_config=protein_default

Fig. 4.2 | LSD1 homologs share conserved structure. (A) General structure of LSD1 homologs with arrows indicating an N-terminal intrinsically disordered domain conserved across humans, mice, and flies. This figure was generated at https://www.ncbi.nlm.nih.gov/homologene **(B)** NCBI blastP multiple sequence alignment showing detailed primary structure of LSD1 homologs. Arrows denote N-terminal intrinsically disordered domain in conserved species. This figure was generated using https://www.ncbi.nlm.nih.gov/projects/msaviewer/

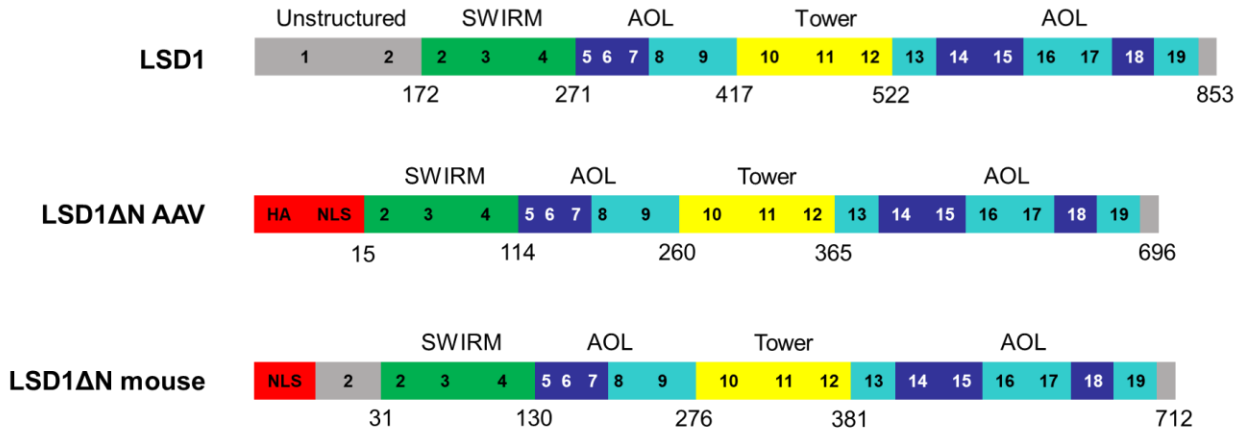

Fig. 4.3 | N-terminally truncated LSD1 constructs. Number of amino acids encoded by each exon in *Lsd1* **(LSD1)** in the endogenous mouse protein, as well as the HA-tagged protein product produced by the LSD1ΔN viral vector **(LSD1ΔN AAV)**, and the protein produced by the *Lsd1ΔN* allele in the mouse that we designed **(LSD1ΔN mouse)**.

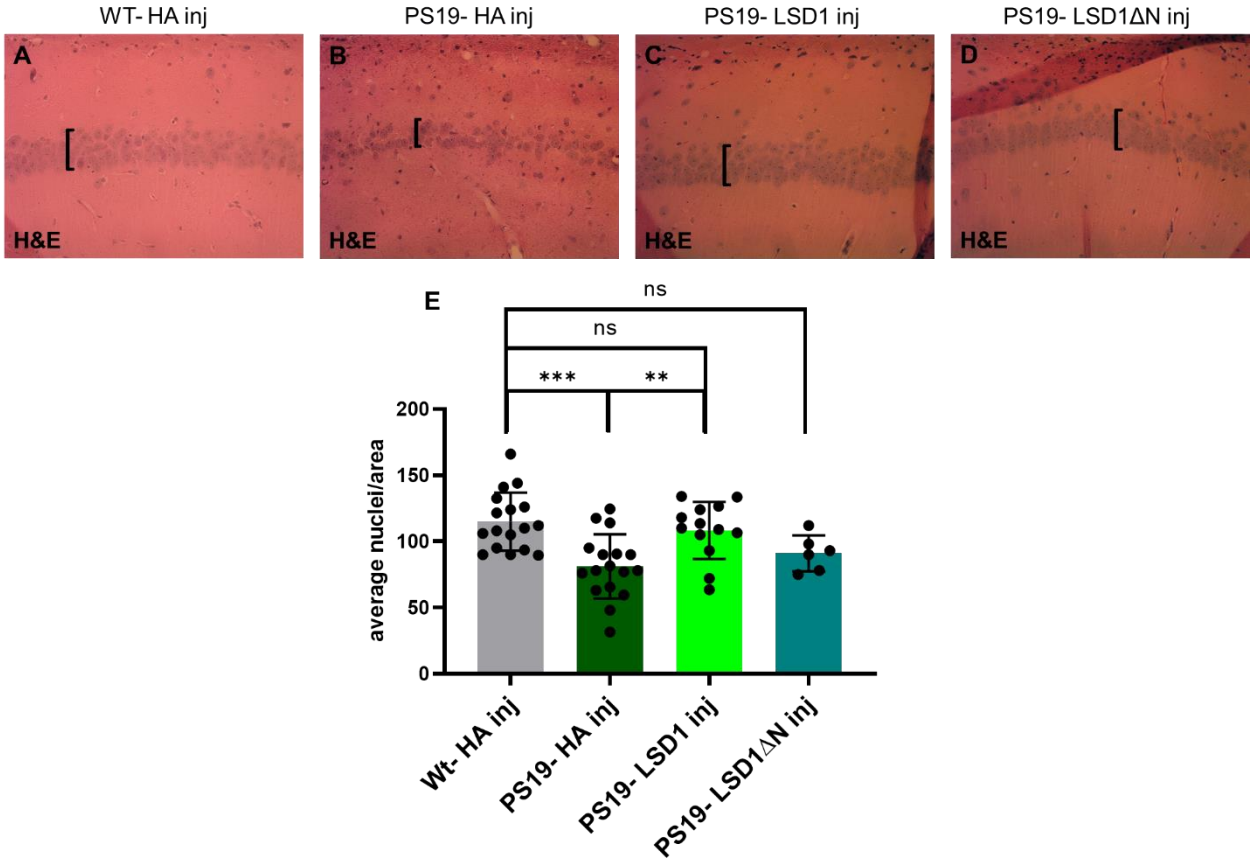

Fig. 4.4 | Overexpression of LSD1ΔN rescues as well as full length. (A-D) Representative images of histology used to collect the counts quantified in **(E)**. **(A)** WT- HA inj mouse aged 11.4 months, **(B)** PS19- HA inj mouse aged 11.7 months, **(C)** PS19- LSD1 inj mouse aged 10.8 months, **(D)** PS19- LSD1ΔN inj mouse aged 10.8 months. Hippocampal thickness denoted by square bracket ([), which is the same size for **(A, C, D)** but smaller in **(B)**. All images taken on 20X objective. **(E)** Quantification of the average number of nuclei in the pyramidal layer of the

hippocampus per area per mouse (<12 months old) from histology represented in **Fig. 4.4A-D**. WT- HA inj *n=17*, PS19- HA inj *n=17*, PS19- LSD1 inj *n=13*, PS19- LSD1ΔN inj *n=6*. Values are mean ± SD (one-way analysis of variance (ANOVA) with Tukey's post hoc test, ***p=0.0002, **p=0.0079, ns=not significant; PS19- HA inj – PS19- LSD1ΔN inj also ns, p=0.7803).

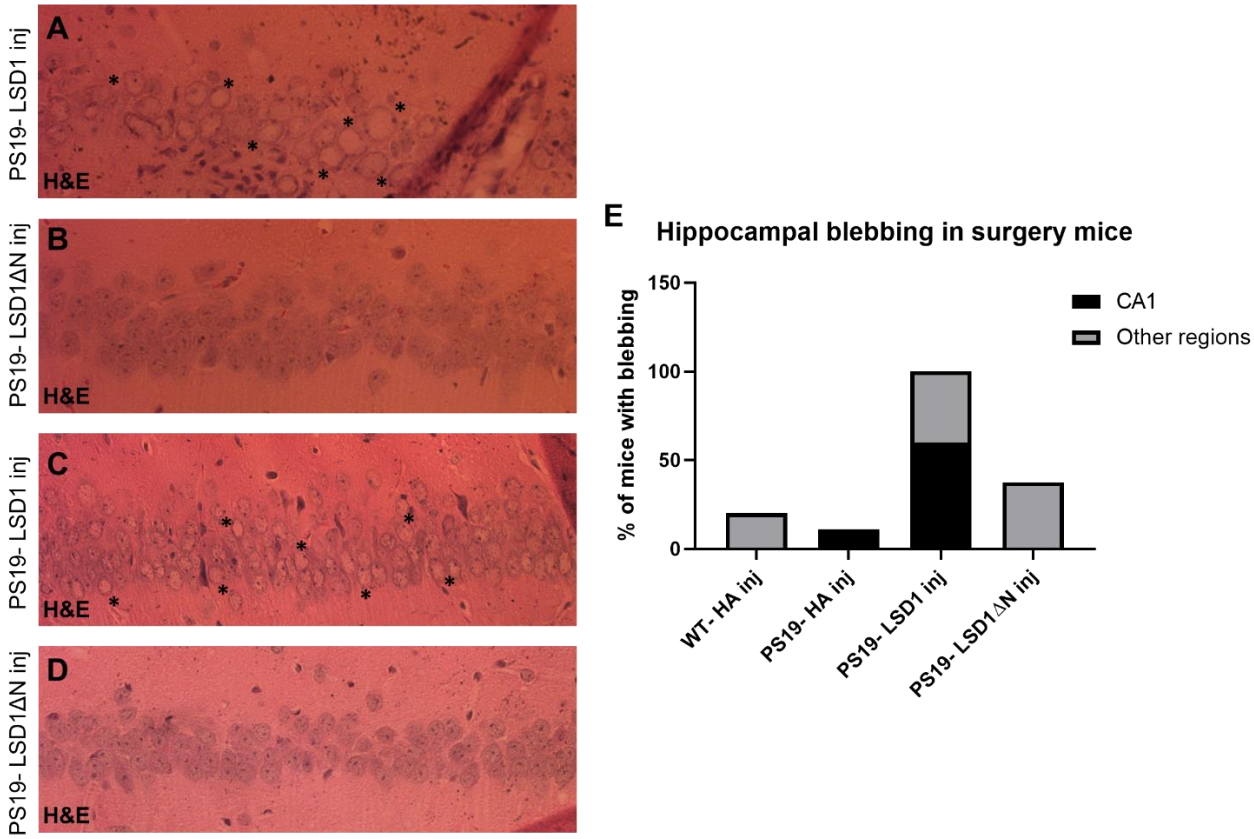

Fig. 4.5 | Only mice injected with the full length LSD1 virus show blebbing in the CA1. (A-D) Representative images of age-matched histology showing blebbing in the CA1 quantified in **(E)**. **(A-B)** show 10 month old mice, while **(C-D)** show 12 month old mice. **(E)** Quantification (%) of mice with CA1 blebbing (black) superimposed over the % of mice with blebbing in the rest of the hippocampus (gray). Every mouse with CA1 blebbing also shows blebbing elsewhere.

Therefore, 100% of PS19- LSD1 inj mice show blebbing somewhere in the hippocampus, 60% of which also show blebbing in the CA1. None of the PS19- LSD1ΔN inj mice show CA1 blebbing, even past 1 year of age **(D)**. All images taken on 20X objective.

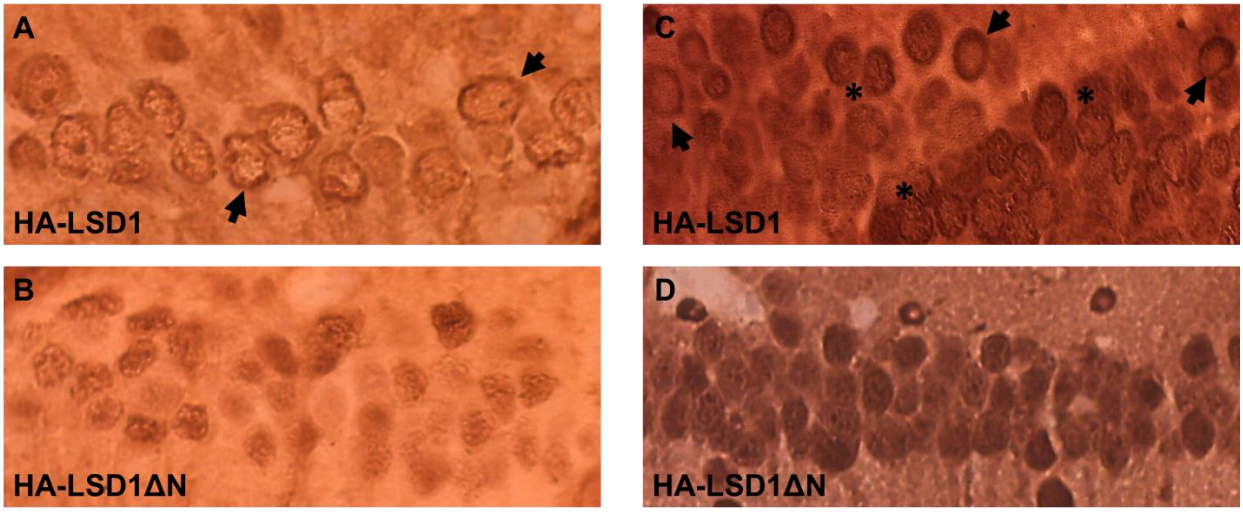

Fig. 4.6 | LSD1ΔN virus remains nuclear even after sequestration in age-matched PS19-LSD1 inj. (A) 10 month old PS19- LSD1 inj mouse shows sequestration of exogenous LSD1 tagged with HA **(B)** 10 month old PS19- LSD1ΔN inj mouse shows nuclear localization of exogenous LSD1ΔN **(C)** 12.2 month old PS19- LSD1 inj mouse shows both cytoplasmic diffuse (*) and nuclear exclusion (→) HA staining, demonstrating sequestration. **(D)** 12.3 month old PS19- LSD1ΔN inj mouse shows consistent nuclear localization of the HA-tagged viral product despite the presence of tau aggregates. All images taken on 20X objective.

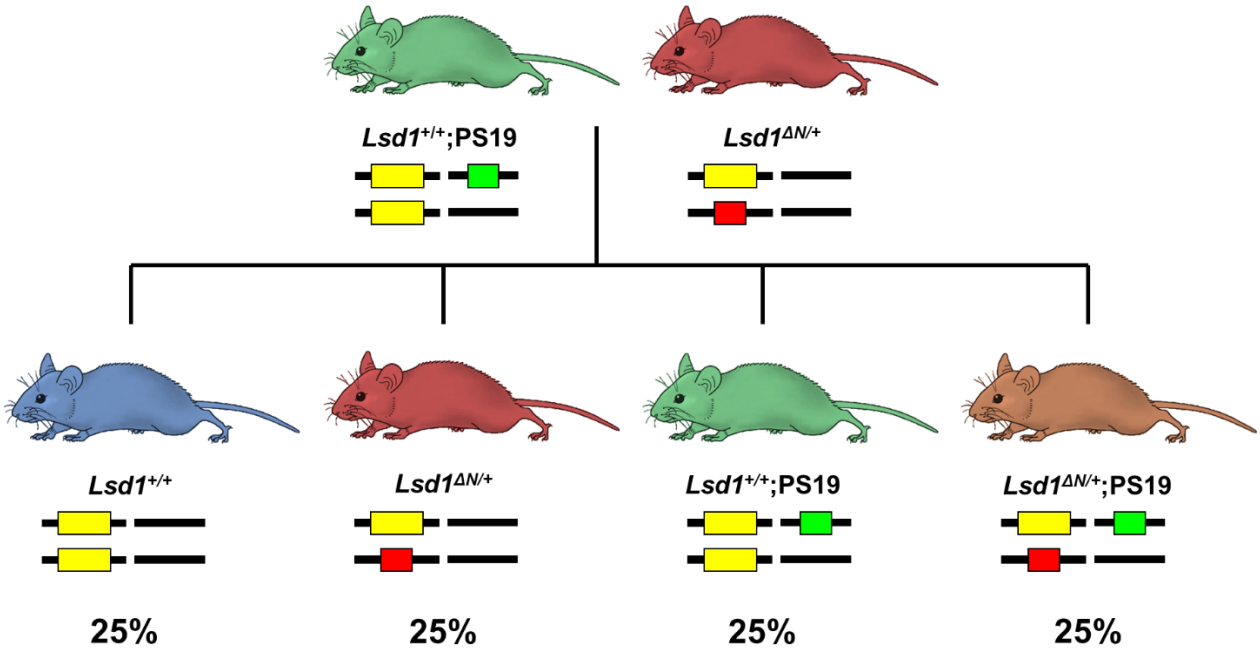

Figure 4.7 | Generation of mice heterozygous for the exon 1 deletion of *Lsd1* in the tau background. Cross of a PS19 hemizygote to a mouse heterozygous for the exon 1 deletion of *Lsd1* generates four experimental genotypes at equal ratios: wildtype (blue), *Lsd1*$^{\Delta N/+}$ (red), PS19 (green), and PS19;*Lsd1*$^{\Delta N/+}$ (brown).

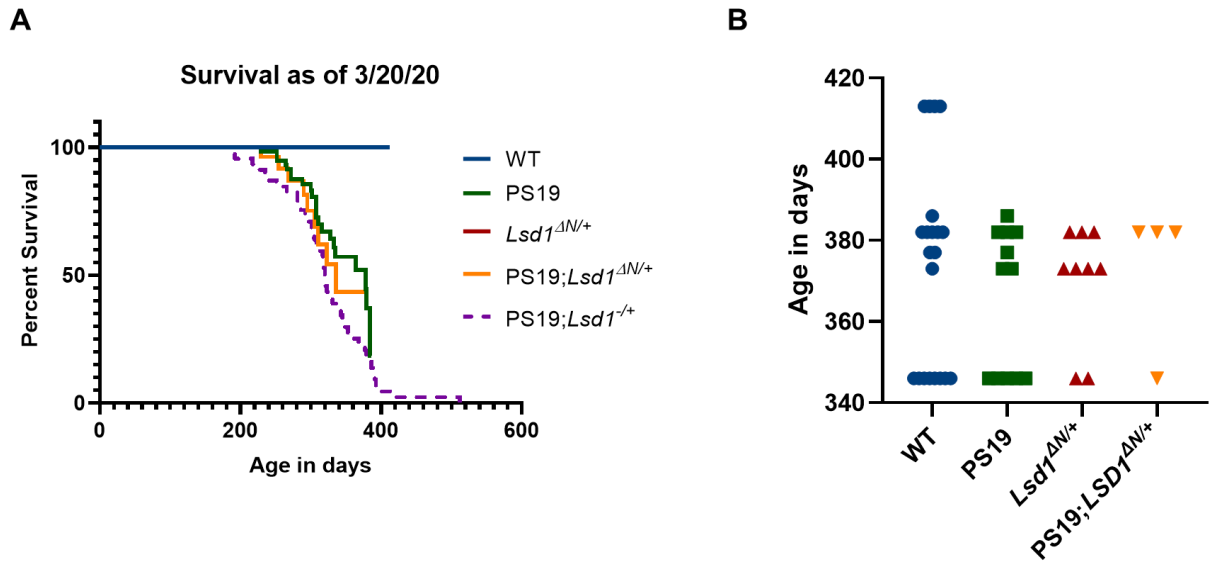

Fig. 4.8 | PS19;*Lsd1*$^{\Delta N/+}$ mice show a survival phenotype intermediate of PS19 and PS19;*Lsd1*$^{-/+}$ mice. (A) Ongoing survival curve: WT (blue) *n=66*, PS19 (green) *n=66*, *Lsd1*$^{\Delta N/+}$ (red) *n=34*, and PS19;*Lsd1*$^{\Delta N/+}$ (orange) *n=28* are all progeny >7 months old from the cross shown in **Fig. 4.10**. PS19;*Lsd1*$^{-/+}$ (purple) *n=44* data is taken from **Fig 3.2A**, which is why the line is dotted and all of the mice are deceased. **(B)** Remaining living mice >11 months old in the same colony: WT (blue) *n=21*, PS19 (green) *n=12*, *Lsd1*$^{\Delta N/+}$ (red) *n=9*, and PS19;*Lsd1*$^{\Delta N/+}$ (orange) *n=4*.

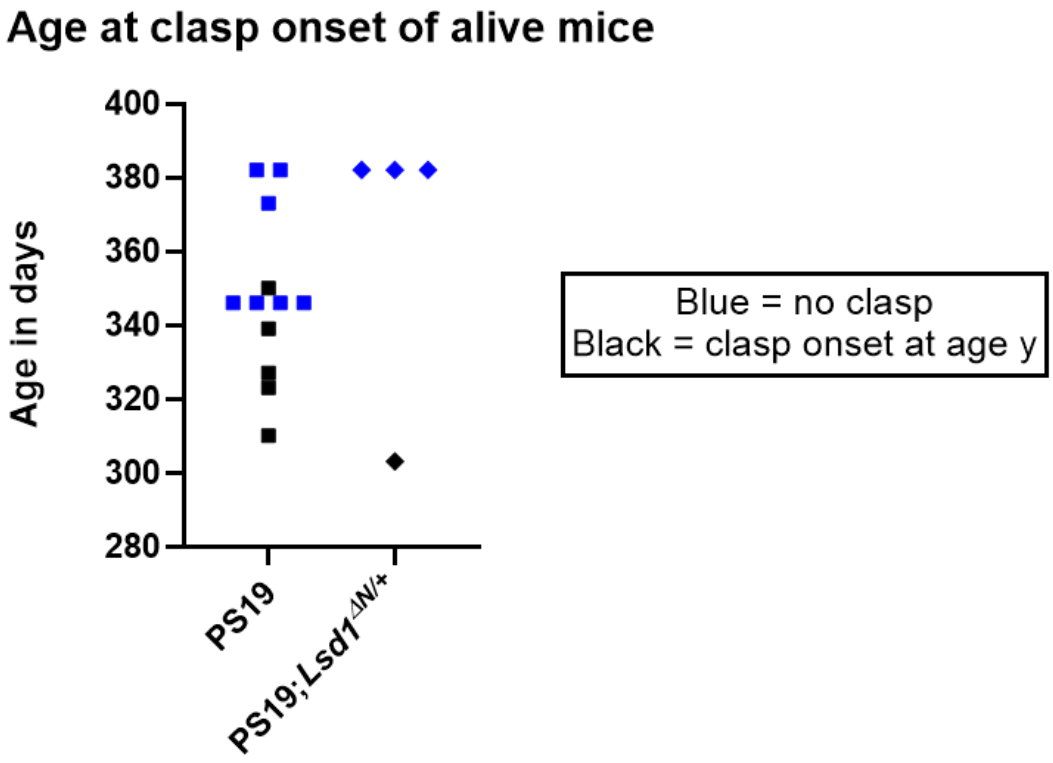

Fig. 4.9 | Some PS19;*Lsd1*$^{\Delta N/+}$ mice have no paralysis despite old age. Age at clasp onset of living mice >11 months only (represented in **Fig. 4.8B**); black points represent animals living with hindlimb paralysis and show y = age at clasp onset, blue points represent animals without a clasp and show y = current age in days. PS19 *n=12* and PS19;*Lsd1*$^{\Delta N/+}$ *n=4*.

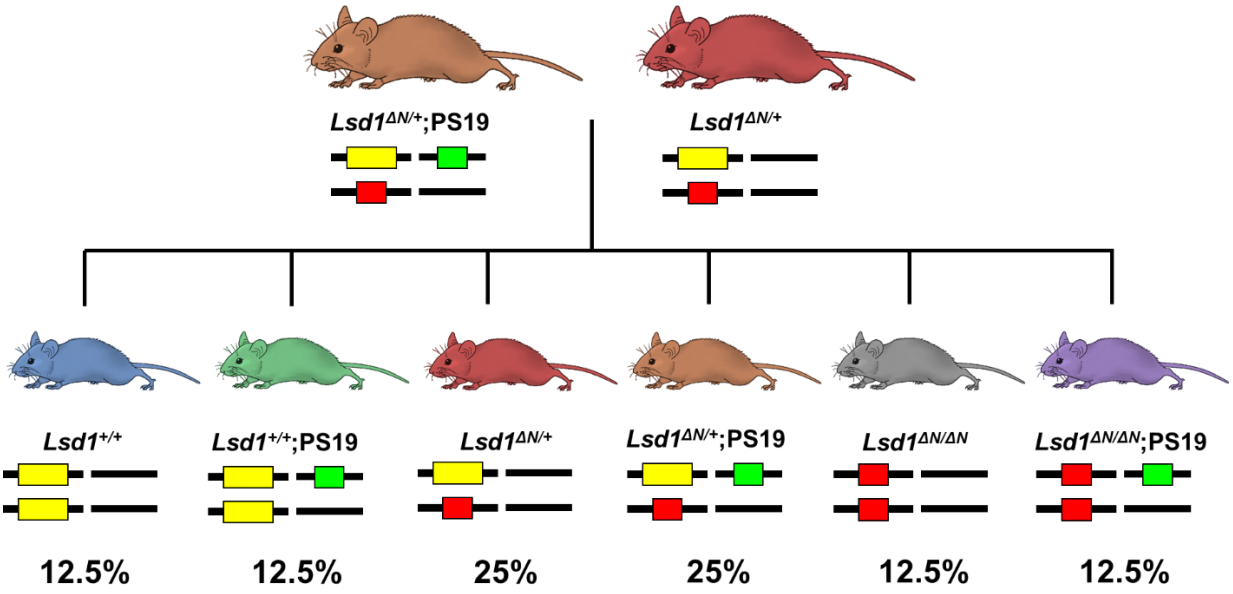

Figure 4.10 | Generation of mice homozygous for the exon 1 deletion of *Lsd1* in the tau background. Cross of a mouse heterozygous for the exon 1 deletion of *Lsd1* with another of these mice which also expresses the tau transgene (PS19;$Lsd1^{\Delta N/+}$) is expected to yield six experimental genotypes: wildtype (blue, ~12.5%), PS19 (green, ~12.5%), $Lsd1^{\Delta N/+}$ (red, ~25%), PS19;$Lsd1^{\Delta N/+}$ (brown, ~25%), $Lsd1^{\Delta N/\Delta N}$ (gray, ~12.5%), PS19;$Lsd1^{\Delta N/\Delta N}$ (purple, ~12.5%).

CHAPTER V

Conclusions and Future Directions

Because the results in Chapter 4 represent a project that is very much ongoing, we are taking some 'future' directions more immediately than others. The most imminent of these is conclusive determination whether the exon 1 deletion of *Lsd1* is embryonic lethal, which we will be able to determine once we have optimized the PCR genotyping.

Based on our preliminary data from the PS19;*Lsd1*$^{\Delta N/+}$ mice, objective measures of paralysis such as a rotarod and/or grid performance assay for grip strength for these mice relative to their *Lsd1*$^{\Delta N/+}$, PS19, and PS19;*Lsd1*$^{-/+}$ counterparts at different ages will inform which genotypes share the most similar phenotype, providing more reliable evidence for the contribution of LSD1's N-terminal disordered domain *in vivo*. To better understand if the paralysis in a majority of the PS19;*Lsd1*$^{\Delta N/+}$ mice is due to tau sequestering truncated LSD1 by continued interaction with the remainder of the disordered domain in exon 2, we can create an AAV viral construct that matches the PS19;*Lsd1*$^{\Delta N/+}$ mouse's *Lsd1* exon 1 deletion. If this exon 2-mediated sequestration model is the case, we would expect this virally produced LSD1 to continue to localize to tau aggregates in the cytoplasm. We are also interested in determining whether overexpression of only the N-terminal disordered domain in PS19 mice can effectively 'coat' tau and prevent it from sequestering endogenous LSD1 in the cytoplasm; this would provide a promising drug target for AD. Finally, we could also create a viral construct in which the N-terminal disordered domain remains intact, but the NLS is moved to the C-terminus. Assuming that moving the NLS to the C-terminus is far enough away to avoid tau aggregates from masking the NLS when LSD1 localizes to tau aggregates, this construct could enable a fully functioning LSD1 protein to evade sequestration. If this works, we could then create a mouse with the NLS moved to the C-terminus. This mouse would be expected to fully block tau from causing neurodegeneration.

To assess the validity of our speculation that the disordered domain is partially required for LSD1 flexibility, and is therefore required for binding with specific chromatin targets, we can perform RNA Sequencing and H3K4me2 ChIP of PS19;*Lsd1*$^{\Delta N/+}$ mice (and ideally PS19;*Lsd1*$^{\Delta N/\Delta N}$ if we can generate them). These experiments will tell us which targets truncated LSD1 fails to interact with, and how the neuronal transcriptional program has changed as a result. Taking the project in this direction would focus the story back on chromatin and has the potential to provide new insights into the mechanism of LSD1 functionality *in vivo*.

In summary, the preceding chapters have demonstrated several important findings. We have identified a novel role for the histone demethylase LSD1 in protection against neurodegeneration – canonical LSD1 is required for neuronal survival (Christopher et al., 2017), while conditional knockout of a neuronal-specific LSD1 isoform does not induce cell death (Wang et al., 2015). We have shown that pathological tau sequesters LSD1 from the nucleus, interfering with this critical role, and resulting in neuronal cell death in mouse models of AD. This conclusion is corroborated by the fact that genetic reduction of *Lsd1* in a PS19 tauopathy mouse model exacerbates tau-mediated neurodegeneration, while overexpression of *Lsd1* temporarily rescues cell death (Engstrom et al., 2020). Additionally, we provide preliminary evidence suggesting that the interaction between tau and LSD1 occurs via the chromatin modifier's N-terminal disordered domain, which we have hypothesized may be partially required for LSD1 functionality *in vivo*. These projects provide exciting new discoveries with the potential to pioneer both the neurodegeneration and epigenetics fields.

CHAPTER VI

References

Afgan E, Baker D, van den Beek M, Blankenberg D, Bouvier D, Cech M, Chilton J, Clements D, Coraor N, Eberhard C, Gruning B, Guerler A, Hillman-Jackson J, Von Kuster G, Rasche E, Soranzo N, Turaga N, Taylor J, Nekrutenko A, Goecks J (2016) The Galaxy platform for accessible, reproducible and collaborative biomedical analyses: 2016 update. Nucleic Acids Res 44:W3-w10.

Afgan E, Baker D, Batut B, van den Beek M, Bouvier D, Čech M, Chilton J, Clements D, Coraor N, Grüning BA, Guerler A, Hillman-Jackson J, Hiltemann S, Jalili V, Rasche H, Soranzo N, Goecks J, Taylor J, Nekrutenko A, Blankenberg D (2018) The Galaxy platform for accessible, reproducible and collaborative biomedical analyses: 2018 update. Nucleic Acids Research 46:W537-W544.

Alonso AD, Cohen LS, Corbo C, Morozova V, ElIdrissi A, Phillips G, Kleiman FE (2018) Hyperphosphorylation of Tau Associates With Changes in Its Function Beyond Microtubule Stability. Front Cell Neurosci 12:338-338.

Arendt T, Stieler JT, Holzer M (2016) Tau and tauopathies. Brain Res Bull 126:238-292.

Arriagada PV, Growdon JH, Hedley-Whyte ET, Hyman BT (1992) Neurofibrillary tangles but not senile plaques parallel duration and severity of Alzheimer's disease. Neurology 42:631-639.

B. B. Gregory R. Warens LB, Robert Gentleman, Wolfgang Huber Andy Liaw, Thomas Lumley, Martin Maechler, Arni Magnusson, Steffen Moeller, Marc Schwartz, Bill Venables (2019).

Ballas N, Grunseich C, Lu DD, Speh JC, Mandel G (2005) REST and Its Corepressors Mediate Plasticity of Neuronal Gene Chromatin throughout Neurogenesis. Cell 121:645-657.

Barage SH, Sonawane KD Amyloid cascade hypothesis: Pathogenesis and therapeutic strategies in Alzheimer's disease. Neuropeptides 52:1-18.

Bejanin A, Schonhaut DR, La Joie R, Kramer JH, Baker SL, Sosa N, Ayakta N, Cantwell A, Janabi M, Lauriola M, O'Neil JP, Gorno-Tempini ML, Miller ZA, Rosen HJ, Miller BL, Jagust WJ, Rabinovici GD (2017) Tau pathology and neurodegeneration contribute to cognitive impairment in Alzheimer's disease. Brain 140:3286-3300.

Bellucci A, Westwood AJ, Ingram E, Casamenti F, Goedert M, Spillantini MG (2004) Induction of Inflammatory Mediators and Microglial Activation in Mice Transgenic for Mutant Human P301S Tau Protein. The American journal of pathology 165:1643-1652.

Bishof I, Dammer EB, Duong DM, Kundinger SR, Gearing M, Lah JJ, Levey AI, Seyfried NT (2018) RNA-binding proteins with basic-acidic dipeptide (BAD) domains self-assemble and aggregate in Alzheimer's disease. The Journal of biological chemistry 293:11047-11066.

Blighe K (2019) EnhancedVolcano: Publication-ready volcano plotswith enhanced colouring and labeling. In: R. package version 1.2.0.

Bloom GS (2014) Amyloid-β and Tau: The Trigger and Bullet in Alzheimer Disease PathogenesisAmyloid-β and TauAmyloid-β and Tau. JAMA Neurology 71:505-508.

Braak H, Braak E (1997) Frequency of Stages of Alzheimer-Related Lesions in Different Age Categories. Neurobiology of Aging 18:351-357.

Castellani RJ, Perry G (2019) Tau Biology, Tauopathy, Traumatic Brain Injury, and Diagnostic Challenges. Journal of Alzheimer's disease : JAD 67:447-467.

Cataldo AM, Hamilton DJ, Nixon RA (1994) Lysosomal abnormalities in degenerating neurons link neuronal compromise to senile plaque development in Alzheimer disease. Brain Res 640:68-80.

Chen-Plotkin AS, Geser F, Plotkin JB, Clark CM, Kwong LK, Yuan W, Grossman M, Van Deerlin VM, Trojanowski JQ, Lee VM (2008) Variations in the progranulin gene affect global gene expression in frontotemporal lobar degeneration. Hum Mol Genet 17:1349-1362.

Choi SH, Kim YH, Hebisch M, Sliwinski C, Lee S, D/'Avanzo C, Chen H, Hooli B, Asselin C, Muffat J, Klee JB, Zhang C, Wainger BJ, Peitz M, Kovacs DM, Woolf CJ, Wagner SL, Tanzi RE, Kim DY (2014) A three-dimensional human neural cell culture model of Alzheimer/'s disease. Nature 515:274-278.

Chong JA, Tapia-Ramirez J, Kim S, Toledo-Aral JJ, Zheng Y, Boutros MC, Altshuller YM, Frohman MA, Kraner SD, Mandel G (1995) REST: a mammalian silencer protein that restricts sodium channel gene expression to neurons. Cell 80:949-957.

Christopher MA, Myrick DA, Barwick BG, Engstrom A, Porter-Stransky KA, Boss JM, Weinshenker D, Levey AI, Katz DJ (2017) LSD1 protects against hippocampal and cotical neurodegeneration. Nature Communications In press.

Cragg BG (1970) What is the signal for chromatolysis? Brain Res 23:1-21.

Diner I, Hales CM, Bishof I, Rabenold L, Duong DM, Yi H, Laur O, Gearing M, Troncoso J, Thambisetty M, Lah JJ, Levey AI, Seyfried NT (2014) Aggregation properties of the small nuclear ribonucleoprotein U1-70K in Alzheimer disease. The Journal of biological chemistry 289:35296-35313.

Duyckaerts C, Delatour B, Potier M-C (2009) Classification and basic pathology of Alzheimer disease. Acta Neuropathologica 118:5-36.

Eftekharzadeh B et al. (2018) Tau Protein Disrupts Nucleocytoplasmic Transport in Alzheimer's Disease. Neuron 99:925-940.e927.

Engstrom AK, Walker AC, Moudgal RA, Myrick DA, Kyle SM, Katz DJ (2020) The inhibition of LSD1 via sequestration contributes to tau-mediated neurodegeneration. bioRxiv:745133.

Falcon S, Gentleman R (2007) Using GOstats to test gene lists for GO term association. Bioinformatics 23:257-258.

Forneris F, Binda C, Vanoni MA, Mattevi A, Battaglioli E (2005) Histone demethylation catalysed by LSD1 is a flavin-dependent oxidative process. FEBS Lett 579:2203-2207.

Foster CT, Dovey OM, Lezina L, Luo JL, Gant TW, Barlev N, Bradley A, Cowley SM (2010) Lysine-specific demethylase 1 regulates the embryonic transcriptome and CoREST stability. Molecular and cellular biology 30:4851-4863.

Frost B, Bardai FH, Feany MB (2016) Lamin Dysfunction Mediates Neurodegeneration in Tauopathies. Curr Biol 26:129-136.

Gentleman RC et al. (2004) Bioconductor: open software development for computational biology and bioinformatics. Genome Biol 5:R80.

Giasson BI, Mushynski WE (1996) Aberrant stress-induced phosphorylation of perikaryal neurofilaments. J Biol Chem 271:30404-30409.

Goedert M, Wischik CM, Crowther RA, Walker JE, Klug A (1988) Cloning and sequencing of the cDNA encoding a core protein of the paired helical filament of Alzheimer disease:

identification as the microtubule-associated protein tau. Proc Natl Acad Sci U S A 85:4051-4055.

Gomez-Isla T, Hollister R, West H, Mui S, Growdon JH, Petersen RC, Parisi JE, Hyman BT (1997) Neuronal loss correlates with but exceeds neurofibrillary tangles in Alzheimer's disease. Ann Neurol 41:17-24.

Hanger DP, Betts JC, Loviny TL, Blackstock WP, Anderton BH (1998) New phosphorylation sites identified in hyperphosphorylated tau (paired helical filament-tau) from Alzheimer's disease brain using nanoelectrospray mass spectrometry. J Neurochem 71:2465-2476.

Hardy J, Selkoe DJ (2002) The amyloid hypothesis of Alzheimer's disease: progress and problems on the road to therapeutics. Science (New York, NY) 297:353-356.

Hayashi S, McMahon AP (2002) Efficient recombination in diverse tissues by a tamoxifen-inducible form of Cre: a tool for temporally regulated gene activation/inactivation in the mouse. Dev Biol 244:305-318.

He Z, Guo JL, McBride JD, Narasimhan S, Kim H, Changolkar L, Zhang B, Gathagan RJ, Yue C, Dengler C, Stieber A, Nitla M, Coulter DA, Abel T, Brunden KR, Trojanowski JQ, Lee VM (2018) Amyloid-beta plaques enhance Alzheimer's brain tau-seeded pathologies by facilitating neuritic plaque tau aggregation. Nat Med 24:29-38.

Holtzman DM, Carrillo MC, Hendrix JA, Bain LJ, Catafau AM, Gault LM, Goedert M, Mandelkow E, Mandelkow EM, Miller DS, Ostrowitzki S, Polydoro M, Smith S, Wittmann M, Hutton M (2016) Tau: From research to clinical development. Alzheimers Dement 12:1033-1039.

Hurtado DE, Molina-Porcel L, Iba M, Aboagye AK, Paul SM, Trojanowski JQ, Lee VM (2010) A{beta} accelerates the spatiotemporal progression of tau pathology and augments tau amyloidosis in an Alzheimer mouse model. Am J Pathol 177:1977-1988.

Iba M, McBride JD, Guo JL, Zhang B, Trojanowski JQ, Lee VM (2015) Tau pathology spread in PS19 tau transgenic mice following locus coeruleus (LC) injections of synthetic tau fibrils is determined by the LC's afferent and efferent connections. Acta Neuropathol 130:349-362.

Ingelsson M, Fukumoto H, Newell KL, Growdon JH, Hedley-Whyte ET, Frosch MP, Albert MS, Hyman BT, Irizarry MC (2004) Early Abeta accumulation and progressive synaptic loss, gliosis, and tangle formation in AD brain. Neurology 62:925-931.

Iqbal K, Liu F, Gong CX, Grundke-Iqbal I (2010) Tau in Alzheimer disease and related tauopathies. Curr Alzheimer Res 7:656-664.

Jiang D, Yang W, He Y, Amasino RM (2007) Arabidopsis relatives of the human lysine-specific Demethylase1 repress the expression of FWA and FLOWERING LOCUS C and thus promote the floral transition. Plant Cell 19:2975-2987.

Jin L, Hanigan CL, Wu Y, Wang W, Park BH, Woster PM, Casero RA (2013) Loss of LSD1 (lysine-specific demethylase 1) suppresses growth and alters gene expression of human colon cancer cells in a p53- and DNMT1(DNA methyltransferase 1)-independent manner. The Biochemical journal 449:459-468.

Jin Y, Kim TY, Kim MS, Kim MA, Park SH, Jang YK (2014) Nuclear import of human histone lysine-specific demethylase LSD1. J Biochem 156:305-313.

Karran E, Mercken M, De Strooper B (2011) The amyloid cascade hypothesis for Alzheimer's disease: an appraisal for the development of therapeutics. Nature reviews Drug discovery 10:698-712.

Katz DJ, Edwards TM, Reinke V, Kelly WG (2009) A C. elegans LSD1 demethylase contributes to germline immortality by reprogramming epigenetic memory. Cell 137:308-320.

Kim D, Pertea G, Trapnell C, Pimentel H, Kelley R, Salzberg SL (2013) TopHat2: accurate alignment of transcriptomes in the presence of insertions, deletions and gene fusions. Genome Biology 14:R36.

Kinney JW, Bemiller SM, Murtishaw AS, Leisgang AM, Salazar AM, Lamb BT (2018) Inflammation as a central mechanism in Alzheimer's disease. Alzheimer's & Dementia: Translational Research & Clinical Interventions 4:575-590.

Laurent B, Ruitu L, Murn J, Hempel K, Ferrao R, Xiang Y, Liu S, Garcia BA, Wu H, Wu F, Steen H, Shi Y (2015) A specific LSD1/KDM1A isoform regulates neuronal differentiation through H3K9 demethylation. Molecular cell 57:957-970.

Lawrence M, Gentleman R, Carey V (2009) rtracklayer: an R package for interfacing with genome browsers. Bioinformatics 25:1841-1842.

Lee TW, Katz DJ (2020) Hansel, Gretel, and the Consequences of Failing to Remove Histone Methylation Breadcrumbs. Trends in Genetics 36:160-176.

Liao Y, Wang J, Jaehnig EJ, Shi Z, Zhang B (2019) WebGestalt 2019: gene set analysis toolkit with revamped UIs and APIs. Nucleic Acids Res 47:W199-w205.

Lindwall G, Cole RD (1984) Phosphorylation affects the ability of tau protein to promote microtubule assembly. The Journal of biological chemistry 259:5301-5305.

Liu YL, Guo YS, Xu L, Wu SY, Wu DX, Yang C, Zhang Y, Li CY (2008) Alternation of neurofilaments in immune-mediated injury of spinal cord motor neurons. Spinal Cord 47:166.

Lyons DB, Allen WE, Goh T, Tsai L, Barnea G, Lomvardas S (2013) An epigenetic trap stabilizes singular olfactory receptor expression. Cell 154:325-336.

Masliah E, Mallory M, Alford M, DeTeresa R, Hansen LA, McKeel DW, Jr., Morris JC (2001) Altered expression of synaptic proteins occurs early during progression of Alzheimer's disease. Neurology 56:127-129.

Mito Y, Henikoff JG, Henikoff S (2005) Genome-scale profiling of histone H3.3 replacement patterns. Nature genetics 37:1090-1097.

Moon LDF (2018) Chromatolysis: Do injured axons regenerate poorly when ribonucleases attack rough endoplasmic reticulum, ribosomes and RNA? Dev Neurobiol 78:1011-1024.

Mootha VK et al. (2003) PGC-1α-responsive genes involved in oxidative phosphorylation are coordinately downregulated in human diabetes. Nature genetics 34:267-273.

Morishima-Kawashima M, Hasegawa M, Takio K, Suzuki M, Yoshida H, Watanabe A, Titani K, Ihara Y (1995) Hyperphosphorylation of tau in PHF. Neurobiol Aging 16:365-371; discussion 371-380.

Muramoto T, Müller I, Thomas G, Melvin A, Chubb JR (2010) Methylation of H3K4 Is Required for Inheritance of Active Transcriptional States. Current Biology 20:397-406.

Ng HH, Robert F, Young RA, Struhl K (2003) Targeted Recruitment of Set1 Histone Methylase by Elongating Pol II Provides a Localized Mark and Memory of Recent Transcriptional Activity. Molecular cell 11:709-719.

Orr ME, Sullivan AC, Frost B (2017) A Brief Overview of Tauopathy: Causes, Consequences, and Therapeutic Strategies. Trends in pharmacological sciences 38:637-648.

Riancho J, Ruiz-Soto M, Villagra NT, Berciano J, Berciano MT, Lafarga M (2014) Compensatory Motor Neuron Response to Chromatolysis in the Murine hSOD1(G93A) Model of Amyotrophic Lateral Sclerosis. Front Cell Neurosci 8:346.

Rubio-Perez JM, Morillas-Ruiz JM (2012) A review: inflammatory process in Alzheimer's disease, role of cytokines. TheScientificWorldJournal 2012:756357-756357.

Sanders David W, Kaufman Sarah K, DeVos Sarah L, Sharma Apurwa M, Mirbaha H, Li A, Barker Scarlett J, Foley Alex C, Thorpe Julian R, Serpell Louise C, Miller Timothy M, Grinberg Lea T, Seeley William W, Diamond Marc I (2014) Distinct Tau Prion Strains Propagate in Cells and Mice and Define Different Tauopathies. Neuron 82:1271-1288.

Sandhu KS (2009) Intrinsic disorder explains diverse nuclear roles of chromatin remodeling proteins. Journal of Molecular Recognition: An Interdisciplinary Journal 22:1-8.

Scharer CD, Barwick BG, Youngblood BA, Ahmed R, Boss JM (2013) Global DNA methylation remodeling accompanies CD8 T cell effector function. Journal of immunology (Baltimore, Md : 1950) 191:3419-3429.

Sheffield LG, Miskiewicz HB, Tannenbaum LB, Mirra SS (2006) Nuclear Pore Complex Proteins in Alzheimer Disease. Journal of Neuropathology & Experimental Neurology 65:45-54.

Shi Y, Lan F, Matson C, Mulligan P, Whetstine JR, Cole PA, Casero RA, Shi Y (2004) Histone demethylation mediated by the nuclear amine oxidase homolog LSD1. Cell 119:941-953.

Shilatifard A (2012) The COMPASS Family of Histone H3K4 Methylases: Mechanisms of Regulation in Development and Disease Pathogenesis. Annual Review of Biochemistry 81:65-95.

Shrinivas K, Sabari BR, Coffey EL, Klein IA, Boija A, Zamudio AV, Schuijers J, Hannett NM, Sharp PA, Young RA, Chakraborty AK (2019) Enhancer Features that Drive Formation of Transcriptional Condensates. Molecular cell 75:549-561.e547.

Sil S, Goswami AR, Dutta G, Ghosh T (2014) Effects of naproxen on immune responses in a colchicine-induced rat model of Alzheimer's disease. Neuroimmunomodulation 21:304-321.

Skrabana R, Skrabanova M, Csokova N, Sevcik J, Novak M (2006) Intrinsically disordered tau protein in Alzheimer's tangles: a coincidence or a rule? Bratisl Lek Listy 107:354-358.

Subramanian A, Tamayo P, Mootha VK, Mukherjee S, Ebert BL, Gillette MA, Paulovich A, Pomeroy SL, Golub TR, Lander ES, Mesirov JP (2005) Gene set enrichment analysis: A knowledge-based approach for interpreting genome-wide expression profiles. Proceedings of the National Academy of Sciences 102:15545.

Suzuki R, Shimodaira H (2006) Pvclust: an R package for assessing the uncertainty in hierarchical clustering. Bioinformatics 22:1540-1542.

Trapnell C, Williams BA, Pertea G, Mortazavi A, Kwan G, van Baren MJ, Salzberg SL, Wold BJ, Pachter L (2010) Transcript assembly and quantification by RNA-Seq reveals unannotated transcripts and isoform switching during cell differentiation. Nature Biotechnology 28:511-515.

Wang J, Duncan D, Shi Z, Zhang B (2013) WEB-based GEne SeT AnaLysis Toolkit (WebGestalt): update 2013. Nucleic Acids Res 41:W77-83.

Wang J, Vasaikar S, Shi Z, Greer M, Zhang B (2017) WebGestalt 2017: a more comprehensive, powerful, flexible and interactive gene set enrichment analysis toolkit. Nucleic Acids Res 45:W130-w137.

Wang J, Hevi S, Kurash JK, Lei H, Gay F, Bajko J, Su H, Sun W, Chang H, Xu G, Gaudet F, Li E, Chen T (2009) The lysine demethylase LSD1 (KDM1) is required for maintenance of global DNA methylation. Nature genetics 41:125-129.

Wang J, Scully K, Zhu X, Cai L, Zhang J, Prefontaine GG, Krones A, Ohgi KA, Zhu P, Garcia-Bassets I, Liu F, Taylor H, Lozach J, Jayes FL, Korach KS, Glass CK, Fu XD, Rosenfeld MG (2007) Opposing LSD1 complexes function in developmental gene activation and repression programmes. Nature 446:882-887.

Wang J, Telese F, Tan Y, Li W, Jin C, He X, Basnet H, Ma Q, Merkurjev D, Zhu X, Liu Z, Zhang J, Ohgi K, Taylor H, White RR, Tazearslan C, Suh Y, Macfarlan TS, Pfaff SL, Rosenfeld MG (2015) LSD1n is an H4K20 demethylase regulating memory formation via transcriptional elongation control. Nature neuroscience 18:1256-1264.

Wang Y, Mandelkow E (2016) Tau in physiology and pathology. Nat Rev Neurosci 17:5-21.

Weingarten MD, Lockwood AH, Hwo SY, Kirschner MW (1975) A protein factor essential for microtubule assembly. Proceedings of the National Academy of Sciences of the United States of America 72:1858-1862.

Wheeler DL, Church DM, Lash AE, Leipe DD, Madden TL, Pontius JU, Schuler GD, Schriml LM, Tatusova TA, Wagner L, Rapp BA (2001) Database resources of the National Center for Biotechnology Information. Nucleic acids research 29:11-16.

Whyte WA, Bilodeau S, Orlando DA, Hoke HA, Frampton GM, Foster CT, Cowley SM, Young RA (2012) Enhancer decommissioning by LSD1 during embryonic stem cell differentiation. Nature 482:221-225.

Wischik CM, Novak M, Thogersen HC, Edwards PC, Runswick MJ, Jakes R, Walker JE, Milstein C, Roth M, Klug A (1988) Isolation of a fragment of tau derived from the core of the paired helical filament of Alzheimer disease. Proc Natl Acad Sci U S A 85:4506-4510.

Wright PE, Dyson HJ (1999) Intrinsically unstructured proteins: re-assessing the protein structure-function paradigm. J Mol Biol 293:321-331.

Yoshiyama Y, Higuchi M, Zhang B, Huang SM, Iwata N, Saido TC, Maeda J, Suhara T, Trojanowski JQ, Lee VM (2007) Synapse loss and microglial activation precede tangles in a P301S tauopathy mouse model. Neuron 53:337-351.

Zhang B, Kirov S, Snoddy J (2005) WebGestalt: an integrated system for exploring gene sets in various biological contexts. Nucleic Acids Res 33:W741-748.

Zhang B et al. (2013) Integrated systems approach identifies genetic nodes and networks in late-onset Alzheimer's disease. Cell 153:707-720.

Zibetti C, Adamo A, Binda C, Forneris F, Toffolo E, Verpelli C, Ginelli E, Mattevi A, Sala C, Battaglioli E (2010) Alternative splicing of the histone demethylase LSD1/KDM1 contributes to the modulation of neurite morphogenesis in the mammalian nervous system. J Neurosci 30:2521-2532.